NASA CONTRACTOR REPORT

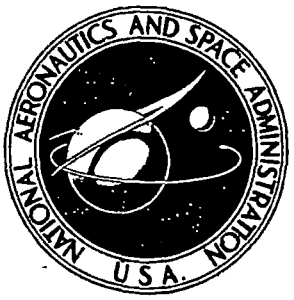

NASA CR-2516

NASA CR-2516

INSTABILITY OF A GRAVITY GRADIENT SATELLITE DUE TO THERMAL DISTORTION

Robert L. Goldman

Prepared by
MARTIN MARIETTA CORPORATION
Baltimore, Md. 21227
for Goddard Space Flight Center

NATIONAL AERONAUTICS AND SPACE ADMINISTRATION • WASHINGTON, D. C. • MARCH 1975

TECHNICAL REPORT STANDARD TITLE PAGE

1 Report No	2 Government Accession No	3 Recipient's Catalog No
NASA CR-2516		

4 Title and Subtitle
Instability of a Gravity Gradient Satellite Due to Thermal Distortion

5 Report Date
March 1975

6 Performing Organization Code

7 Author(s)
Robert L. Goldman

8 Performing Organization Report No
TR-74-02c

9 Performing Organization Name and Address
Martin Marietta Corporation
Martin Marietta Laboratories
1450 South Rolling Road
Baltimore, Maryland 21227

10 Work Unit No

11 Contract or Grant No
NAS5-22230

12 Sponsoring Agency Name and Address
National Aeronautics and Space Administration
Washington, D.C. 20546

13 Type of Report and Period Covered
Contractor Report

14 Sponsoring Agency Code

15 Supplementary Notes
Final Report. Harold P. Frisch, Technical Monitor, Goddard Space Flight Center

16 Abstract

A nonlinear analytical model and a corresponding computer program have been developed to study the influence of solar heating on the anomalous low frequency, orbital instability of the Naval Research Laboratory's gravity gradient satellite 164. The model's formulation was based on a quasi-static approach in which deflections of the satellite's booms were determined in terms of thermally induced bending without consideration of boom vibration. Calculations, which were made for variations in absorptivity, sun angle, thermal lag and hinge stiffness, demonstrated that, within the confines of a relatively narrow stability criteria, the quasi-static model of NRL 164 not only becomes unstable, but, in a number of cases, responses were computed that closely resembled flight data.

17. Key Words (Selected by Author(s))	18. Distribution Statement
Gravity gradient satellites Booms Thermoelasticity Spacecraft stability	Unclassified - unlimited STAR Category 18

19 Security Classif (of this report)	20 Security Classif (of this page)	21 No of Pages	22 Price*
Unclassified	Unclassified	109	$5.25

*For sale by the National Technical Information Service, Springfield, Virginia 22151

Page intentionally left blank

Page intentionally left blank

SUMMARY

This report is concerned with the problem of determining the influence of solar heating on the low frequency, dynamic stability of a gravity gradient satellite. The scope of the effort includes the development of a computer program that uses a quasi-static approach for describing a satellite's unsteady orbital motion. Tied to this objective is a requirement to explain the source of the observed anomalous unstable behavior of the Naval Research Laboratory's gravity gradient satellite 164 (NRL 164).

The basic equations describing the rotational dynamics of NRL 164 are obtained in terms of kinematic, dynamic, orbital mechanic and thermal distortion equations. The resulting derivation leads to a set of fifteen first order, nonlinear differential equations of motion. The essential feature of the quasi-static approach is that the satellite's long, slender booms reach their thermal equilibrium position solely as a result of thermal bending and thermal lag without consideration of the dynamic effects of boom vibration. A computer program based on this formulation has been developed and used to examine the effects of absorptivity, sun angle, thermal lag and hinge stiffness on the stability of the satellite's motion.

It is concluded that within the confines of relatively narrow stability criteria, the quasi-static model provides a valid means of predicting the anomalous behavior of NRL 164. The occurrence of computed unstable responses closely resembling flight data tended to confirm that the source of the instability is related to thermal distortion and is particularly sensitive to sun angle.

If future gravity gradient spacecraft stabilization systems are to be considered, a quasi-static mathematical model of sufficient generality should be developed for determining optimum stable configurations.

Page intentionally left blank

IV

Page intentionally left blank

CONTENTS

INTRODUCTION 1

SATELLITE CHARACTERISTICS 3

SIMULATION 4

Reference Frames 4
Kinematic Equations 7
Dynamic Equations 9
Orbital Mechanics 10
Thermal Deformation 11
Computer Program 14

RESULTS AND DISCUSSION 14

Stability Criteria 15
Basic Characteristics 17
Effect of Absorptivity 19
Effect of Sun Angle 20
Effect of Thermal Lag 20
Effect of Hinge Stiffness 27

CONCLUSIONS 30

RECOMMENDATIONS 31

ACKNOWLEDGEMENT 32

REFERENCES 33

APPENDIX A Body Rotations A-1

APPENDIX B Inertia Dyadics and Torque Elements B-1

APPENDIX C Occultation C-1

APPENDIX D Computer Program Guide D-1

APPENDIX E Examination of The Anomalous Behavior of Three Gravity Gradient Satellites . . . E-1

INSTABILITY OF A GRAVITY GRADIENT SATELLITE DUE TO THERMAL DISTORTION

By Robert L. Goldman
Martin Marietta Laboratories
Martin Marietta Corporation

INTRODUCTION

The apparent simplicity offered by the concept of gravity gradient control of an earth orbiting satellite (References 1 to 3) has had a stimulating effect on the design of several spacecraft configurations. From an analytical point of view it seemed clear that three-axis passive stabilization of a spacecraft could be achieved through the clever use of tip weighted extendable booms. If stability were possible, a desirable earth-pointing equilibrium attitude of a satellite could be attained solely by a judicious arrangement of these booms (e. g. References 4 to 6).

However, discovery of actual flight instabilities on several three-axis gravity gradient satellites made much of the earlier theoretical analysis suspect. Such instabilities were seen in the flight data collected during a series of gravity gradient experiments conducted by the Naval Research Laboratory (NRL) and examined in Reference 7.* Here it was observed that the unstable satellite response was primarily characterized by low frequency rigid body oscillations dominated by large yaw motions and, in some cases, yaw inversions. The satellite's behavior was clearly related to the angle between the sun's vector and the normal to the satellite's orbital plane (sun angle), a condition that led directly to the conclusion that a satellite's thermal distortion properties play an important role in the instability mechanism.

If a correct analytical model of this instability mechanism could be developed, it might be possible to design gravity gradient satellites in such a way as to eliminate the detrimental effects of thermal distortion. As reported in Reference 8, a specific analytical attempt was made to determine the influence that thermal distortion might have had on the attitude stability of the Naval Research Laboratory's gravity gradient satellite 164 (NRL 164) shown in Figure 1. As described in Reference 7, NRL 164 was unstable in yaw while in full sunlight.

The analytical model selected was the IMP Dynamics Computer Program, Reference 9. Although the program was developed to simulate the dynamics of IMP class satellites, it retains sufficient generality to be applicable to NRL 164. Internal and external effects due to gravity gradient forces, solar pressure, magnetic torques, eccentricity, thermal bending, boom vibration and a single-axis libration damper can be simulated by the program.

---

*This report is reproduced as Appendix E.

Unfortunately the planned analysis of NRL 164 with the IMP Dynamics Computer Program was unsuccessful. In retrospect the IMP Program was not at all suitable for the attempted investigation. In addition to a number of unanticipated program errors, the method proved to be much too cumbersome for the specific problem under investigation. Boom vibrations, for example, had an adverse influence on the computational procedure, since they led to excessively long computer runs.

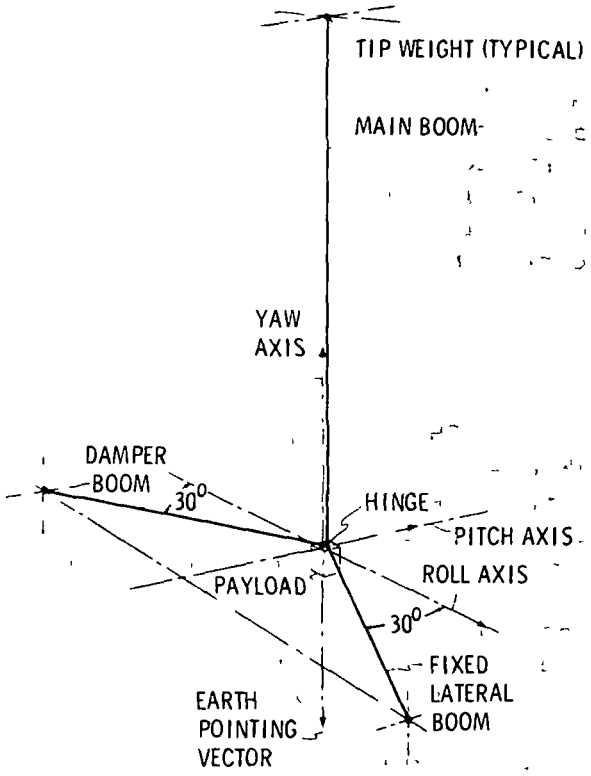

Figure 1 - Satellite geometry, NRL 164.

An alternative, quasi-static procedure, based on the dynamical equations described by Hooker in Reference 10, was suggested in Reference 8 as a means of simplifying the analytical model and the resulting computational procedures. In essence, this approach, which is similar to that used by Kanning in Reference 11, would eliminate entirely consideration of a boom's flexural modes of vibration. Assumptions of importance in the quasi-static approach are that:

1. The boom reaches its thermal equilibrium position solely as a result of thermal bending and thermal lag without any consideration of boom vibration;

2. The inertial and geometric properties of the satellite are altered as the tip weights at the ends of massless booms are displaced by boom deformation;

3. The sun line and thermal properties of a boom determine the magnitude and direction of a boom's tip deflection.

The quasi-static approach eliminates the numerical analysis problem that arises from boom vibration and is justified by the relatively large ratio between the satellite's boom vibration frequencies and its gravity induced rigid body frequencies. Boom bending is considered solely in terms of static thermal deformation without the local dynamic effects of boom inertia.

In the present report the problem of ascertaining the influence of thermal deformation due to solar radiation on the low frequency, dynamic stability of NRL 164 is re-examined. In this case the effort is directed

toward the development of a digital computer program that uses the quasi-static approach for describing the rotational dynamics of the satellite. The principal disturbance mechanism considered is assumed to be due to geometrical and subsequent inertial changes resulting from thermal distortion. The essential objective is to determine under what conditions the resulting re-orientation process becomes unstable.

SATELLITE CHARACTERISTICS

The basic geometry of satellite 164 is illustrated in Figure 1. The three-axis, two-body gravity gradient stabilization system consisted of three extendable, interlocked nonperforated, SPAR BI-STEM booms arranged in a symmetric pattern about the plane of the pitch-yaw axes. The primary body was made up of the payload, main boom and front lateral boom (fixed to the payload); the secondary body consisted solely of the lateral damper boom. Nominally, the lateral booms were located in the horizontal pitch-roll plane. The damper boom was connected to the primary body through a single-axis hinge mechanism that constrained boom motion to a vertical plane. The hinge provided hysteresis damping torques and torsion wire spring restoring torques.

By skewing the horizontal principal axis of the damper boom out of the orbital plane, all motions become strongly coupled. Under these conditions, three-axis damping of the entire satellite is achieved by the single-degree-of-freedom motion of the damper boom about its hinge (Reference 12).

Satellite 164 was stable throughout its initial period of eclipsing orbits (passage through the earth's shadow) and unstable in yaw sometime after its first excursion into a fully sunlit orbit. In fact, during the entire first passage through eclipsing orbits and first entrance into full sunlight, all attitude errors were small. The perturbations were confined to approximately one-cycle-per-orbit oscillations in pitch and 1/2 cycle-per-orbit oscillations in yaw.

As the satellite, in full sunlight, approached the 0° sun angle position* the amplitude of the 1/2 cycle-per-orbit oscillations in yaw unexpectedly increased. The satellite rapidly became unstable with several yaw inversions and large amplitude oscillations in both pitch and roll. After passing through the 0° sun angle position, the instability ceased and was followed by a period of stable operation.

---

*In References 7 and 8 this is the 180° sun angle position. The difference lies in whether the sun vector is defined as either being toward or away from the sun. In the present report it is always toward the sun.

SIMULATION

For NRL 164 the vector dynamical equations developed by Hooker in Reference 10 are used since their application eliminates many of the difficulties common to the Lagrangian approach (e.g. Reference 4). With respect to the basic equations, the final quasi-static attitude of the two-body satellite, including associated kinematics, dynamics, orbital mechanics, and thermal distortion, leads eventually to a set of 15 first-order, non-linear differential equations of motion.

Reference Frames

In the present derivation the three orthogonal frames illustrated in Figures 2 and 3 have been chosen. The basic inertial frame,

$$[\vec{a}] = [\vec{a}_1 \vec{a}_2 \vec{a}_3]$$

is fixed in space with its origin at the earth's center.

Here

$\vec{a}_1$ is a unit vector towards the perigee of the satellite's orbit,

$\vec{a}_3$ is a unit vector parallel to the satellite's orbital angular momentum vector, and

$$\vec{a}_2 = \vec{a}_3 \times \vec{a}_1$$

It has been assumed that the satellite's orbital plane is perpendicular to the $\vec{a}_3$ vector. The local inertial frame is simply obtained by a parallel translation of the $[\vec{a}]$ frame from the earth's center to the satellite's center of mass.

The second frame is the local vertical, or orbital reference frame,

$$[\vec{E}] = [\vec{E}_1 \vec{E}_2 \vec{E}_3]$$

which has its origin fixed at the satellite's center of mass and moves with it along its orbital path.

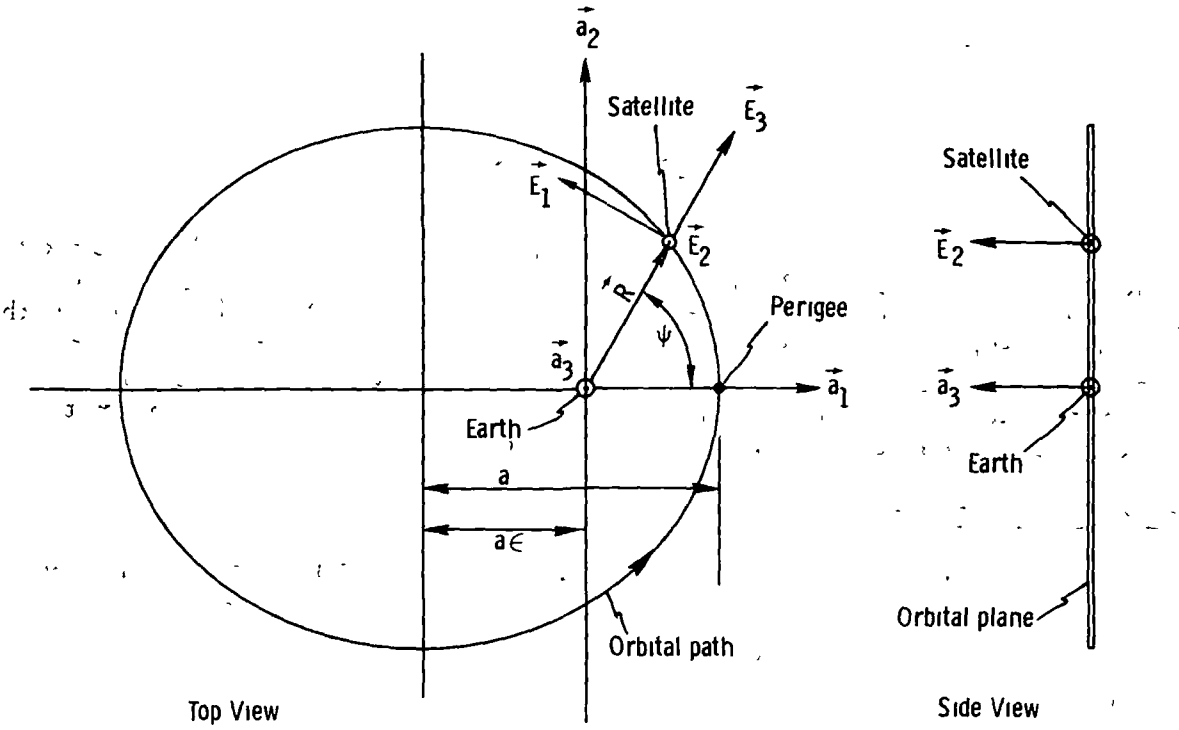

Figure 2 - Inertial and orbital reference frames.

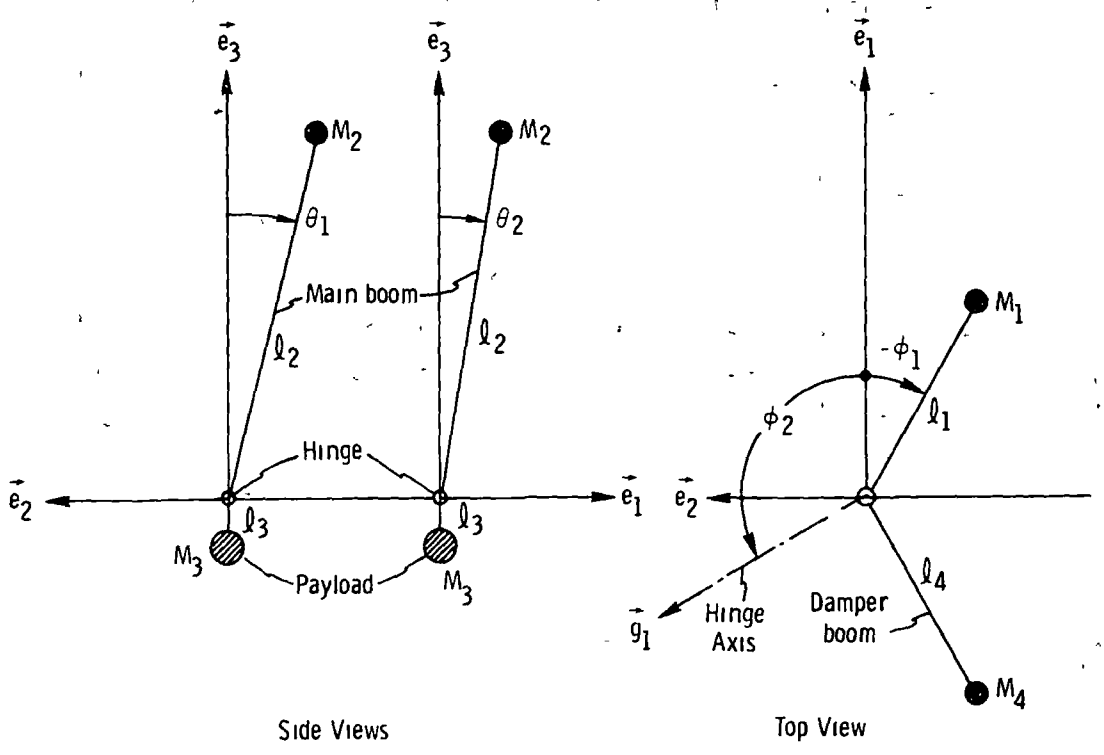

Figure 3 - Body frame and satellite orientation.

Here

$\vec{E}_3$ is a unit vector in the direction of the radius vector, $\vec{R}$, from the earth's center to the satellite's center of mass,

$\vec{E}_2$ is a unit vector parallel to $\vec{a}_3$, and

$$\vec{E}_1 = \vec{E}_2 \times \vec{E}_3.$$

The first two reference frames are related through the direction cosine matrix [B], leading to the orthogonal transformation

$$\begin{bmatrix} \vec{E}_1 \\ \vec{E}_2 \\ \vec{E}_3 \end{bmatrix} = \begin{bmatrix} B_{11} & B_{12} & B_{13} \\ B_{21} & B_{22} & B_{23} \\ B_{31} & B_{32} & B_{33} \end{bmatrix} \begin{bmatrix} \vec{a}_1 \\ \vec{a}_2 \\ \vec{a}_3 \end{bmatrix} \tag{1}$$

where

$$B_{11} = -B_{32} = -\sin\psi, \quad B_{23} = 1$$

$$B_{12} = B_{31} = \cos\psi, \quad B_{13} = B_{21} = B_{22} = B_{33} = 0$$

and ψ = true anomaly.

The third frame is a body frame,

$$[\vec{e}] = [\vec{e}_1\ \vec{e}_2\ \vec{e}_3]$$

that has its origin fixed in the satellite and is used in conjunction with the inertial frame and local vertical frame to define the satellite's motion. The nominal orientation of the undeformed NRL 164 satellite in terms of the unit vectors $\vec{e}_1$, $\vec{e}_2$ and $\vec{e}_3$ is depicted in Figure 3.

The rotational position of this body frame with respect to the local vertical frame is described through the orthogonal matrix transformation [S] such that

$$\begin{bmatrix} \vec{e}_1 \\ \vec{e}_2 \\ \vec{e}_3 \end{bmatrix} = \begin{bmatrix} S_{11} & S_{12} & S_{13} \\ S_{21} & S_{22} & S_{23} \\ S_{31} & S_{32} & S_{33} \end{bmatrix} \begin{bmatrix} \vec{E}_1 \\ \vec{E}_2 \\ \vec{E}_3 \end{bmatrix} \tag{2}$$

where S_{ij} are direction cosines. These direction cosines are derived in Appendix A in terms of the usual Euler angles β, α, and γ (designated as pitch, roll and yaw respectively).

Combining Equations 1 and 2 results in the relationship

$$\{\vec{e}\} = [S][B]\{\vec{a}\} = [A]^T\{\vec{a}\} \tag{3}$$

where $[A]^T$ is now the direction cosine matrix relating the body frame to the inertial frame.

Kinematic Equations

The kinematic equations in the present derivation consist of the set of direction cosine rate equations that relate the elements of matrix $[A]$ to the inertial angular velocity vector, $\vec{\omega}_0$, where, in the body frame,

$$\vec{\omega}_0 = \omega_1\vec{e}_1 + \omega_2\vec{e}_2 + \omega_3\vec{e}_3 \tag{4}$$

and ω_i are the body axis components of inertial rotation. For a system of moving axes (see Reference 13) the inertial derivatives of vector $\{\vec{e}\}$ are given by

$$\dot{\{\vec{e}\}} = -[\Omega_B]\{\vec{e}\} \tag{5}$$

where

$$[\Omega_B] = \begin{bmatrix} 0 & -\omega_3 & \omega_2 \\ \omega_3 & 0 & -\omega_1 \\ -\omega_2 & \omega_1 & 0 \end{bmatrix} \tag{6}$$

Since in inertial space $\{\dot{\vec{a}}\} \equiv 0$

the same inertial derivatives of vector $\{\vec{e}\}$ obtained from Equation (3) results in the expression

$$\{\dot{\vec{e}}\} = [\dot{A}]^T \{\vec{a}\} \tag{7}$$

Equations (3), (5) and (7) yield the identity condition that

$$[\dot{A}]^T = -[\Omega_B] [A]^T$$

which when transposed becomes

$$[\dot{A}] = [A] [\Omega_B]$$

When expanded this leads directly to the desired set of kinematic equations given by the six first order differential equations

$$\begin{aligned}
\dot{A}_{11} &= A_{12}\omega_3 - A_{13}\omega_2 \\
\dot{A}_{12} &= A_{11}\omega_3 + A_{13}\omega_1 \\
\dot{A}_{13} &= A_{11}\omega_2 - A_{12}\omega_1 \\
\dot{A}_{21} &= A_{22}\omega_3 - A_{23}\omega_2 \\
\dot{A}_{22} &= A_{21}\omega_3 + A_{23}\omega_1 \\
\dot{A}_{23} &= A_{21}\omega_2 - A_{22}\omega_1
\end{aligned} \tag{8}$$

Only six kinematic equations are necessary since the orthogonality of the direction cosine matrix [A] requires that

$$\begin{aligned}
A_{31} &= A_{12}A_{23} - A_{13}A_{22} \\
A_{32} &= A_{13}A_{21} - A_{11}A_{23} \\
A_{33} &= A_{11}A_{22} - A_{12}A_{21}
\end{aligned} \tag{9}$$

Dynamic Equations

The complete dynamic equations for NRL 164 are developed using the results of Reference 10. The vector dynamical equations with constraint torques can be written in the form

$$(\tilde{\Phi}_{00} + \tilde{\Phi}_{10}) \cdot \dot{\vec{\omega}}_0 + (\tilde{\Phi}_{01} + \tilde{\Phi}_{11}) \cdot (\dot{\vec{\omega}}_0 + \ddot{\delta}\vec{g}_1) = \vec{E}_0^* + \vec{E}_1^*$$

$$\vec{g}_1 \cdot [\tilde{\Phi}_{10} \cdot \dot{\vec{\omega}}_0 + \tilde{\Phi}_{11} \cdot (\dot{\vec{\omega}}_0 + \ddot{\delta}\vec{g}_1)] = \vec{g}_1 \cdot \vec{E}_1^* \tag{10}$$

Here a tilde over an element is used to identify a dyadic, and a dot over a vector denotes its time derivative with respect to inertial space.

$\tilde{\Phi}_{ij}$ = the set of reduced inertia dyadics derived in Appendix B,

δ = the angular rotation of the damper boom about its hinge axis,

$\vec{g}_1$ = the vector direction of the hinge axis (see Figure 3), and

$\vec{E}_1^*$ = the torque vector (gyroscopic torques, gravity gradient torques, hinge acceleration torques, interaction torques, etc.) as defined in Appendix B.

Written together in matrix notation Equation (10) becomes

$$\begin{bmatrix} \tilde{a}_{00} & \vec{a}_{01} \\ \vec{a}_{10} & a_{11} \end{bmatrix} \begin{bmatrix} \dot{\vec{\omega}}_0 \\ \ddot{\delta} \end{bmatrix} = \begin{bmatrix} \vec{E}_0^* + \vec{E}_1^* \\ \vec{g}_1 \cdot \vec{E}_1^* \end{bmatrix} \tag{11}$$

where $\tilde{a}_{00}$ is the dyadic

$$\tilde{a}_{00} = \tilde{\Phi}_{00} + \tilde{\Phi}_{10} + \tilde{\Phi}_{01} + \tilde{\Phi}_{11} \tag{12}$$

$\vec{a}_{01}$ and $\vec{a}_{10}$ are the vectors

$$\vec{a}_{01} = (\tilde{\Phi}_{01} + \tilde{\Phi}_{11}) \cdot \vec{g}_1 \tag{13}$$

$$\vec{a}_{10} = \vec{g}_1 \cdot (\tilde{\Phi}_{10} + \tilde{\Phi}_{11}) \tag{14}$$

and a_{11} is the scalar

$$a_{11} = \vec{g}_1 \cdot \tilde{\Phi}_{11} \cdot \vec{g}_1 \tag{15}$$

Introducing the new dependent variable, Δ, such that

$$\dot{\delta} = \Delta \tag{16}$$

permits the vector dynamical relationship of Equation (11) to be expanded into the scalar form

$$\begin{bmatrix} & & & \\ & I_{00} & & \\ & & & \end{bmatrix} \begin{bmatrix} \dot{\omega}_1 \\ \dot{\omega}_2 \\ \dot{\omega}_3 \\ \dot{\Delta} \end{bmatrix} = \begin{bmatrix} T_1 \\ T_2 \\ T_3 \\ T_4 \end{bmatrix} \tag{17}$$

At this point Equation (17) is premultiplied by $[I_{00}]^{-1}$ so that, along with Equation (16), the final complete set of dynamic equations is given by the five first-order differential equations

$$\begin{bmatrix} \dot{\omega}_1 \\ \dot{\omega}_2 \\ \dot{\omega}_3 \\ \dot{\Delta} \end{bmatrix} = \begin{bmatrix} & & & \\ & I_{00} & & \\ & & & \end{bmatrix}^{-1} \begin{bmatrix} T_1 \\ T_2 \\ T_3 \\ T_4 \end{bmatrix} \tag{18}$$

$$\dot{\delta} = \Delta$$

Orbital Mechanics

The orbital path of the satellite is derived directly from the solution of Kepler's equation based on a spherical earth model. This solution is carried out under the assumption that perigee occurs at $t = 0$ at which time the orbit path crosses the inertial $\vec{a}_1$ axis. Referring to Figure 2 the complete

formulation of the decoupled Keplerian orbit is given by the first order differential equation

$$\dot{\psi} = \frac{\Omega_0}{(1-\epsilon^2)^{3/2}} (1 + \epsilon \cos \psi)^2 \tag{19}$$

where

$$\Omega_0 = \left(\frac{\mu}{a^3}\right)^{\frac{1}{2}} = \text{mean orbital rate}$$

a = semi-major axis

ϵ = orbital eccentricity

μ = gravitational constant

ψ = true anomaly

The magnitude of the radius vector, $\vec{R}$, is determined from

$$|\vec{R}| = \frac{a(1-\epsilon^2)}{1 + \epsilon \cos\psi} \tag{20}$$

and it therefore follows that

$$\begin{aligned} R_x &= |\vec{R}| \cos \psi \\ R_y &= |\vec{R}| \sin \psi \end{aligned} \tag{21}$$

Thermal Deformation

Thermal deformation of each of the satellite's three booms is presumed to be due solely to a thermal bending moment induced by solar heating. The resulting deformation alters the position of each boom's tip weight and, in accordance with the quasi-static approach, changes the satellites inertial properties. As the inertial properties vary, a new set of principal axes appear, and reorientation of the satellite occurs.

Deflection of a typical long, slender boom exposed to solar heating is illustrated in Figure 4. The undeformed boom lies along the unit vector axis, $\vec{U}$, with the sun's unit vector, $\vec{\sigma}$, tilted so that it makes an angle ξ with the boom. The thermal bending moment induced by solar heating is considered to cause a tip deflection

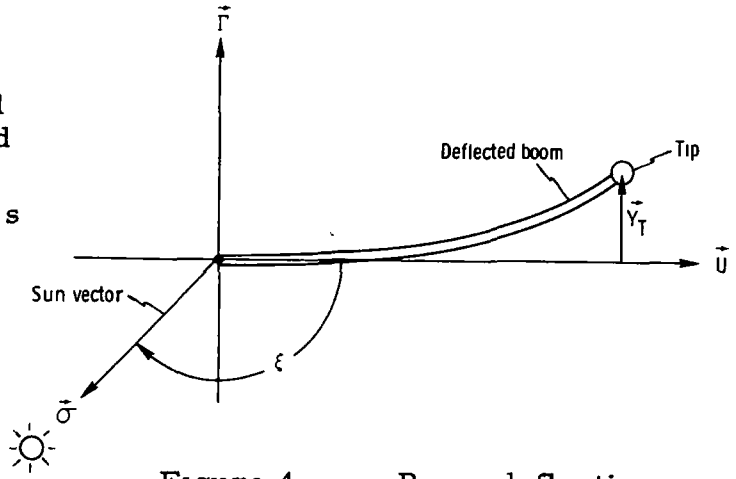

Figure 4 - Boom deflection.

$$\vec{Y}_T = y_T \vec{\Gamma} \qquad (22)$$

whose direction $\vec{\Gamma}$, is normal to $\vec{U}$ in a plane containing the sun's vector. The magnitude of the tip deflection, y_T, in turn, is a function of the boom's thermal properties as well as the position of the satellite with respect to the earth's shadow.

Let the unit sun vector, $\vec{\sigma}$, be defined such that

$$\vec{\sigma} = \sin\alpha\, \vec{a}_1 + \cos\alpha\, \vec{a}_3 \qquad (23)$$

where α = sun angle. Since the direction of the unit tip deflection vector, $\vec{\Gamma}$, is assumed to always be away from the sun it can be derived from the vector triple product relationship

$$\vec{\Gamma} = \frac{(\vec{\sigma} \times \vec{U}) \times \vec{U}}{|(\vec{\sigma} \times \vec{U}) \times \vec{U}|} \qquad (24)$$

Similarly the sun angle on the boom, ξ, is obtained from the equation

$$\cos\xi = \vec{U} \cdot \vec{\sigma} \qquad (25)$$

where, in view of the restrictions of Equation (24)

$$0 \leq \xi \leq \pi$$

The tip deflection, y_T, for each boom is computed from the first-order differential equation

$$\dot{y}_T + \frac{1}{\tau} y_T = \frac{1}{\tau} y_{T0} \tag{26}$$

where τ = thermal lag and y_{T0} is the static thermal tip deflection of the boom.

The static deflection, y_{T0}, is assumed to be the tip deflection that the boom would attain if thermal lag were ignored. The computation of y_{T0} is based in part on the analysis described in Reference 14.

For a seamless, thin-walled cantilevered boom of circular cross section it has been found that y_{T0} can be approximated by the equation

$$y_{T0} = \frac{A_T \ell^2}{2} \sin \xi \left[1 + \frac{A_T \ell \cos \xi}{3} \right] \tag{27}$$

where ℓ = boom length, ft, and A_T is the thermal constant

$$A_T = \frac{\alpha_0 e D J_s}{4hk} \tag{28}$$

whose elements are

α_0 = absorptivity

D = boom diameter, in.

e = linear thermal coefficient of expansion, in./in.-^oF

h = thickness, in.

J_s = solar radiation intensity, Btu/hr-ft^2

k = thermal conductivity, Btu/hr-ft-^oF

On the other hand if the satellite is in the earth's shadow, solar radiation can be ignored and

$$y_{T0} = 0 \tag{29}$$

The sun model used for finding out whether the satellite is either in full sunlight or in the earth's shadow is described in Appendix C.

The three tip deflection vectors $\vec{Y}_{TM}$, $\vec{Y}_{TS}$, and $\vec{Y}_{TD}$ for the main boom, side boom and damper boom respectively are determined from the relationships of Equations (22) to (29). It should be noted that the imposition of Equation (26) requires the solution of three first-order differential equations.

Computed changes in the magnitudes and directions of the three tip deflections are used to rederive the reduced inertia dyadics $\tilde{\Phi}_{ij}$ (see Appendix B) and subsequently to alter the inertia matrix $[I_{00}]$ in Equation (17).

Computer Program

The equations of motion describing the quasi-static response of NRL 164 to solar radiation are fully represented by Equations (8), (18), (19) and (26). The 15 first-order nonlinear differential equations of motion and associated supplementary equations have been programmed for digital solution on an IBM 360 computer. The resulting FORTRAN IV program, entitled GGSAT, is described in Appendix D. GGSAT consists of a main program and a series of subroutines designed to solve the equations of motion.

A solution is obtained using Hammings predictor-corrector method, with starting values determined by a Runge-Kutta procedure. A plotting routine, compatible with a CalComp 210/665 plotter, permits the user to generate plots of calculated variations of satellite yaw, pitch and roll as a function of time.

RESULTS AND DISCUSSION

The essential aspects of the results presented here cover a selective investigation of the effect of boom thermal bending on the stability of the quasi-static model of NRL 164 in a circular orbit ($\epsilon = 0$). Particular emphasis has been placed on the influence of absorptivity, sun angle, thermal lag and hinge stiffness on the satellites responses in yaw, pitch and roll.

The nominal physical and thermal properties of the satellite as well as its orbital characteristics are summarized in Table 1. The booms were considered to be long, slender beryllium copper tubes with highly reflective, silver-plated outer surfaces. For the sake of simplicity the mass of the booms was ignored.

Stability Criteria

The linear stability of NRL 164 in the absence of solar heating can be inferred from the roots of the linearized equations of motion given in Reference 5. The roots are either real or occur in complex pairs with each imaginary pair corresponding to one frequency of the satellite's normal modes of oscillation. Despite the strong coupling between the degrees of freedom representing yaw, pitch, roll and damper boom motion, each frequency still represents a predominant modal motion in one of these four degrees of freedom. In Figure 5 the computed frequencies (obtained from the imaginary part of each root) along with the predominant modal motion at that frequency are plotted for a variation in damper spring constant. Here all other properties are consistent with Table 1. For $K_D > .0008$ ft-lb/rad the roots are all complex with negative real parts so that four stable frequencies exist. As K_D becomes large the frequencies approach those of a configuration with a locked damper hinge. At the design K_D, two of the roots are simply negative real. The complex roots all have negative real parts so that the three remaining frequencies are still stable. For $K_D < .00064$ ft-lb/rad, however, one of the real roots becomes positive, and roll, pitch and yaw motions diverge exponentially. For reference purposes, this divergence boundary delineates the theoretical region within which linear stability of NRL 164 cannot be attained.

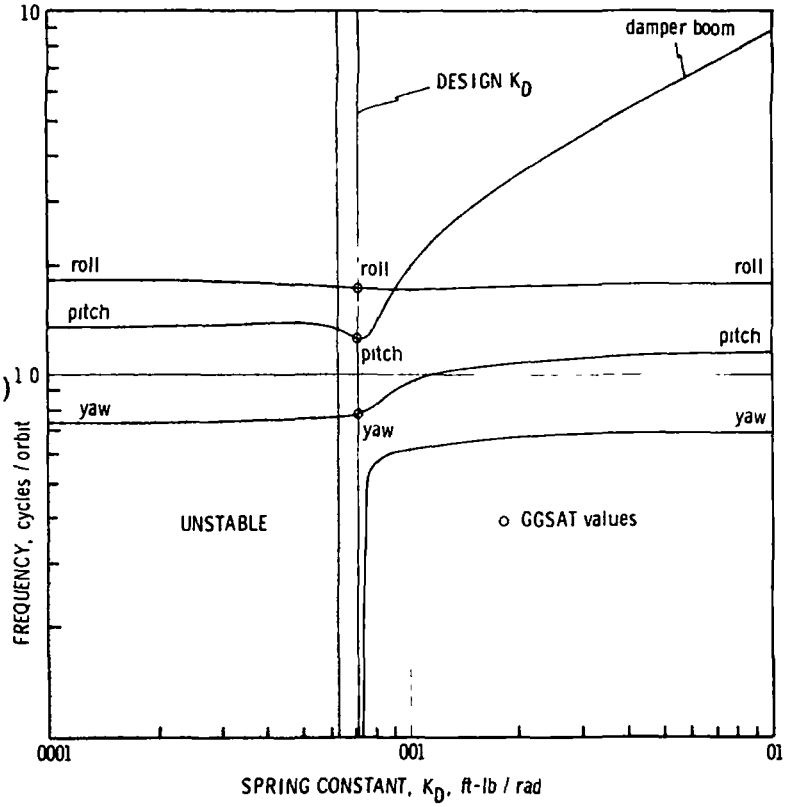

Figure 5 - Linearized frequency variation.

The nonlinear stability of NRL 164 exposed to solar radiation has been deduced through a time domain solution of the quasi-static equations of motion. Although the selected variations in parameters were quite broad, it was evident early in the study that nonlinearities in the simulation and economic limitations on computer usage required a narrow definition of stability.

The stability criteria eventually adopted assumed that the satellite was unstable if, after the model was initially perturbed by a set of "prime conditions" in yaw, pitch and roll, a yaw inversion occurred within the

TABLE 1

PHYSICAL PROPERTIES AND ORBITAL PARAMETERS
OF NRL GRAVITY GRADIENT SATELLITE 164

Lateral and damper boom tip mass, slugs	0.118
Main boom tip mass, slugs	0.159
Payload mass, slugs	8.800
Lateral and damper boom length, ft	35.0
Main boom length, ft	60.0
Distance from payload C.G. to hinge, ft	1.375
Lateral and damper boom diameter, in	0.25
Main boom diameter, in	0.50
Lateral and damper boom wall thickness, in	0.14×10^{-2}
Main boom wall thickness, in	0.20×10^{-2}
Payload moment of inertia, slug-ft^2	4.0
Yaw rotation of lateral boom, deg	-30.0
Yaw rotation of hinge axis, deg	120.0
Roll rotation of main boom, deg	0.0
Pitch rotation of main boom, deg	0.0
Null position of damper boom, deg	0.0
Damper spring constant, ft-lb/rad	0.714×10^{-3}
Damper damping constant, ft-lb-sec/rad	0.395
Eccentricity	0.0
Semi-major axis, km	7302.4
Earth radius, km	6378.2
Gravitational constant, km^3/sec^2	3.986×10^5
Mean orbital rate, rad/sec	0.1012×10^{-2}
Initial true anomaly, deg	0.0
Sun angle, deg	0.0
Absorptivity	0.13
Linear, thermal coefficient of expansion, in/in-$^\circ$F	0.104×10^{-4}
Thermal conductivity, Btu/hr-in-$^\circ$F	4.167
Heat radiation of source, Btu/hr-in^2	3.065
Thermal lag, min	0.0
Initial roll angle, deg	-10.0
Initial pitch angle, deg	-30.0
Initial yaw angle, deg	30.0

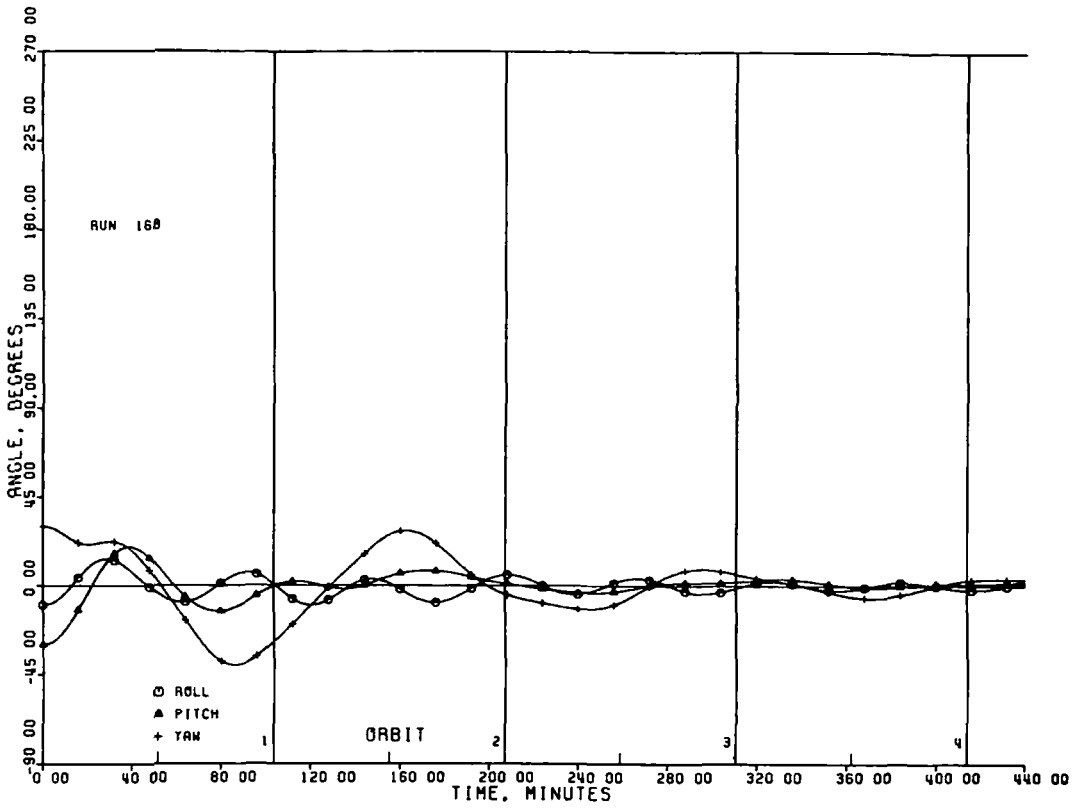

Figure 6 - Nominal satellite response, no sun.

first four orbits of the earth. These prime conditions (established somewhat arbitrarily by trial and error) were $\gamma = 30^{\circ}$, $\beta = -30^{\circ}$, $\alpha = -10^{\circ}$ and $\dot{\gamma} = \dot{\beta} = \dot{\alpha} = 0$.

Although this definition provided a way of evaluating the effect on stability of a parametric change it was strictly limited by its singular specification of initial prime conditions and the number of orbits examined. Despite these limitations, the criteria still led to some particularly revealing observations.

Basic Characteristics

The motions of NRL 164 in the absence of sunlight and initially perturbed by the prime conditions are plotted in Figure 6. This figure serves as an instructive indicator of the basic nonlinear dynamic behavior of the nominal configuration and should be used in gaging the changes in response that are brought about by a parameter variation. As expected in this case, the satellite is very stable. Although yaw motions are initially quite large they damp out rapidly and the system is close to an equilibrium attitude soon after the fourth orbit.

Since the study is particularly concerned with yaw instabilities, some insight into large amplitude yaw responses without sunlight is needed in order to evaluate basic system performance. Two such responses are plotted in Figure 7 for an initial yaw perturbation of 30°. The difference

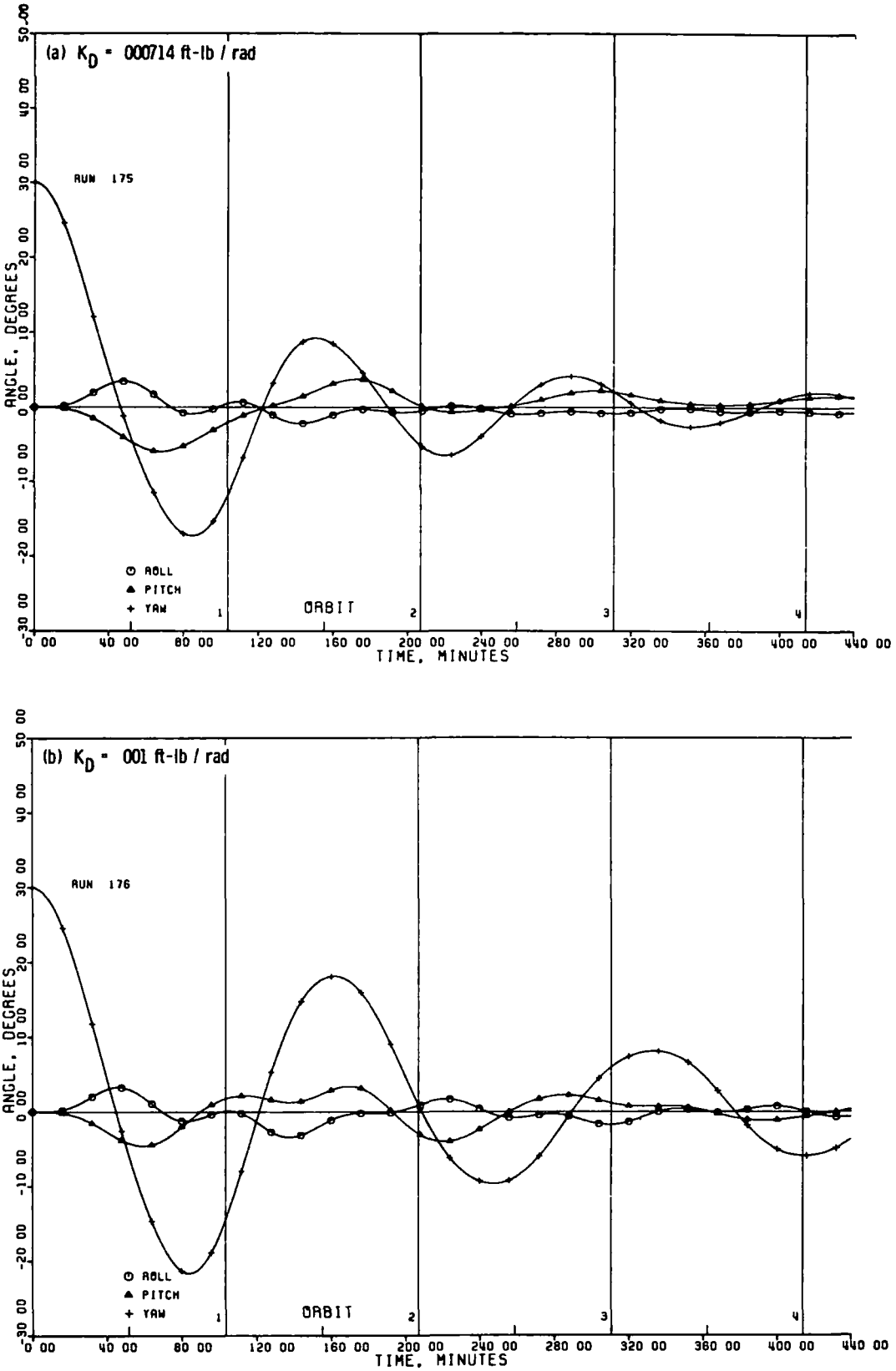

Figure 7 - Basic yaw frequency, no sun.

between the two responses arises simply from the change in the damper spring constant. As can be seen, yaw damping and frequency decrease as the damper spring is stiffened above its nominal value (the drop in frequency is also apparent in Figure 5). The appearance of both pitch and roll coupling with a yaw perturbation is a basic characteristic of this type of gravity gradient configuration and is necessary in order to achieve three-axis damping of the entire satellite.

Frequencies associated with the nonlinear response were, as expected, amplitude dependent. For a small initial perturbation, however, the nonlinear influence on frequency was negligible, and the quasi-static frequencies agreed closely with the linear analysis (see Figure 5).

Effect of Absorptivity

The present thermal instability supposition rests on the assumption that thermally induced changes in the satellite's inertial properties due to boom bending may cause a yaw instability. To examine this possibility, satellite responses were computed for variations in tip deflections brought about by a change in absorptivity. Figure 8 shows the linear variation of the main boom's static tip deflection with increasing absorptivity for normal sun incidence.

Since the outer surfaces of the booms were assumed to be highly reflective, a low absorptivity, $\alpha_0 = 0.13$, was specified as the nominal value. On the other hand, as indicated in Reference 15, data accumulated by GSFC suggests that factors other than absorptivity tend to influence thermal bending, and large deflections may occur in spite of a low value of absorptivity. To compensate for these factors, an effective absorptivity of 0.5 was considered to represent the high end of the deflection scale.

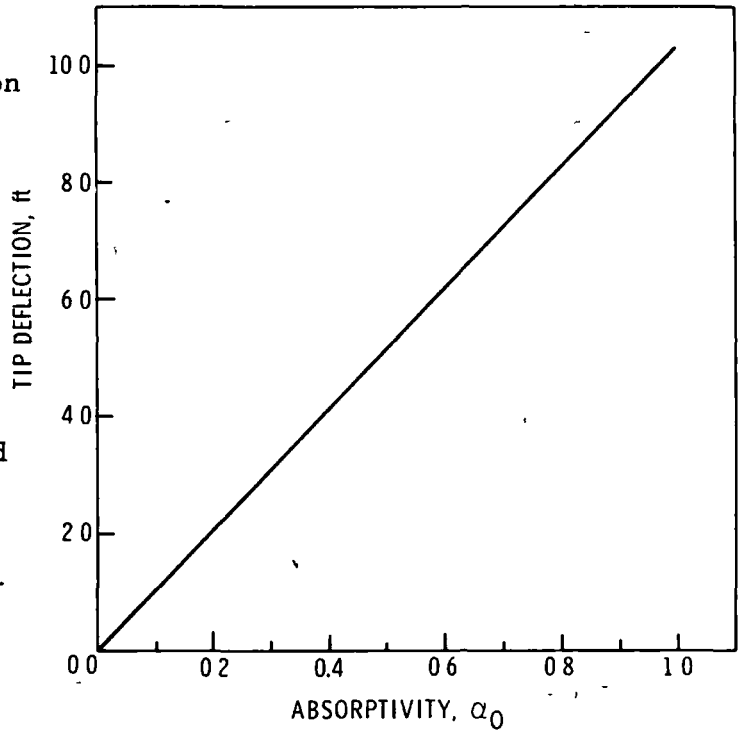

Figure 8 - Main boom tip deflection for normal sun incidence.

The computed influence of absorptivity on the attitude motion of NRL 164 is illustrated in Figure 9. For these responses, the sun is normal to the orbital plane (sun angle at 0^{o}), and thermal lag is zero. The plots reveal the existence of a yaw instability that is particularly sensitive to thermal distortion. For $\alpha_0 = 0.3$ and 0.4, the calculated yaw attitude, though large, seems to be stable. Conversely for $\alpha_0 = 0.45$ and 0.6, a yaw inversion occurs prior to the second orbit, and the configuration is considered to be unstable. The onset of an inversion appears to be closely dependent upon yaw reaching an angle of -90^{o}.

Effect of Sun Angle

The investigation of absorptivity led directly to the observation that the satellite's computed response and stability could be strongly influenced by a small change in sun angle. This was previously noted in the flight data of Reference 7 and now tends to be confirmed by the present quasi-static analysis.

The sensitivity to a change in sun angle is typified by the computer plots shown in Figure 10, which depict the yaw, pitch and roll motions of NRL 164 for sun angles of 0^{o}, 10^{o}, 20^{o} and 30^{o}. Here thermal lag is zero, and the magnitude of boom thermal absorptivity is 0.5, a value which for the 60 ft. main boom and normal sun incidence results in a computed static tip deflection of approximately 5 ft. (see Figure 8).

In Figure 10(a), with the sun angle at 0^{o}, a yaw inversion starts almost immediately and, as previously seen in Figure 9, the satellite response is unstable. In Figure 10(b), however, by just shifting the sun angle to 10^{o} the inversion is suppressed and the motion is surprisingly stable. In fact, in Figure 10(c), a further increase in the sun angle to 20^{o} still leads to a stable configuration. Finally, in Figure 10(d), at a sun angle of 30^{o}, occultations* begin to occur, and the satellite is again unstable. The latter instability is probably involved with the deflection transient that arises as the satellite enters the earth's shadow.

Effect of Thermal Lag

Figure 11 shows the effect on stability of a change in thermal lag with the sun angle at 0^{o} and $\alpha_0 = 0.5$. Previously, with no thermal lag, (Figure 10(a)) this condition was unstable. For the time span shown in Figure 11, the inclusion of thermal lag appears to have a stabilizing tendency.

---

*Occultations are indicated by the downward facing steps in the horizontal line across the top of Figure 10(d).

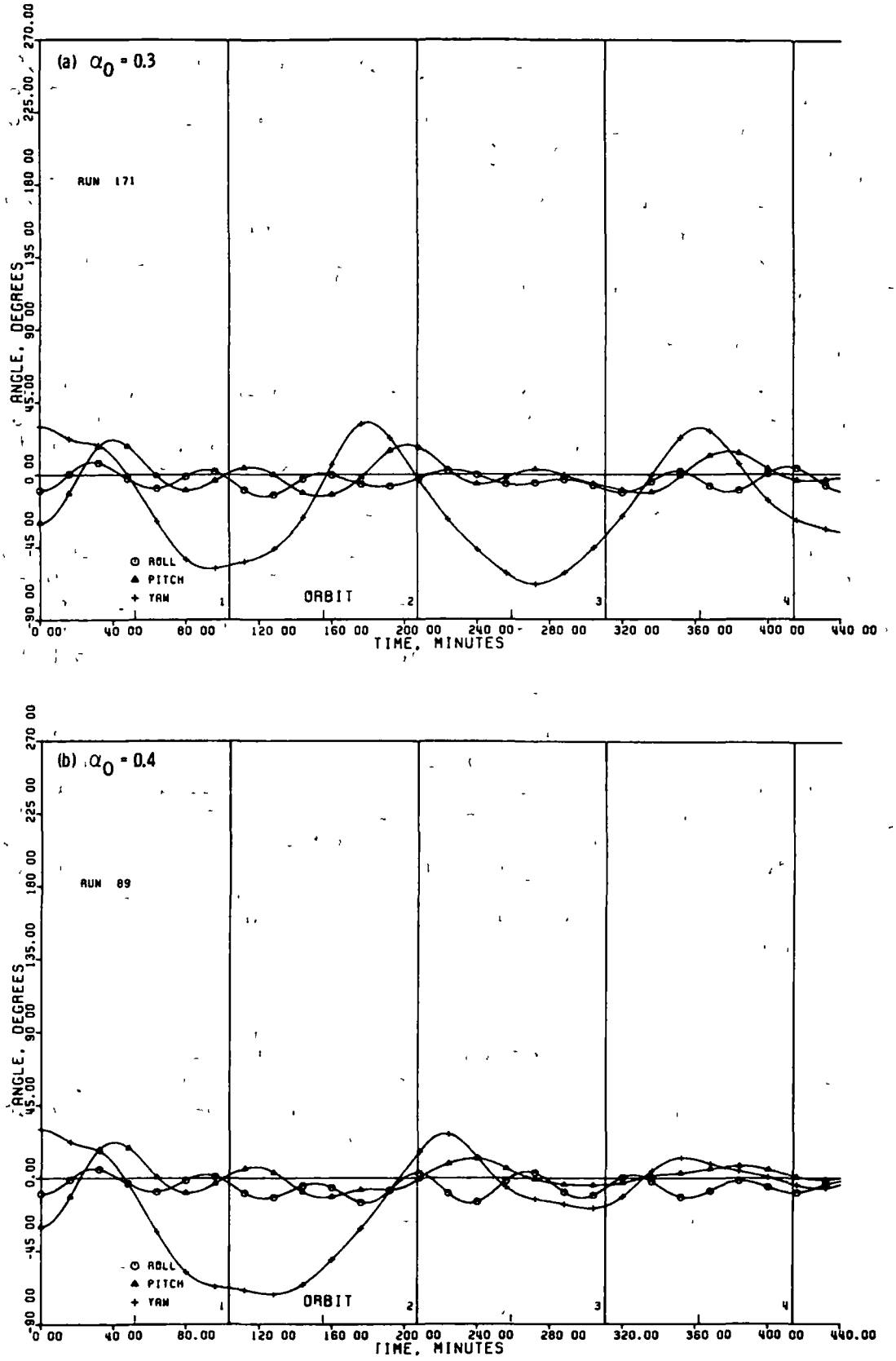

Figure 9 - Effect of absorptivity, K_D = .000714 ft-lb/rad, $\alpha = 0^o$.

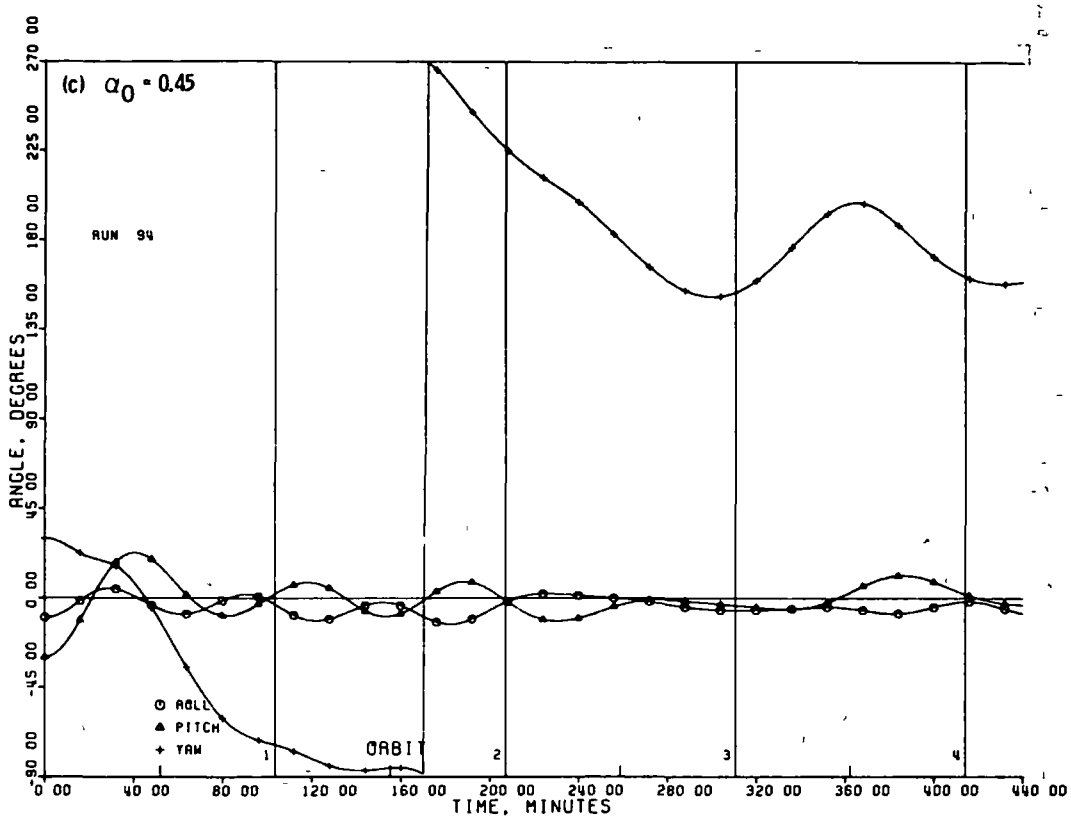

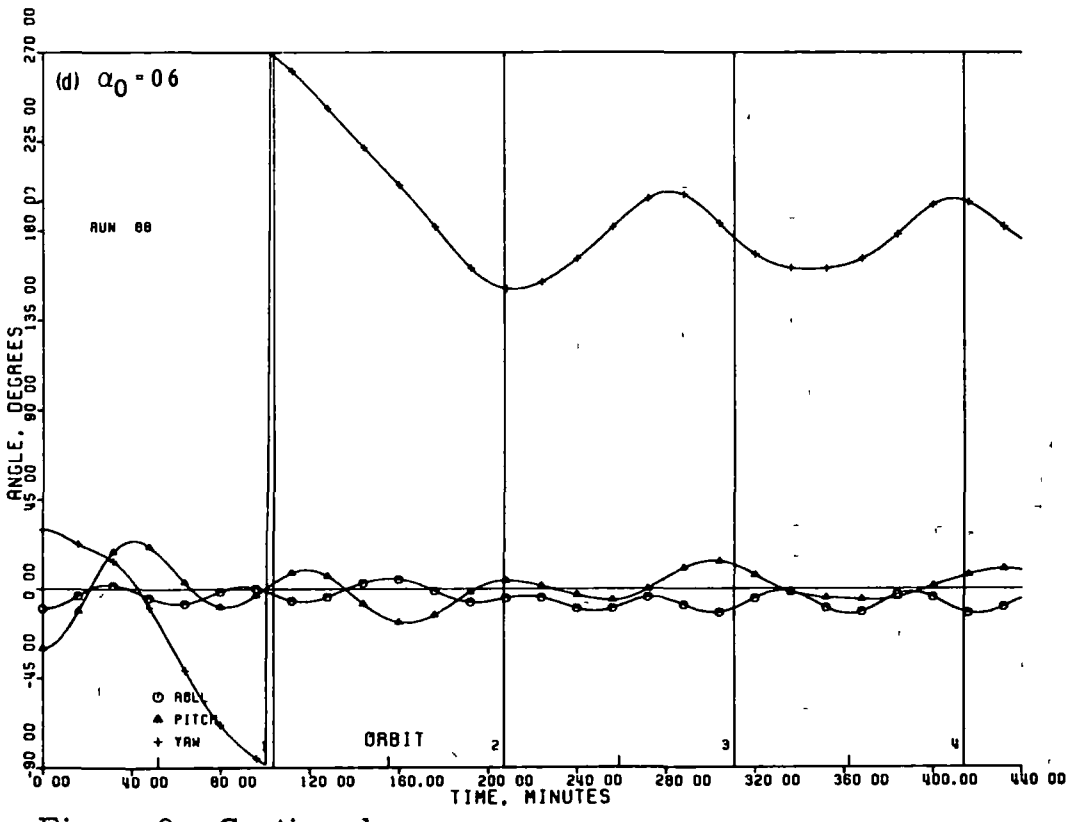

Figure 9 - Continued

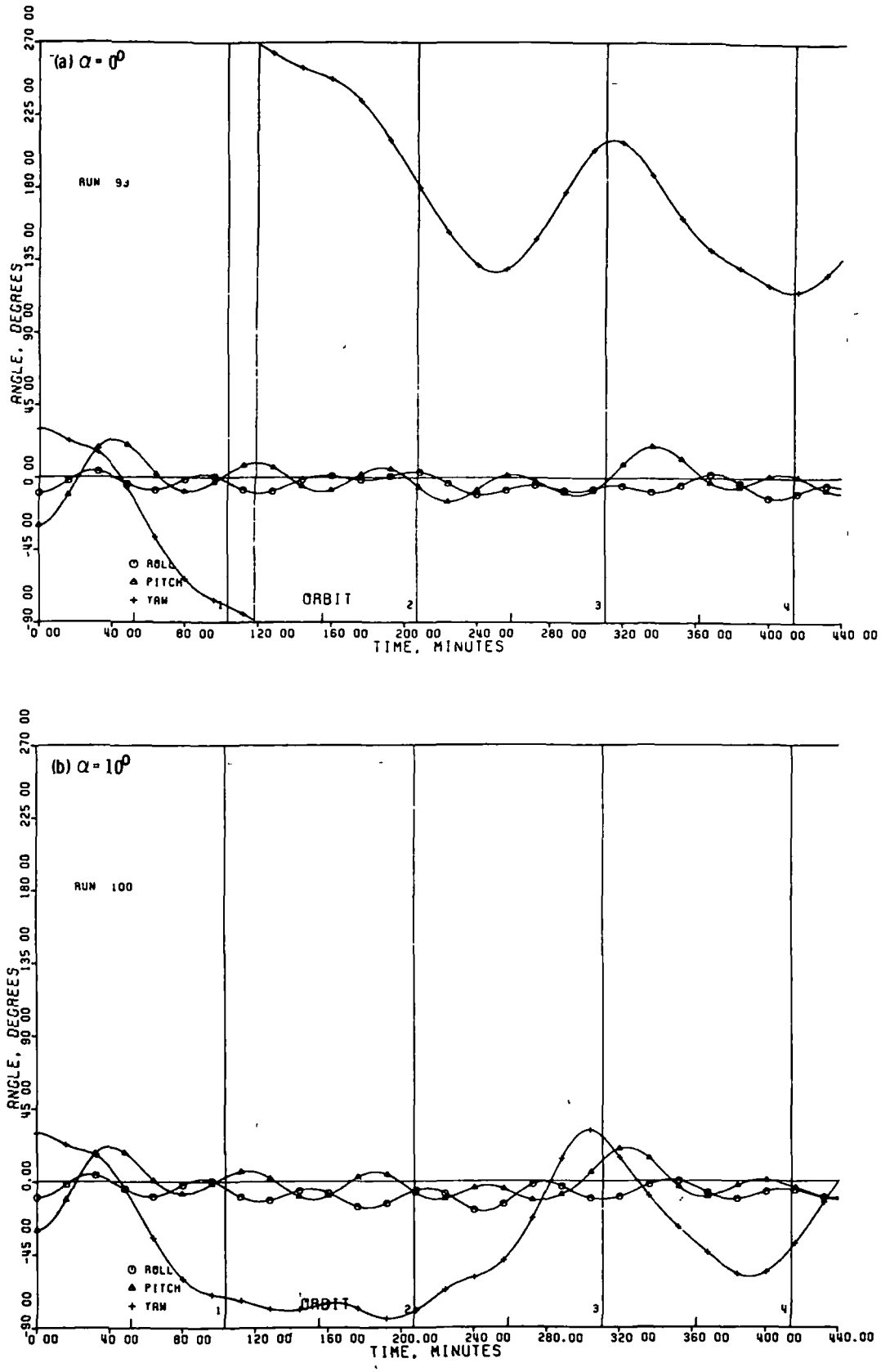

Figure 10 - Effect of sun angle, K_D = .000714 ft-lb/rad, α_0 = 0.5.

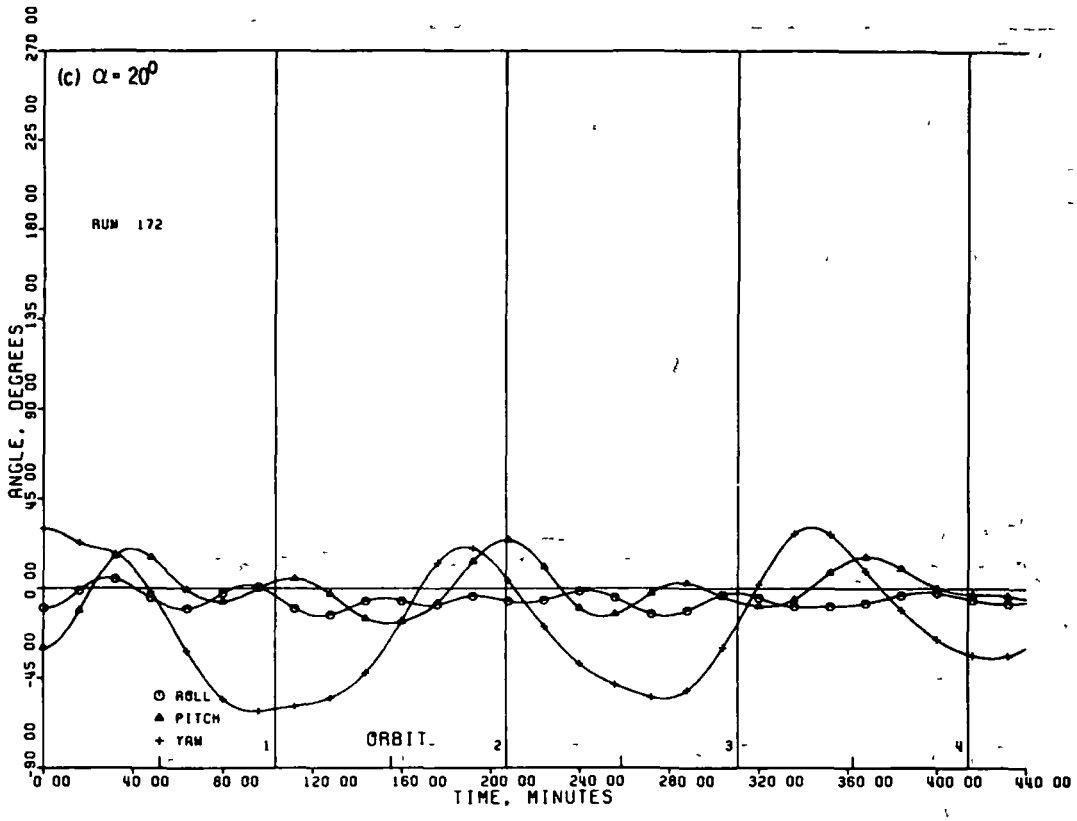

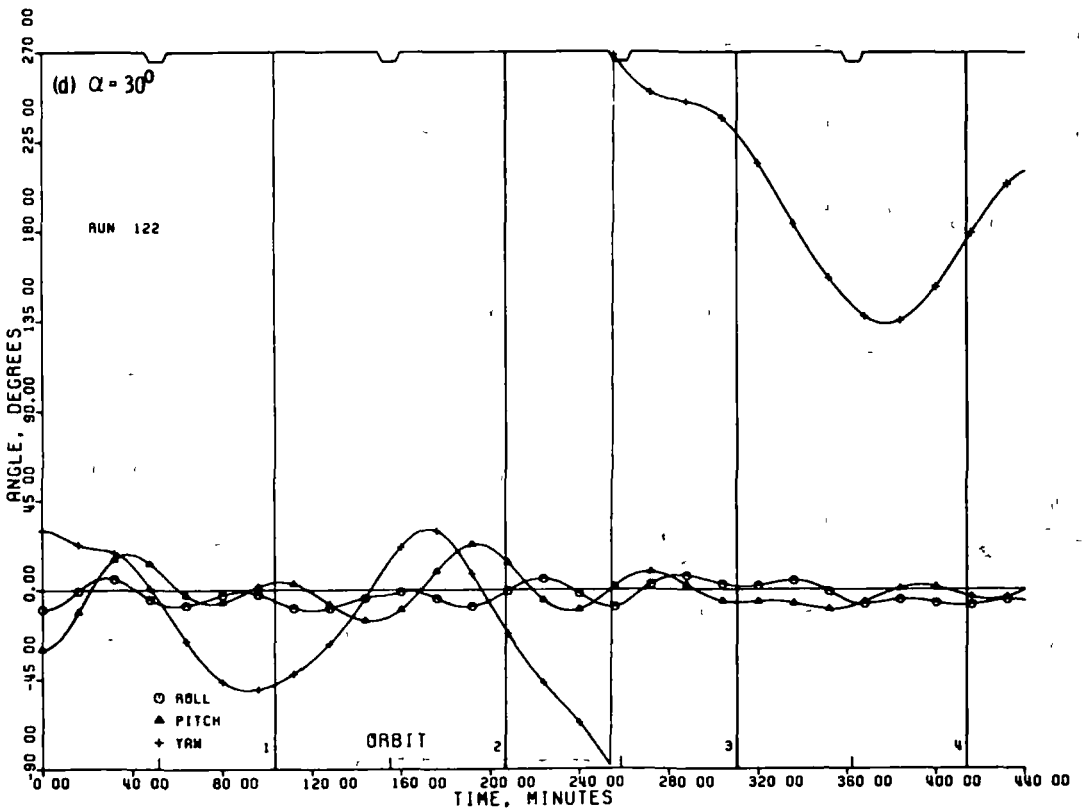

Figure 10 - Continued

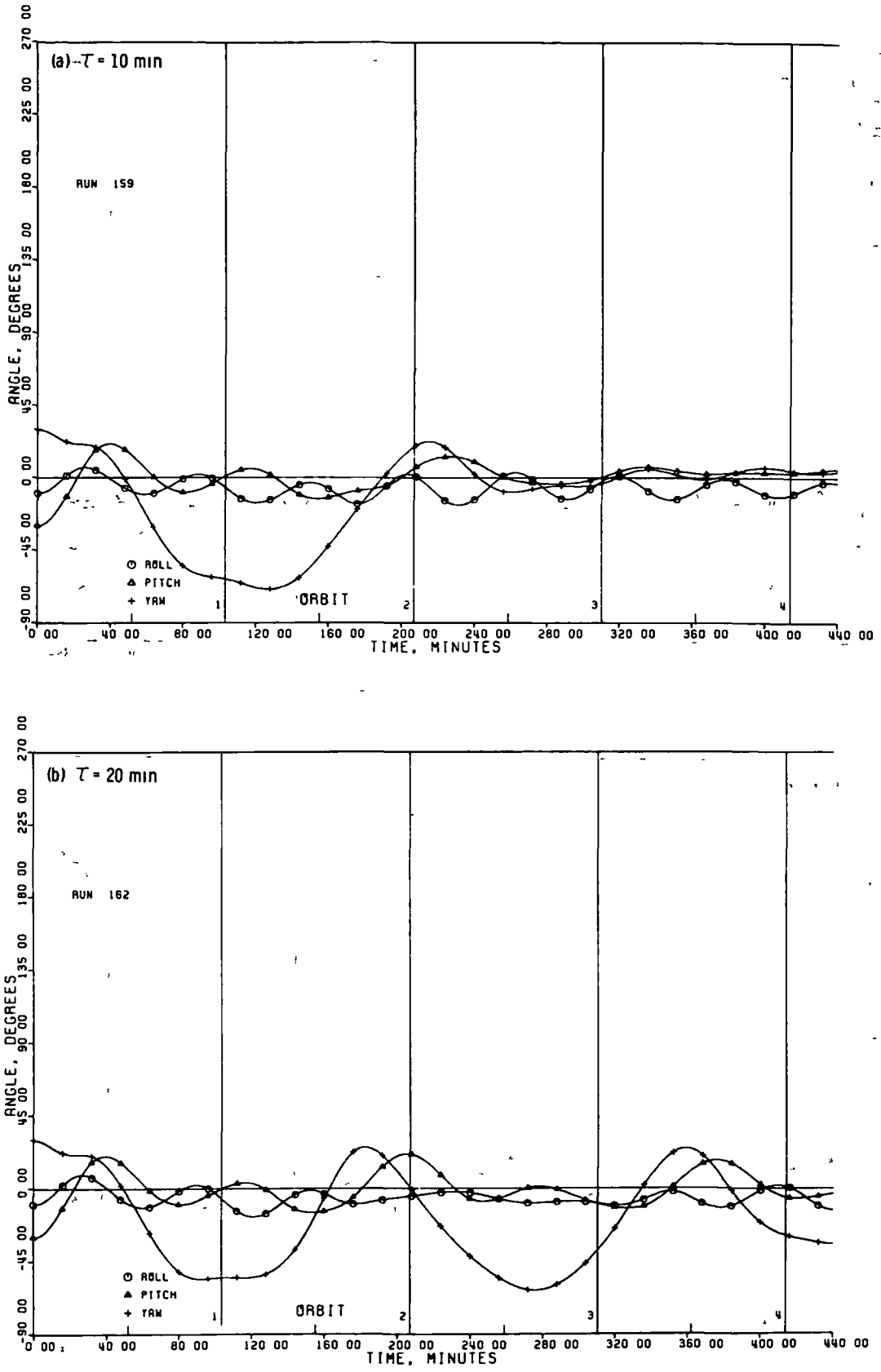

Figure 11 - Effect of thermal lag, K_D = .000714 ft-lb/rad, $\alpha = 0^\circ$. α_0 = 0.5.

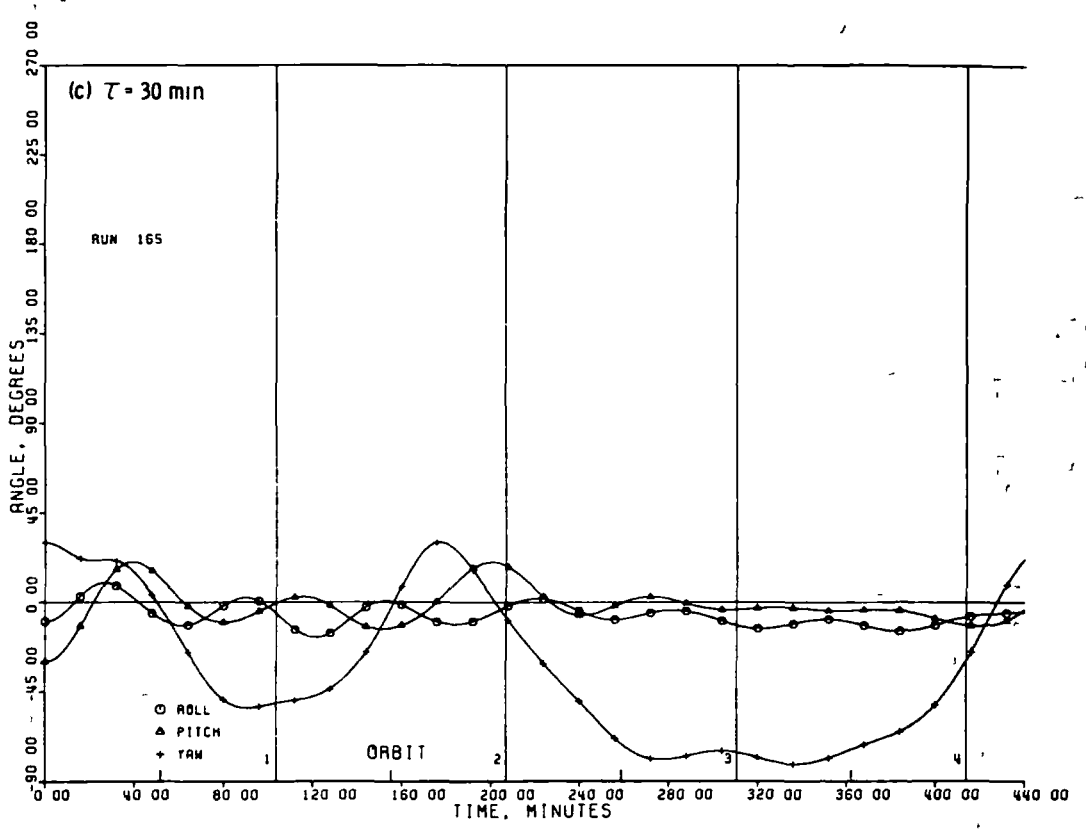

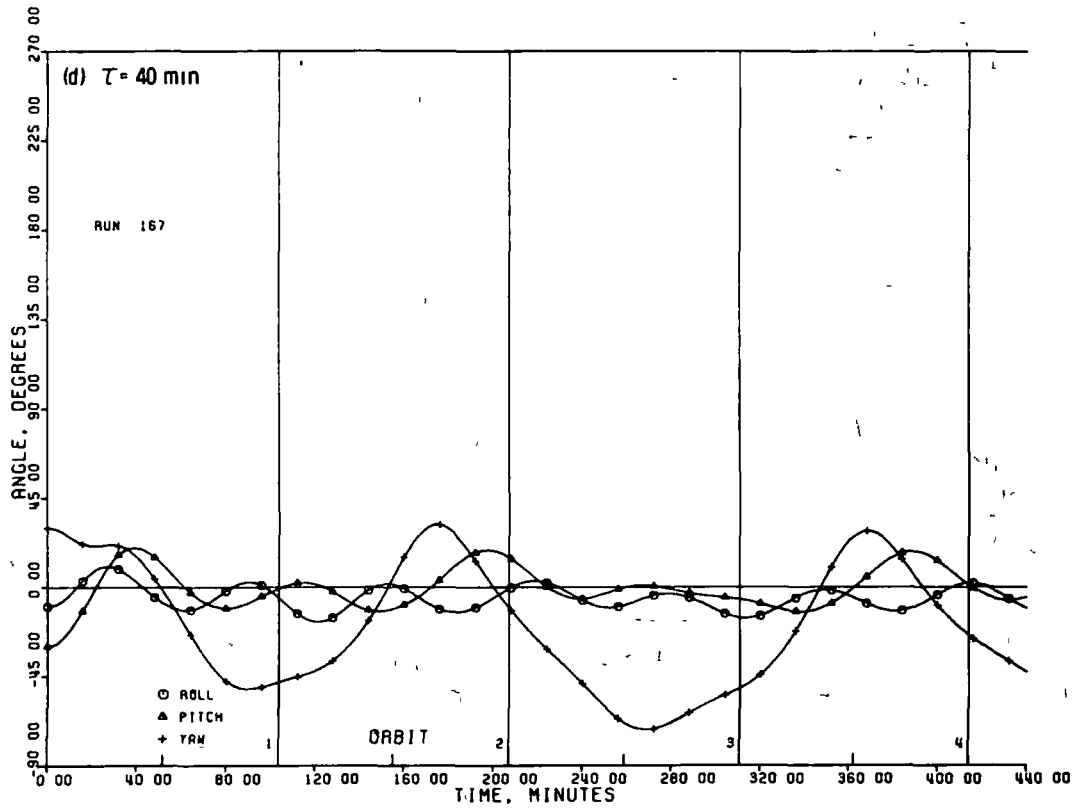

Figure 11 - Continued

Despite this observation, it is not at all clear whether or not certain critical combinations of thermal lag, absorptivity, sun angle and damper spring constant may still result in an instability. In this respect it should be noted that, in Figure 11, as thermal lag is increased from 10 min to 30 min, the magnitude of the second peak in yaw increases substantially. A further increase in thermal lag to 40 min, Figure 11(d), however, has the opposite effect, and the yaw amplitude begins to decrease.

Effect of Hinge Stiffness

The comparison of most of the computed results with flight data is in itself quite remarkable. As in flight, the controlling factor in establishing NRL 164's stability boundary appears to be most closely allied with sun angle. Hinge stiffness, however, also plays an important role in the results.

Some indication of the sensitivity of the computed response to a change in hinge stiffness is shown in the plots of Figure 12. Here the sun angle is 0° and $\alpha_0 = 0.4$. For the nominal hinge stiffness ($K_D = .000714$ ft -lb/rad) the yaw response is stable. By just increasing the stiffness about 10%, so that K_D is equal to .0008 ft -lb/rad, the yaw response becomes unstable.

Figures 13, 14 and 15 illustrate how the computed quasi-static stability boundaries for sun angles of 0°, 10° and 30° were influenced by variations in hinge stiffness (damper spring constant) K_D, and absorptivity, α_0. The illustrations essentially summarize the outputs from a large number of computer runs.

In these figures, the divergence region arises solely from the consideration that, in the absence of sunlight, the system becomes unstable for $K_D < .00064$ ft-lb/rad. Conversely the unstable regions that are shown in the figures encompass areas of yaw instabilities that were deduced by applying the nonlinear stability criteria.

In Figures 13 and 14 the stability boundary is not only favorably influenced by a low value of hinge stiffness, but the stable region increases in area as the sun angle changes from 0° to 10°. For a sun angle of 30°, Figure 15, the satellite passes through the earth's shadow, and the stability picture becomes quite confusing. Now the unstable regions are isolated into two pockets that restrict the onset of an instability to only certain limited combinations of absorptivity and hinge stiffness.

In obtaining Figures 13 to 15 a number of especially interesting cases were found in which the satellite responded in a yaw spin. A

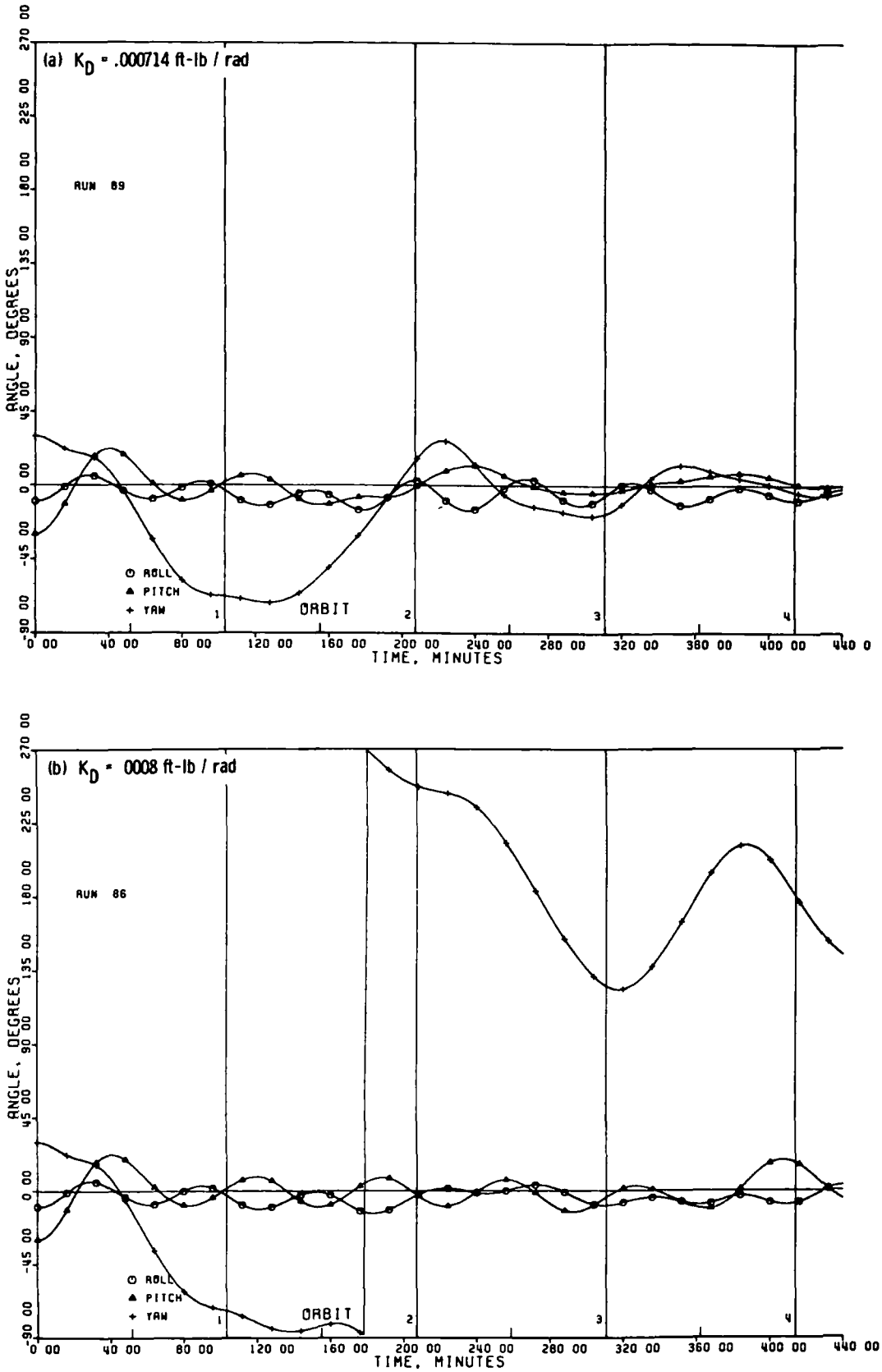

Figure 12 - Effect of hinge stiffness, $\alpha = 0^{\circ}$, $\alpha_0 = 0.4$.

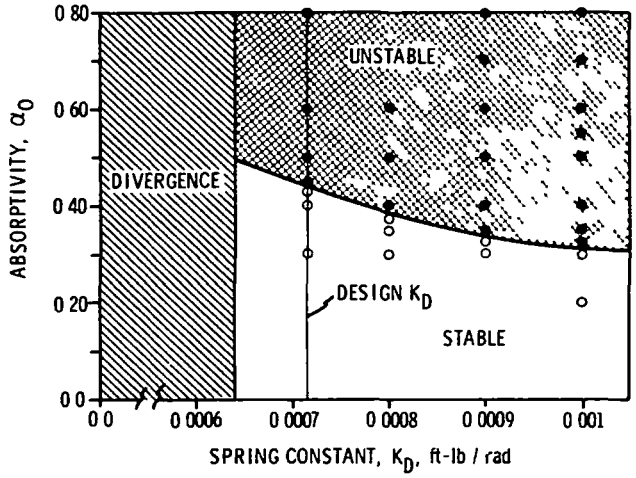

Figure 13 - Stability boundary, $\alpha = 0^{\circ}$.

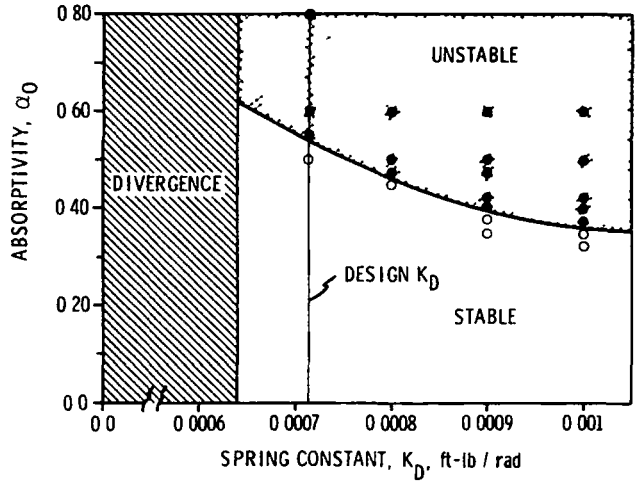

Figure 14 - Stability boundary, $\alpha = 10^{\circ}$.

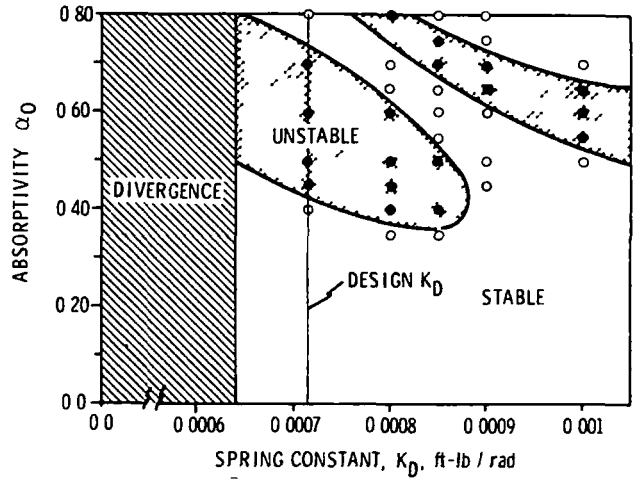

Figure 15 - Stability boundary, $\alpha = 30^{\circ}$.

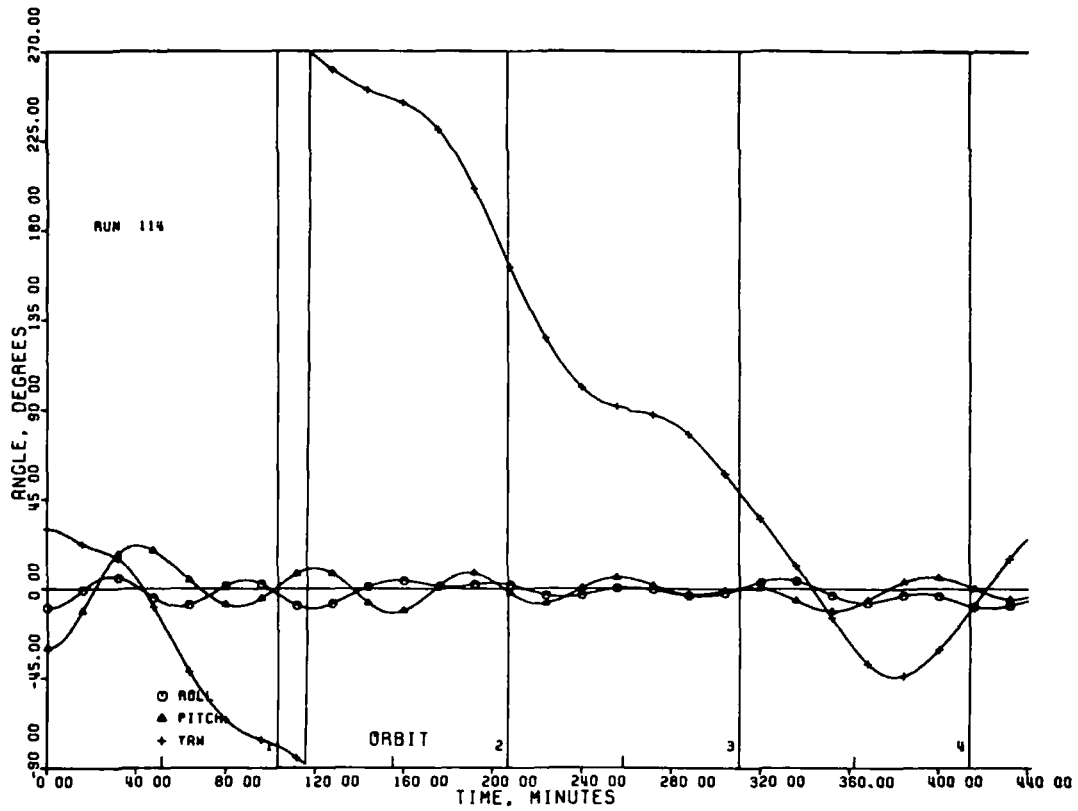

Figure 16 - Yaw spin, K_D = .001 ft-lb/rad, $\alpha = 10^\circ$, $\alpha_0 = 0.425$.

typical occurrence is illustrated in Figure 16, in which the computed response in yaw rotates through 360° in about three orbits. Similar phenomena also were seen in the flight data of NRL 164 and conceivably were caused by parameter combinations of the type studied in the present investigation.

CONCLUSIONS

A nonlinear analytical model and a corresponding computer program have been developed to study the possible influence of solar heating on the anomalous low-frequency, orbital yaw instability of the Naval Research Laboratory's gravity gradient satellite 164 in a circular orbit. The model's formulation was based on a quasi-static approach in which the deflections of the satellite's long, slender booms were determined in

terms of thermally induced bending without consideration of the dynamic effects of boom vibration.

Within the confines of relatively narrow stability criteria, it has been found that, under the quasi-static model, NRL 164 not only becomes unstable but, in a number of cases, responses were computed that closely resembled flight data.

From a review of the results, it has been discovered that:

1. The onset of a yaw instability is particularly sensitive to a small change in sun angle, with the least favorable sun angle at 0°.

2. In order to obtain an adverse effect from thermal distortion, it was necessary to assume a larger thermal deflection than might be inferred from a boom's nominal thermal properties. Some evidence is available, however, to justify this assumption.

3. Occultation of the satellite produces isolated regions of instabilities believed to be related to the abrupt changes in boom deflections that occur as the satellite enters or leaves the earth's shadow.

4. In most cases, an increase in hinge stiffness tends to be destabilizing, while an increase in thermal lag seems to be stabilizing.

By comparing the data collected during the computer study, it has been concluded that the quasi-static approach provides a valid means of predicting the anomalous behavior of NRL 164. In retrospect, the analysis probably could have been used to anticipate the instability seen in the flight data of NRL 164.

RECOMMENDATIONS

If three-axis gravity gradient stabilization of a satellite through the use of long, slender booms is to be considered in future spacecraft designs, adequate consideration must be given to the influence of thermal distortion on system performance. Assuming that such satellites are still of practical consequence, it is important that the designer have available a means of selecting configurations that are free from the thermally induced instabilities.

Since the present investigation has been limited to NRL 164 in a circular orbit, it is difficult to reach any definitive conclusion as to either an optimum configuration or the influence of eccentricity on stability. A general interrelationship between analysis and design selection is therefore necessary before further development of three-axis stabilization systems can be adequately considered. In this respect, the formulation of

a quasi-static model of sufficient generality is recommended as the analytic tool for selecting and evaluating the nonlinear dynamics of a hinged multibody satellite.

Closely related to this suggestion is the need to obtain a much better physical understanding of the behavior of a boom exposed to solar heating. A review is needed of existing GSFC experimental data with a view toward ascertaining the thermal bending process of a boom. This advice includes the possibility of additional experiments aimed at determining the effect of sun angle on the boom and end conditions on actual thermal deflection.

ACKNOWLEDGMENT

The author wishes to acknowledge the contributions made by S. H. Yamamura during the course of this work. In particular, he is indebted to Ms. Yamamura for the many productive suggestions she provided throughout the development and implementation of the computer program.

REFERENCES

1. DeBra, D. B., "The Large Attitude Motions and Stability, Due to Gravity, of a Satellite with Passive Damping in an Orbit of Arbitrary Eccentricity about an Oblate Body," Ph. D. Dissertation, Stanford Univ., SUDAER No. 162, 1962.

2. Fletcher, H. J., Rongved, L., and Yu, E. Y., "Dynamics Analysis of a Two-Body Gravitationally Oriented Satellite," Bell System Tech. J., Sept. 1963, pp. 2239-2266.

3. Raymond, F. W., "Gravity Gradient Torques on Artificial Satellites," Astro. Acta, vol. 12, no. 1, 1966, pp. 33-38.

4. Hartbaum, H., Hooker, W., Leliakov, I., and Margulies, G., "Configuration Selection for Passive Gravity Gradient Satellites," Symposium on Passive Gravity Gradient Stabilization, NASA SP-107, May 1965.

5. Barba, P.M., and Marx, S. H., "An Integrated 3-Axis Gravity Gradient Stabilization System," Symposium on Gravity Gradient Attitude Control, Aerospace Corp., El Segundo, Calif., December 1968.

6. Anon., "Design and Performance of an Integrated, Hysteresis Damped, Gravity Stabilized Satellite," TR-DA 2091, Space and Re-Entry Systems Div., Philco-Ford Corp., July 1969.

7. Goldman, R. L., "Examination of the Anomalous Behavior of Three Gravity Gradient Satellites," TR-71-07c, RIAS, Martin Marietta Corp., Mar. 1971. (This reference is reproduced in its entirety as Appendix E.)

8. Goldman, R. L., "Influence of Thermal Distortion on the Anomalous Behavior of a Gravity Gradient Satellite," TR-72-11c, RIAS, Martin Marietta Corporation, May 1972.

9. Anon., "User's Manual for IMP Dynamics Computer Program-Volume I," AVSD-0191-71-CR, AVCO Systems Div., AVCO Corp., Mar. 1971.

10. Hooker, W.W., "A Set of r Dynamical Attitude Equations for an Arbitrary n-Body Satellite having r Rotational Degrees of Freedom," AIAA J., vol. 8, no. 7, July 1970, pp. 1204-1207.

11. Kanning, G., "The Influence of Thermal Distortion on the Performance of Gravity Stabilized Satellites," NASA TN D-5435, Nov. 1969.

12. Tinling, B.E., and Merrick, V.K., "Exploitation of Inertial Coupling in Passive Gravity Gradient Stabilized Satellites," J. Spacecraft and Rockets, vol. 1, no. 4, July-Aug. 1964, pp. 381-387.

13. Constant, F. W., "Theoretical Physics," Addison-Wesley Pub. Co., Inc., 1954.

14. Fixler, S. Z., "Effects of Solar Environment and Aerodynamic Drag on Structural Booms in Space," J. Spacecraft and Rockets, vol. 4, no. 3, Mar. 1967, pp. 315-321.

15. Herzl, G. G., Walker, W.W., and Ferrera, J. D., "Tubular Spacecraft Booms (Extendible, Reel Stored)," NASA SP-8065, Feb. 1971.

APPENDIX A
BODY ROTATIONS

An Euler rotational sequence of pitch, roll and yaw has been selected in order to define the orientation of the body frame, $\{\vec{e}\}$, relative to the local vertical frame, $\{\vec{E}\}$. The three rotational transformations* are:

1. Pitch rotation

$$\begin{bmatrix} \vec{x} \\ \vec{y} \\ \vec{z} \end{bmatrix} = \begin{bmatrix} c\beta & 0 & -s\beta \\ 0 & 1 & 0 \\ s\beta & 0 & c\beta \end{bmatrix} \begin{bmatrix} \vec{E}_1 \\ \vec{E}_2 \\ \vec{E}_3 \end{bmatrix}$$

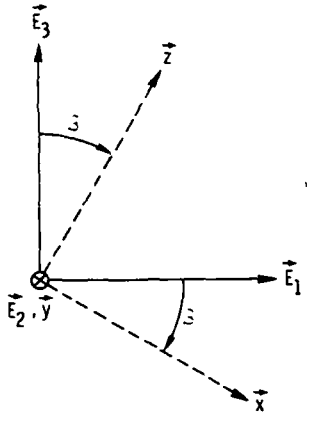

2. Roll rotation

$$\begin{bmatrix} \vec{X} \\ \vec{Y} \\ \vec{Z} \end{bmatrix} = \begin{bmatrix} 1 & 0 & 0 \\ 0 & c\alpha & s\alpha \\ 0 & -s\alpha & c\alpha \end{bmatrix} \begin{bmatrix} \vec{x} \\ \vec{y} \\ \vec{z} \end{bmatrix}$$

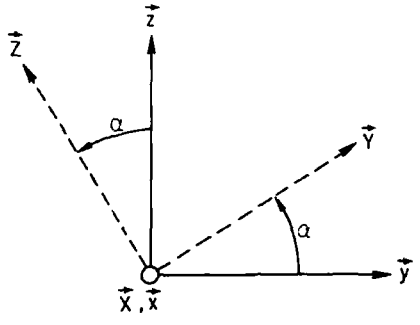

*Here c = cos, s = sin

3. Yaw rotation

$$\begin{bmatrix} \vec{e}_1 \\ \vec{e}_2 \\ \vec{e}_3 \end{bmatrix} = \begin{bmatrix} c\gamma & s\gamma & 0 \\ -s\gamma & c\gamma & 0 \\ 0 & 0 & 1 \end{bmatrix} \begin{bmatrix} \vec{X} \\ \vec{Y} \\ \vec{Z} \end{bmatrix}$$

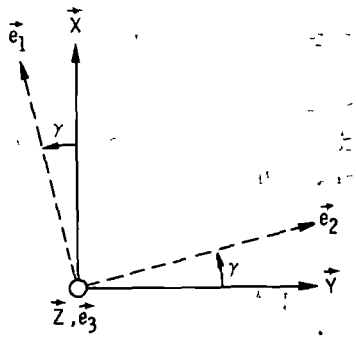

The total transformation is given by the matrix product

$$\begin{bmatrix} \vec{e}_1 \\ \vec{e}_2 \\ \vec{e}_3 \end{bmatrix} = \begin{bmatrix} c\gamma & s\gamma & 0 \\ -s\gamma & c\gamma & 0 \\ 0 & 0 & 1 \end{bmatrix} \begin{bmatrix} 1 & 0 & 0 \\ 0 & c\alpha & s\alpha \\ 0 & -s\alpha & c\alpha \end{bmatrix} \begin{bmatrix} c\beta & 0 & -s\beta \\ 0 & 1 & 0 \\ s\beta & 0 & c\beta \end{bmatrix} \begin{bmatrix} \vec{E}_1 \\ \vec{E}_2 \\ \vec{E}_3 \end{bmatrix}$$

$$= \begin{bmatrix} c\beta c\gamma + s\alpha s\beta s\gamma & c\alpha s\gamma & -s\beta c\gamma + s\alpha c\beta s\gamma \\ -c\beta s\gamma + s\alpha s\beta c\gamma & c\alpha c\gamma & s\beta s\gamma + s\alpha c\beta c\gamma \\ c\alpha s\beta & -s\alpha & c\alpha c\beta \end{bmatrix} \begin{bmatrix} \vec{E}_1 \\ \vec{E}_2 \\ \vec{E}_3 \end{bmatrix}$$

$$= \begin{bmatrix} S_{11} & S_{12} & S_{13} \\ S_{21} & S_{22} & S_{23} \\ S_{31} & S_{32} & S_{33} \end{bmatrix} \begin{bmatrix} \vec{E}_1 \\ \vec{E}_2 \\ \vec{E}_3 \end{bmatrix} \qquad \text{(A1)}$$

where S_{ij} are now the desired direction cosines that provide the relationship between the body frame and the local vertical frame.

In a similar manner, the angular velocity vector, $\vec{\omega}_0$, can be expressed in terms of the Euler angles and orbital motion by the matrix relationship

$$\begin{bmatrix} \omega_1 \\ \omega_2 \\ \omega_3 \end{bmatrix} = \begin{bmatrix} S_{12} & c\gamma & 0 \\ S_{22} & -s\gamma & 0 \\ S_{32} & 0 & 1 \end{bmatrix} \begin{bmatrix} \dot{\beta} \\ \dot{\alpha} \\ \dot{\gamma} \end{bmatrix} + \dot{\psi} \begin{bmatrix} S_{12} \\ S_{22} \\ S_{32} \end{bmatrix} \quad \text{(A2)}$$

APPENDIX B

INERTIA DYADICS AND TORQUE ELEMENTS

Derivation of the elements of Equation (10) and (11) in the section on Dynamic Equations has been carried out in numerous references and is quite straightforward.

The inertia dyadics are obtained from the geometrical and inertial properties of the satellite through the equations

$$
\begin{aligned}
\tilde{\Phi}_{00} &= \tilde{\Phi}_0 + \bar{m}\,\{\vec{L}_{01}\cdot\vec{L}_{01}\,\tilde{1} - \vec{L}_{01}\,\vec{L}_{01}\} \\
\tilde{\Phi}_{10} &= -\bar{m}\,\{\vec{L}_{01}\cdot\vec{L}_{11}\,\tilde{1} - \vec{L}_{01}\,\vec{L}_{11}\} \\
\tilde{\Phi}_{01} &= -\bar{m}\,\{\vec{L}_{11}\cdot\vec{L}_{01}\,\tilde{1} - \vec{L}_{11}\,\vec{L}_{01}\} \\
\tilde{\Phi}_{11} &= \bar{m}\,\{\vec{L}_{11}\cdot\vec{L}_{11}\,\tilde{1} - \vec{L}_{11}\,\vec{L}_{11}\}
\end{aligned}
\qquad \text{(B1)}
$$

where

$\tilde{\Phi}_0$ = inertia dyadic of main body about its center of mass

$\bar{m}$ = reduced mass, $M_0 M_4 / M$

M_0 = mass of main body, $M_1 + M_2 + M_3$

M_1 = mass of lateral boom tip mass

M_2 = mass of main boom tip mass

M_3 = mass of payload

M_4 = mass of damper boom tip mass

M = mass of satellite, $M_0 + M_4$

$\vec{L}_{01}$ = vector from center of mass of main body to hinge point

$\vec{L}_{11}$ = vector from center of mass of damper boom to hinge point

$\tilde{1}$ = unit dyadic, $\vec{e}_1\vec{e}_1 + \vec{e}_2\vec{e}_2 + \vec{e}_3\vec{e}_3$

To illustrate the mechanics of deriving the elements of Equation (B1), consider Figure B-1, which shows the main body and hinge of NRL 164 with the booms deformed due to solar heating.

The hinge vector, $\vec{L}_{01}$ is given by the equation

$$\vec{L}_{01} = -\frac{(M_1\vec{P}_1 + M_2\vec{P}_2 + M_3\vec{P}_3)}{M_0} \qquad (B2)$$

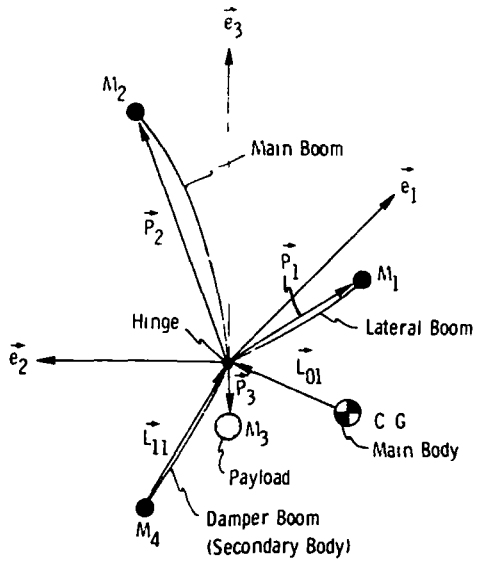

Figure B-1 Geometry of deformed satellite.

where

$\vec{P}_1$ = vector from hinge to deflected lateral boom tip mass

$\vec{P}_2$ = vector from hinge to deflected main boom tip mass

$\vec{P}_3$ = vector from hinge to payload center of mass

Let

$$\vec{R}_1 = \vec{P}_1 + \vec{L}_{01}$$

$$\vec{R}_2 = \vec{P}_2 + \vec{L}_{01}$$

$$\vec{R}_3 = \vec{P}_3 + \vec{L}_{01}$$

Then the inertia dyadic $\tilde{\Phi}_0$ for the main body can be written as

$$\tilde{\Phi}_0 = \sum_{i=1}^{3} M_i \left(|\vec{R}_i|^2 \tilde{1} - \vec{R}_i \vec{R}_i \right) + \tilde{\Phi}_3 \qquad \text{(B3)}$$

where

$\tilde{\Phi}_3$ = the local inertia dyadic of the payload about its own center of mass

The critical element in the quasi-static approach is the inclusion of the vector displacements $\vec{Y}_{TM}$, $\vec{Y}_{TS}$ and $\vec{Y}_{TD}$ of each boom due to thermal distortion in the determination of the vectors $\vec{P}_1$, $\vec{P}_2$ and $\vec{L}_{11}$. In terms of the nominal characteristics of NRL 164 (see Figure 3), the deformed position vectors are given by the equations

$$\begin{aligned}
\vec{P}_1 &= \ell_1 \cos\phi_1 \vec{e}_1 + \ell_1 \sin\phi_1 \vec{e}_2 + \vec{Y}_{TS} \\
\vec{P}_2 &= \ell_2 \sin\theta_2 \vec{e}_1 - \ell_2 \sin\theta_1 \cos\theta_2 \vec{e}_2 + \ell_2 \cos\theta_1 \cos\theta_2 \vec{e}_3 + \vec{Y}_{TM} \qquad \text{(B4)} \\
\vec{P}_3 &= -\ell_3 \vec{e}_3 \\
\vec{L}_{11} &= \ell_4 \sin\phi_2 \cos\delta \vec{e}_1 - \ell_4 \cos\phi_2 \cos\delta \vec{e}_2 - \ell_4 \sin\delta \vec{e}_3 - \vec{Y}_{TD}
\end{aligned}$$

The torque elements on the right of Equation (11) have been derived in Reference 10 and for the present case can be expanded into the following expressions:

$$\begin{aligned}
\vec{E}_0^* + \vec{E}_1^* &= 3G[\vec{\rho} \times (\tilde{\Phi}_{00} + \tilde{\Phi}_{11}) \cdot \vec{\rho}] - \dot{\delta}^2 [\vec{g}_1 \times \tilde{\Phi}_{11} \cdot \vec{g}_1] - \vec{\omega}_0 \times (\tilde{\Phi}_{00} + \tilde{\Phi}_{11}) \cdot \vec{\omega}_0 \\
&+ \bar{m} \vec{L}_{01} \times [\vec{\omega}_0 \times (\vec{\omega}_0 \times \vec{L}_{11})] - \dot{\delta} [\vec{\omega}_0 \times \tilde{\Phi}_{00} \cdot \vec{g}_1 + \vec{g}_1 \times \tilde{\Phi}_{11} \cdot \vec{\omega}_0] \\
&+ \dot{\delta} \bar{m} \vec{L}_{01} \times [\vec{\omega}_0 \times (\vec{g}_1 \times \vec{L}_{11}) + \vec{g}_1 \times (\vec{\omega}_0 \times \vec{L}_{11})] \qquad \text{(B5)} \\
&+ \dot{\delta}^2 \bar{m} \vec{L}_{01} \times [\vec{g}_1 \times (\vec{g}_1 \times \vec{L}_{11})]
\end{aligned}$$

$$+ \quad G\bar{m}[\vec{L}_{01} \times (\tilde{1} - 3\vec{\rho}\vec{\rho}) \cdot \vec{L}_{11} + \vec{L}_{11} \times (\tilde{1} - 3\vec{\rho}\vec{\rho}) \cdot \vec{L}_{01}]$$

$$- \quad \dot{\delta}[(\tilde{\Phi}_{01} + \tilde{\Phi}_{11}) \cdot \dot{\vec{g}}_1 + \vec{\omega}_0 \times \tilde{\Phi}_{11} \cdot \vec{g}_1 + \vec{g}_1 \times \tilde{\Phi}_{11} \cdot \vec{\omega}_0] \qquad \text{(B5-Cont.)}$$

$$\vec{g}_1 \cdot \vec{E}_1^* = 3G\vec{g}_1 \cdot [\vec{\rho} \times \tilde{\Phi}_{11} \cdot \vec{\rho}] - \vec{g}_1 \cdot [\vec{\omega}_0 \times \tilde{\Phi}_{11} \cdot \vec{\omega}_0]$$

$$- \quad \dot{\delta}\vec{g}_1 \cdot [\tilde{\Phi}_{11} \cdot \dot{\vec{g}}_1 + \vec{\omega}_0 \times \tilde{\Phi}_{11} \cdot \vec{g}_1 + \vec{g}_1 \times \tilde{\Phi}_{11} \cdot \vec{\omega}_0]$$

$$- \quad \dot{\delta}^2 \vec{g}_1 \cdot [\vec{g}_1 \times \tilde{\Phi}_{11} \cdot \vec{g}_1] + \bar{m}\vec{g}_1 \cdot \left[\vec{L}_{11} \times [\vec{\omega}_0 \times (\vec{\omega}_0 \times \vec{L}_{01})]\right] \qquad \text{(B6)}$$

$$+ \quad G\bar{m}\vec{g}_1 \cdot [\vec{L}_{11} \times (\tilde{1} - 3\vec{\rho}\vec{\rho}) \cdot \vec{L}_{01}]$$

$$- \quad C_D \dot{\delta} - K_D \dot{\delta}$$

where $\vec{\rho}$ = unit vector from the earth's center toward the satellites composite center of mass

$$G = \frac{\Omega_0^2}{(1-\epsilon^2)^3} (1 + \epsilon \cos \psi)^3$$

C_D = hinge damper damping constant

K_D = hinge damper spring constant

in terms of the prescribed reference frames:

$$\vec{\rho} = \cos\psi \vec{a}_1 + \sin\psi \vec{a}_2 = s_{13}\vec{e}_1 + s_{23}\vec{e}_2 + s_{33}\vec{e}_3$$

$$\vec{g}_1 = \cos \phi_2 \vec{e}_1 + \sin \phi_2 \vec{e}_2 \qquad \text{(B7)}$$

$$\dot{\vec{g}}_1 = -\sin \phi_2 \omega_3 \vec{e}_1 + \cos \phi_2 \omega_3 \vec{e}_2 + (\sin \phi_2 \omega_1 - \cos \phi_2 \omega_2)\vec{e}_3$$

APPENDIX C

OCCULTATION

When the effect of solar heating on the bending of the booms is included, consideration must be given to that portion of the satellite's orbit during which the sun is occulted by the earth.

In Figure C-1, occultation begins when the satellite in its orbital path reaches the occultation point, Q_2. Since the sun is assumed to be in the direction of the vector, $\vec{\sigma}$, the distances Q_1Q_2 and Q_2Q_3 at the occultation point are given by

$$Q_1Q_2 = |\vec{R}|\cos\psi \qquad (C1)$$

$$Q_2Q_3 = Q_1Q_2 \sin\alpha = |\vec{R}|\cos\psi\sin\alpha$$

where ψ is the true anomaly of the satellite and $\cos\psi\sin\alpha \leq 0$.

Let the angle between the two radials OQ_2 and OQ_3 be defined by the occultation angle ν, where in general

$$\sin\nu = \cos\psi\sin\alpha \qquad (C2)$$

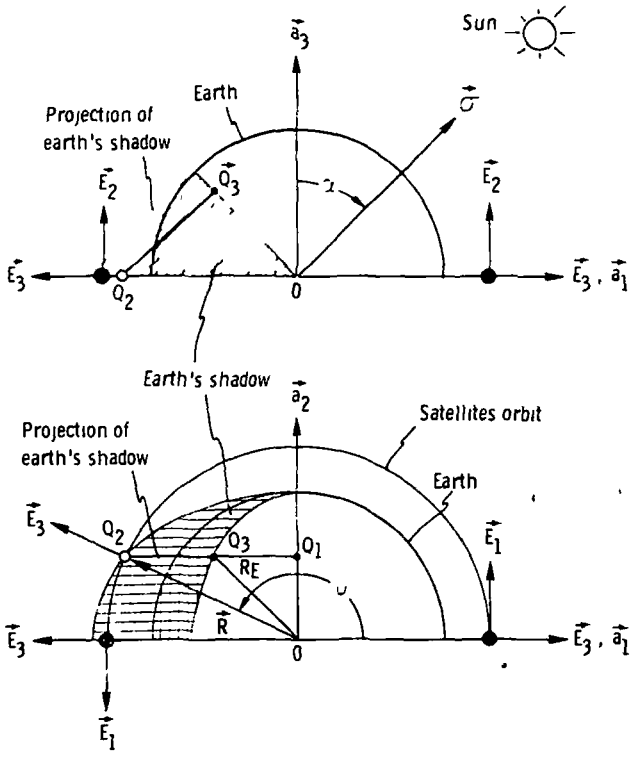

Figure C-1 Location of occultation point.

Here $OQ_2 = |\vec{R}|$ and $OQ_3 = R_E$, where R_E is the radius of the earth. Now since Q_3 must be perpendicular to Q_2Q_3 at occultation it follows that occultation occurs when

$$|\vec{R}|\cos\nu = R_E \qquad (C3)$$

or

$$\sin\nu = \sqrt{1 - \left(\frac{R_E}{|\vec{R}|}\right)^2} \qquad (C4)$$

Furthermore from consideration of the geometrical relationship between the sun vector, $\vec{\sigma}$, and the occultation point, Q_2, it is clear that the satellite must be in the sunlight as long as

$$\sin \nu > -\sqrt{1 - \left(\frac{R_E}{|\vec{R}|}\right)^2} \tag{C4}$$

APPENDIX D

COMPUTER PROGRAM GUIDE

The accompanying information provides a brief description of the utilization of computer program GGSAT. The guide includes the required input data and a program listing as well as a short sample of the program output.

The program is capable of solving for the satellite's unsteady orbital motion under the influence of solar heating. It was written for an IBM/360 operating system with plotting routines compatible with a CalComp 210/665 plotting system.

Program Input

Actual data input is submitted as floating point information on three cards. Starting in column 1, data on each card is read in with a 4E16.8 format. The data must be supplied in the following order:

CARD 1	ALPHA, deg	Sun angle, α.
	EPS, dimensionless	Eccentricity, ϵ, of orbital path.
	ALO, dimensionless	Absorptivity, α_0, $0.0 \leq \alpha_0 \leq 1.0$.
	PSCALE, dimensionless	Plot scale factor (usually 1.0).
CARD 2	ALFAE, deg	Initial roll angle.
	BETAE, deg	Initial pitch angle.
	GAMAE, deg	Initial yaw angle.
	TOW, min	Thermal lag, τ.
CARD 3	V(15), ft-lb/rad	Damper spring constant, K_D, (nominal value = .000714).
	V(16), ft-lb-sec/rad	Damper damping constant, C_D, (nominal value = .395).

RUNUM, dimensionless	Number used to identify case being run.
PLOTR, dimensionless	Plot ordinate selection for $8\frac{1}{2}$" x 12" Cal Comp plots abscissa ranging from 0 to 440 min at 40 min per inch. PLOTR = 1.0; ordinate ranges from -30^{o} to $+50^{o}$ at 10^{o} per inch. PLOTR = 2.0; ordinate ranges from -90^{o} to $+270^{o}$ at 45^{o} per inch.

Program Listing

The FORTRAN IV source deck for GGSAT consists of a main program and nineteen subroutines. Listings for the main program and eleven subroutines are provided below. Of the remaining eight subroutines, subroutine HPCG is available from the IBM Scientific Subroutine Package, while subroutines PLOTS, PLOT, FACTOR, AXIS, SYMBOL, NUMBER and LINE are part of the basic CalComp Software.

```
C*********************MAIN**********************
C
C     V(1)=M1,SIDE BOOM AND M4,DAMPER BOOM TIP MASS
C     V(2)=M2,MAIN BOOM TIP MASS
C     V(3)=M3,PAYLOAD MASS
C     V(4)=L1,SIDE BOOM AND L4,DAMPER BOOM LENGTH
C     V(5)=L2,MAIN BOOM LENGTH
C     V(6)=L3,DISTANCE FROM PAYLOAD C.G. TO HINGE
C     V(7)=I(1,1),PAYLOAD ROLL INERTIA
C     V(8)=I(2,2),PAYLOAD PITCH INERTIA
C     V(9)=I(3,3),PAYLOAD YAW INERTIA
C     V(10)=PHI1,YAW ROTATION OF SIDE BOOM
C     V(11)=PHI2,YAW ROTATION OF HINGE AXIS
C     V(12)=THETA1,ROLL ROTATION OF MAIN BOOM
C     V(13)=THETA2,PITCH ROTATION OF MAIN BOOM
C     V(14)=ALPHA ZERO,NOL POSITION OF DAMPER BOOM
C     V(15)=KD,DAMPER SPRING CONSTANT,FT-LBS/RADIAN
C     V(16)=CD,DAMPER DAMPING CONSTANT,FT-LB-SEC/RADIAN
C
C     MASS IN SLUGS
C     LENGTH IN FEET
C     INERTIAS IN SLUG-FEET**2
C     ROTATIONS IN DEGREES
C     ALPHA = SUN ANGLE(DEGREES)- ANGLE BETWEEN SUN AND NORMAL TO ORBITAL
C             PLANE VECTORS
C     ALFAE = INITIAL ROLL ANGLE(DEGREES)
C     BETAE = INITIAL PITCH ANGLE (DEGREES)
C     GAMAE = INITIAL YAW ANGLE (DEGREES)
C     AZ    = SEMI-MAJOR AXIS (KM) OF ORBITAL PATH
C     EPS   = ECCENTRICITY OF ORBITAL PATH
C     ERRDS = EARTH RADIUS (KM)
C     PSI   = INITIAL TRUE ANOMALY (DEGREES)
C     FMU   = GRAVITATIONAL CONSTANT (KM**3/SEC**2)
C     OMEGA = MEAN ORBITAL RATE (RAD/SEC)
C     ISUN  = 1, CONSTANT ORBIT IN SUN SHADOW(ECLIPSED)
C           = 2, NON-ECLIPSED ORBIT (SUNSHINE)
C     ALO   = ABSORPTIVITY
C     ICE   = LINEAR THERMAL COEFFICIENT OF EXPANSION,IN/(IN-F)
C     D1    = SIDE BOOM DIAMETER, INCHES
C     D2    = MAIN BOOM DIAMETER, INCHES
C     D4    =DAMPER BOOM DIAMETER,INCHES
C     T1    = SIDE BOOM THICKNESS, INCHES
C     T2    = MAIN BOOM THICKNESS, INCHES
C     T4    =DAMPER BOOM THICKNESS,INCHES
C     TC    = THERMAL CONDUCTIVITY,BTU/(HR.-IN.-F)
C     HRS   = HEAT RADIATION OF THE SOURCE, BTU/(HR-IN**2)
C     PSCALE = PLOT SCALE FACTOR
C     TDW    = THERMAL LAG TIME, INPUT IN MINUTES
C     RUNUM  = RUN NUMBER FOR IDENTIFICATION
C
      EXTERNAL OUT ,FCN
      COMMON/BLOCK1/AA,BB,AZ,OMEGA,EPS,NN,ISUN,ALPHA,ERRDS
      COMMON/BLOCK2/T(230),ROLL(230),PITCH(230),YAW(230),IISUN(230),
     C      RX(230),RY(230),R(230)
      COMMON/BLDY/V(16)
      COMMON/CONSTS/PI,TWOPI,RADIAN,FMU,DEGREE,SAR,CAR,OMI,NDIM
      COMMON/XIN2/ALFAE,BETAE,GAMAE,PSI,OMBC(3)
      COMMON/HEATC/ATS,ATM,ATD,ATC1(3),ATC2(3)
      DIMENSION PRMT(5),DEFFNC(9),AUX(16,15),Y(15),DERY(15)
      DIMENSION IBCD(2)
      DATA IBCD/'ORBI','T   '/
```

```
      DATA BLANK/'    '/
      DATA IBRN/'RLN '/
      DIMENSION IBCP(2)
      DIMENSION ESP(230)
      DIMENSION NC(9)
      DATA IBCR/'RLLL'/
      DATA IBCP/'PITC','H   '/
      DATA IBCY/'YAW '/
      DATA NO/119,114,115,116,117,118,119,120,121/
      PI=3.14159265
      CALL PLOTS
      TWOPI=2.*PI
      RADIAN=PI/180.0
      DEGREE=1.0/RADIAN
      AZ=7302.43
      FMU=.398613E+06
      ERADS=6378.165
      LMBC(1)=0.0
      LMBC(2)=0.0
      LMBC(3)=0.0
      PSI=0.0
      DEL=0.0
      DELDOT=0.0
C
      V(1)=0.11754
      V(2)=0.1592
      V(3)=8.7998
      V(4)=35.0
      V(5)=60.0
      V(6)=1.375
      V(7)=4.0
      V(8)=4.0
      V(9)=4.0
      V(10)=-30.0
      V(11)=120.0
      V(12)=0.0
      V(13)=0.0
      V(14)=0.0
      TCE=.104E-4
      U1=.25
      U2=.50
      U4=.25
      H1=1.4E-3
      H2=2.E-3
      H4=1.4E-3
      TC=4.167
      HRS=3.065
C
C     READ SUN ANGLE ALPHA ECCENTRICITY EPS,AND ABSORPTIVITY,ALO FROM
C     INPUT CARDS AS WELL AS PSCALE, PLOT SCALE FACTOR
C     V(15),V(16),RUNUM
C     PLOTR=1. FOR Y RANGE  OF -30 DEGREES TO +50 DEGREES
C           2. FOR Y RANGE   OF -90 DEGREES TO +270 DEGREES
C
    1 READ(5,1000,END=5400)ALPHA,EPS,ALO,PSCALE
 1000 FORMAT(4E16.8)
      READ(5,1000) ALFAE,BETAE,GAMAE,TOW
      READ(5,1000)V(15),V(16),RUNUM,PLOTR
      NDIM=12
      IF(TOW.EQ.0.)GO TO 2
```

```
      IF(TLW.LT.10.) GO TO 5500
      NDIM=15
      GW=TLW*60.
      GW1=1./GW
    2 G1=1./FLOAT(NDIM)
      AR=ALPHA*RADIAN
      SAR=SIN(AR)
      CAR=COS(AR)
      ALFAE1=ALFAE
      BETAE1=BETAE
      GAMAE1=GAMAE
C     CALCULATE LINEAR THERMAL CONSTANT FOR EACH BLOW
      ATC=(3.*ALO*TCE*HRS)/TC
      ATS=ATC*G1/P1
      ATM=ATC*G2/P2
      ATD=ATC*G4/P4
      ATC1(1)=ATS*.5*V(4)*V(4)
      ATC2(1)=(ATS*V(4))/3.
      ATC1(2)=ATM*.5*V(5)*V(5)
      ATC2(2)=(ATM*V(5))/3.
      ATC1(3)=ATD*.5*V(4)*V(4)
      ATC2(3)=(ATD*V(4))/3.
C
      DO 10 I=1,230
      T(I)=0.0
      RHOLL(I)=0.0
      PITCH(I)=0.0
      YAW(I)=0.0
      RX(I)=0.0
      RY(I)=0.0
      R(I)=0.0
   10 CONTINUE
C
      OMEGA=(FMU/(AZ**3))**.5
      PERIOD=(2.*PI/OMEGA)
      PRMT(1)=0.0
      PRMT(2)=26400.
      PRMT(3)=1200.0
      PRMT(4)=.1
C
      CALL INPUT(DEPEND)
      Y(1)=DEPEND(7)
      Y(2)=DEPEND(8)
      Y(3)=DEPEND(9)
      Y(4)=DELDCT*RADIAN
      Y(5)=DEL*RADIAN
      Y(6)=DEPEND(1)
      Y(7)=DEPEND(2)
      Y(8)=DEPEND(3)
      Y(9)=DEPEND(4)
      Y(10)=DEPEND(5)
      Y(11)=DEPEND(6)
      Y(12)=PSI*RADIAN
      Y(13)=0.0
      Y(14)=0.0
      Y(15)=0.0
C
      DO 155 J=1,NDIM
  155 DELY(J)=.1
C
```

```
      IRUN=RUNUM
      WRITE(6,4999)IRUN
 4999 FORMAT(1H1,6CX,'RUN',I4,//)
      WRITE(6,5000)(V(J),J=1,6),D1,D2,H1,H2
      WRITE(6,5010)(V(J),J=7,16)
      WRITE(6,5100) EPS,AZ,EKRDS,PSI,FMU,OMEGA,ALPHA
      WRITE(6,5020)ALO,TLE,TC,HRS,TOW
      WRITE(6,5150) ALFAEI,BETAEI,GAMAEI
      WRITE(6,5160)
C
      AN=0.0
      BN=1.0
      NN=1
      WRITE(6,5200)
C
      CALL HPCG(PRMT,Y,DERY,NDIM,IHLF,FCN,CUT ,AUX)
C
      NN=NN-1
      NN1=NN+1
      NN2=NN+2
      T(NN1)=0.0
      T(NN2)=40.0
      SS=45.
      XL=3.
      FV=-30.
      LV=10.
      IF(PLOTR.EQ.1.)GO TO 156
      SS=265.
      XL=2.
      FV=-90.
      LV=45.
  156 ROLL(NN1)=FV
      ROLL(NN2)=LV
      PITCH(NN1)=FV
      PITCH(NN2)=LV
      YAW(NN1)=FV
      YAW(NN2)=LV
      ESP(NN1)=FV
      ESP(NN2)=LV
C
      DO 160 I=1,NN
      IF(( YAW(I).EQ.BLANK).AND.(PITCH(I).EQ.BLANK))GO TO 157
      WRITE(6,5300)T(I),R(I),RX(I),RY(I),RLLL(I),PITCH(I),YAW(I),
     C          IISUN(I)
      GO TO 160
  157 WRITE(6,5301)T(I),R(I),RX(I),RY(I),ROLL(I),IISUN(I)
 5301 FORMAT(4X,4F10.2,2PF12.2,24X,I5)
  160 CONTINUE
      CALL PLOT(17.,-15.,-3)
      CALL PLOT(0.,1.5,-3)
      IF(PSCALE.EQ.1.0)GO TO 165
      CALL FACTOR(PSCALE)
  165 CALL AXIS(0.,0.,13HTIME, MINUTES,-13,11.,0.,0.,40.)
      CALL AXIS(0.,0.,14HANGLE, DEGREES ,14,6.,90.,FV,DV)
      CALL PLOT(0.,ZL,3)
      CALL PLOT(11.,ZL,2)
      SPACE=0.
      IFPN=0
      DO 200 I=2,9
      SPACE=SPACE+PERIOD/(120.*40)
```

```
      CALL PLOT(SPACE,0.,3)
      YLEN=.125+MOD(I,2)*7.875
      CALL PLOT(SPACE,YLEN,2)
      IF(MOD(I,2).EQ.0) GO TO 190
      IFPN=IFPN+1
      YP=SPACE-.125
      CALL SYMBOL(YP,.25,.10,BC(IFPN),0.,-1)
      GO TO 200
  190 IF(I.NE.2)GO TO 191
      XPAGE=SPACE
      XQ=XPAGE+.2
      CALL SYMBOL(XPAGE,.80,.10,1,0.,-1)
      CALL SYMBOL(XQ,.75,.10,IBCK,0.,4)
      CALL SYMBOL(XPAGE,.55,.10,2,0.,-1)
      CALL SYMBOL(XQ,.50,.10,IBCP,0.,8)
      CALL SYMBOL(XPAGE,.30,.10,3,0.,-1)
      CALL SYMBOL(XQ,.25,.10,IBCY,0.,4)
      XPG=XPAGE-.75
      CALL SYMBOL(XPG,.6,.1,IBKN,0.,4)
      XX=XPG+.5
      CALL NUMBER(XX,.6,.1,RLALM,0.,-1)
  191 IF(I.NE.4) GO TO 200
      XPAGE=SPACE-.25
      CALL SYMBOL(XPAGE,.25,.14,IBCD,0.,8)
  200 CONTINUE
      CALL LINE(T(1),RLLL(1),NN ,1,+8,1)
      CALL LINE(T(1),PITCH(1),NN ,1,+8,2)
      CALL LINE(T(1),YAW(1),NN ,1,+8,3)
      DO 30 K=1,NN
      ESP(K)= SS+5.*FLLAT(IISLN(K)-1)
   30 CONTINUE
      CALL LINE(T(1),ESP(1),NN,1,+0,11)
      GO TO 1
   20 FORMAT(//,(4X,8F17.7))
   21 FORMAT(//,(4X,5F17.7))
   22 FORMAT(//,(4X,4F17.7))
   23 FORMAT(//,(4X,F17.7))
 5000 FORMAT(/,20X,'M1,SIDE BOOM AND M4,DAMPER BOOM TIP MASS=',F10.5,1X,1
     C' SLUGS'/                                                        2
     C20X,'M2,MAIN BOOM TIP MASS                    =',F9.4,2X,' SLUGS'/
     C20X,'M3,PAYLOAD MASS                          =',F9.4,2X,' SLUGS'/
     C20X,'L1,SIDE BOOM AND L4,DAMPER BOOM LENGTH   =',F7.2,4X,' FEET'/
     C20X,'L2,MAIN BOOM LENGTH                      =',F7.2,4X,' FEET'/
     C20X,'L3,DISTANCE FROM PAYLOAD C.G. TO HINGE   =',F8.3,3X,' FEET'/
     C20X,'D1,SIDE BOOM AND L4,DAMPER BOOM DIAMETER=',F7.2,4X,' INCHES'/
     C20X,'D2,MAIN BOOM DIAMETER                    =',F7.2,4X,' INCHES'/
     C20X,'H1,SIDE,AND H4,DAMPER, BOOM THICKNESS    =',1PE11.2,' INCHES'/
     C20X,'H4,MAIN BOOM THICKNESS                   =',1PE11.2,' INCHES')
 5010 FORMAT(/,
     C20X,'I(1,1),PAYLOAD ROLL INERTIA              =',F7.2,4X,' SLUG-FT2
     C'/
     C20X,'I(2,2),PAYLOAD PITCH INERTIA             =',F7.2,4X,' SLUG-FT2
     C'/
     C20X,'I(3,3),PAYLOAD YAW INERTIA               =',F7.2,4X,' SLUG-FT2
     C'/
     C20X,'PHI1,YAW ROTATION OF SIDE BOOM           =',F7.2,4X,' DEG'/
     C20X,'PHI2,YAW ROTATION OF HINGE AXIS          =',F7.2,4X,' DEG'/
     C20X,'THETA1,ROLL ROTATION OF MAIN BOOM        =',F7.2,4X,' DEG'/
     C20X,'THETA2,PITCH ROTATION OF MAIN BOOM       =',F7.2,4X,' DEG'/
     C20X,'DELTA ZERO,NULL POSITION OF DAMPER BOOM =',F7.2,4X,' DEG'/
```

```
     C,20X,'KD,DAMPER SPRING CONSTANT                    =',,2PE11.2,' FT-LB/RA
     CD'/,
     C,20X,'CD,DAMPER DAMPING CONSTANT                   =',CPF8.3,3X,' FT-LB-
     CSEC/RAD'//)
5100 FORMAT(/,20X,'ECCENTRICITY                                  =',F11.6/    1
     D,20X,'SEMI-MAJOR AXIS                              =',4PE11.2,' KM'/    2
     D,20X,'EARTH RADIUS                                 =',4PE11.2,' KM',/
     D,20X,'INITIAL TRUE ANOMALY                         =',4PE11.2,' DEG',/
     D,20X,'GRAVITATIONAL CONSTANT                       =',4PE11.2,' KM3/SEC23
     D'/20X,'OMEGA,MEAN ORBITAL RATE                       =',4PE11.2,' RAD/SE4
     DC'/
     D,20X,'SUN ANGLE                                    =',CPF7.2,4X,' DEG',/
     D/)
5C20 FORMAT(/,
     F,20X,'ABSORPTIVITY                                 =',F7.2,4X,/,
     F,20X,'LINEAR THERMAL COEFFICIENT OF EXPANSION      =',4PE11.2,' IN/IN-F'
     F,/
     F,20X,'THERMAL CONDUCTIVITY                         =',4PE11.2,' BTU/HR-I
     FN-F'/
     F,20X,'HEAT RADIATION OF THE SOURCE                 =',4PE11.2,' BTU/HR-I
     FN2',/,20X,'THERMAL LAG TIME                              =',CPF7.2,4X,'
     GMIN',//)
5150 FORMAT(/,20X,'INITIAL ROLL ANGLE                            =',F11.6,' D
     EG',/
     E,20X,'INITIAL PITCH ANGLE                          =',F11.6,' DEG',/
     E,20X,'INITIAL YAW ANGLE                            =',F11.6,' DEG',/)
5160 FORMAT(1H1)
5200 FORMAT(//,9X,'TIME',8X,'R',8X,'RX',8X,'RY',7X,'ROLL',7X,'PITCH',
     C8X,'YAW',5X,'ECLIPSED',/)
5300 FORMAT(4X,4F10.2,2P3E12.2,I5)
5500 WRITE(6,5600)TOW
5600 FORMAT(1H1,' THERMAL LAG TIME =',E16.8,' AND IS OUT OF RANGE.'    )
     GO TO 1
5400 CALL PLOT(12.,0.,999)
      STOP
      END
```

```
C*******************SUBROUTINE LUT*******
      SUBROUTINE  LUT(X,Y,LERR,IHLF,NDIM,PRMT)
C
      COMMON/BLOCK1/AN,BN,AZ,OMEGA,EPS,NN,ISUN,ALPHA,ERRDS
      COMMON/BLOCK2/T(230),ROLL(230),PITCH(230),YAW(230),IISUN(230),
     C       RX(230),RY(230),R(230)
      COMMON/CONSTS/PI,TWOPI,RADIAN,FMU,DEGREE,SAR,CAR
      DIMENSION PRMT(5),Y(1),DERY(1),A(3,3),B(3,3),S(3,3)
      DATA ALPOLD,BETOLD,GAMOLD/3*0.0/
      DATA BLANK/'  '/
      Z=X-AN*PRMT(3)
      IF(Z)500,20,10
   10 PRMT(5)=1.0
      GO TO 500
C
   20 A1=AZ*(1.-EPS**2)
      CY12=COS(Y(12))
      SY12=SIN(Y(12))
      A2=(1.+EPS*CY12)
      R(NN)=A1/A2
      RX(NN)=R(NN)*CY12
      RY(NN)=R(NN)*SY12
      T(NN)=X/60.0
      IISUN(NN)=ISUN
C
      CALL EULER(Y,A,B,S)
      IF(S(3,1).EQ.0.0.AND.S(3,3).EQ.0.0)GO TO 50
      W=-S(3,2)
      ALFAE=ARSIN(W)
      IF(ABS(ALFAE*DEGREE).GT.89.0.AND.ABS(ALFAE*DEGREE).LT.91.0)
     1GO TO 30
      SN=COS(ALFAE)
      SNI=1./SN
      TEST1=S(3,3)*SNI
      W=S(3,1)*SNI
C
      BETAE=ARSIN(W)
      IF(TEST1.LT.0.0)BETAE=-ARSIN(W)+PI
C
      TEST2=S(2,2)*SNI
      W=S(1,2)*SNI
      GAMAE=ARSIN(W)
      IF(TEST2.LT.0.0)GAMAE=-ARSIN(W)+PI
C
      ALFAE=ALFAE*DEGREE
      BETAE=BETAE*DEGREE
      GAMAE=GAMAE*DEGREE
C
      ALPOLD=ALFAE
      BETOLD=BETAE
      GAMOLD=GAMAE
C
      GO TO 110
C
   30 ALFAE=ALFAE*DEGREE
      ALPOLD=ALFAE
      GO TO 100
   50 IF(S(3,2)-1.0)60,80,60
   60 IF(S(3,2)+1.0)100,70,100
   70 ALFAE=90.0
      ALPOLD=ALFAE
```

```
      GO TO 100
   80 ALFAE=-90.0
      ALPOLD=ALFAE
  100 ROLL(NN)=ALPOLD
      PITCH(NN)=BLANK
      YAW(NN)=BLANK
      GO TO 111
  110 CONTINUE
C
      ROLL(NN)=ALPOLD
      PITCH(NN)=BETOLD
      YAW(NN)=GAMOLD
C
  111 NN=NN+1
      AN=AN+BN
  500 RETURN
      END
```

```
C**********SUBROUTINE FCN*****
      SUBROUTINE FCN(X,Y,DERY)
C
      COMMON/BLOCK1/AP,BN,AZ,OMEGA,EPS,NN,ISUN,ALPHA,ERRUS
      COMMON/BODY/V(16)
      COMMON/CONSTS/PI,TWOPI,RADIAN,FMU,DEGREE,SAR,CAR,DMI,NDIM
      COMMON/HEATC/AIS,ATM,AID,ATC1(3),ATC2(3)
      DIMENSION EYEOU(3,3),EYEIO(3,3),EYEO1(3,3),EYE11(3,3),
     1EL0(1,3),EL11(1,3)
      DIMENSION P(3,3),H(1,3),EYEO(3,3),EYE1(3,3),EYE2(3,3),EYE3(3,3)
      DIMENSION G1(1,3),GT1(3,1),A01(3,1),A10(1,3),A11(1,1),AA(4,4),
     1A110(3,1),EYE4(3,3),T1(3,1),T2(3,1),T3(3,1),T4(3,1),T5(3,1),
     2T6(3,1),T7(3,1),T8(3,1),T9(3,1),T10(3,1),T11(3,1),T12(3,1),
     3T13(3,1),T14(3,1),T15(3,1),T16(3,1),OMEG1(1,3),
     4RHO(3),RHO1(3,1),RHO1(1,3),RHOO(3,3),G2(3),G1DOT(3,1)
      DIMENSION E01ST(3,1),E11ST(3,1),E1ST(1,1),AA1(4,4),
     1LL(4),MM(4),ESTAR(4,1),TLRVUE(4,1)
      DIMENSION Y(1),DERY(1),A(3,3),B(3,3),S(3,3),OMEG(3),W(6)
      DIMENSION AC(3)
      EQUIVALENCE(XC1,AC(1)),(AC2,AC(2)),(XC3,AC(3))
      DIMENSION US(3),UM(3),UD(3)
      EQUIVALENCE(US(1),CP1),(US(2),SP1),(US(3),ZERO)
      EQUIVALENCE(UM(1),ST2),(UM(2),ST1CT2),(UM(3),CT1CT2)
      EQUIVALENCE(UD(1),SP2CDL),(UD(2),CP2CDL),(UD(3),SDLN)
      DIMENSION GS(3),GM(3),GD(3)
      DIMENSION YS(3),YM(3),YD(3)
C
      A1=(1.0-EPS**2)
      A2=A1**1.5
      A3=A1**3
      A4=(1.0+EPS*COS(Y(12)))
      A5=A4**2
      A6=A4**3
      A7=OMEGA*A5/A2
      G=(OMEGA**2)*A6/A3
      RS=A2*A1/A4
      DUM=-SQRT(1.0-(ERRUS/RS)**2)
C
      CALL FULER(Y,A,B,S)
C
      ISUN=1
      SIGE3=SAR*B(3,1)
      IF(SIGE3.GT.DUM) ISUN=2
      OMEG(1)=Y(1)
      OMEG(2)=Y(2)
      OMEG(3)=Y(3)
      DELDET=Y(4)
      DEL=Y(5)
C
      PHI1=V(10)*RADIAN
      PHI2=V(11)*RADIAN
      THETA1=V(12)*RADIAN
      THETA2=V(13)*RADIAN
      DO 1 K=1,3
    1 AC(K)=SAR*A(1,K)+CAR*A(3,K)
      CT1=COS(THETA1)
      CT2=COS(THETA2)
      ST1=SIN(THETA1)
      ST2=SIN(THETA2)
      CP1=COS(PHI1)
      CP2=COS(PHI2)
```

```
      SP1=SIN(PHI1)
      SP2=SIN(PHI2)
      CDL=COS(DEL)
      SDL=SIN(DEL)
      ST1CT2=-ST1*CT2
      CT1CT2=CT1*CT2
      SP2CDL=SP2*CDL
      CP2CDL=-CP2*CDL
      SDLN=-SDL
      ZERO=0.0
      IF(ISUN.EQ.1)GO TO 7
C     CALCULATE SUN ANGLES ON BOOMS FOR THERMAL DEFORMATION
C     XIS IS THE SUN ANGLE ON SIDE BOOM IN RADIANS
C     XIM IS THE SUN ANGLE ON MAIN BOOM IN RADIANS
C     XID IS THE SUN ANGLE ON DAMPER BOOM IN RADIANS
      COSXIS=CP1*XC1+SP1*XC2
      XIS=ARCOS(COSXIS)
      COSXIM=SI2*XC1-ST1*CT2*XC2+CT1*CT2*XC3
      XIM=ARCOS(COSXIM)
      COSXID=SP2*CDL*XC1-CP2*CDL*XC2-SDL*XC3
      XID=ARCOS(COSXID)
      YTS=ATC1(1)*SIN(XIS)*(1.-ATC2(1)*COSXIS   )
      YTM=ATC1(2)*SIN(XIM)*(1.-ATC2(2)*COSXIM   )
      YTD=ATC1(3)*SIN(XID)*(1.-ATC2(3)*COSXID   )
      CALL VECTRI(XC,US,GS)
      CALL VECTRI(XC,UM,GM)
      CALL VECTRI(XC,UD,GD)
      IF(NDIM.EQ.12)GO TO 5
      DERY(13)=(YTS-Y(13))*DWI
      DERY(14)=(YTM-Y(14))*DWI
      DERY(15)=(YTD-Y(15))*DWI
      DO 4 K=1,3
      YS(K)=Y(13)*GS(K)
      YM(K)=Y(14)*GM(K)
      YD(K)=Y(15)*GD(K)
    4 CONTINUE
      GO TO 8
    5 DO 6 K=1,3
      YS(K)=YTS*GS(K)
      YM(K)=YTM*GM(K)
      YD(K)=YTD*GD(K)
    6 CONTINUE
      GO TO 8
C
    7 P(1,1)=V(4)*CP1
      P(1,2)=V(4)*SP1
      P(1,3)=0.0
      P(2,1)=V(5)*ST2
      P(2,2)=-V(5)*ST1*CT2
      P(2,3)=V(5)*CT1*CT2
      GO TO 9
    8 P(1,1)=V(4)*CP1+YS(1)
      P(1,2)=V(4)*SP1+YS(2)
      P(1,3)=YS(3)
C
      P(2,1)=V(5)*ST2+YM(1)
      P(2,2)=-V(5)*ST1*CT2+YM(2)
      P(2,3)=V(5)*CT1*CT2+YM(3)
    9 P(3,1)=0.0
      P(3,2)=0.0
```

```
      P(3,3)=-V(6)
C
      CALL INERTU(P,M,EYE0)
C
      EM0=V(1)+V(2)+V(3)
      EM1=V(1)
      EMBAR=EM0*EM1/(EM0+EM1)
C
      DO 110 I=1,3
  110 EL01(1,I)=-H(1,I)
      IF(ISUN.EQ.1)GO TO 112
      EL11(1,1)=V(4)*SP2*CDL-YD(1)
      EL11(1,2)=-V(4)*CP2*CDL-YD(2)
      EL11(1,3)=-V(4)*SDL-YD(3)
      GO TO 113
  112 EL11(1,1)=V(4)*SP2*CDL
      EL11(1,2)=-V(4)*CP2*CDL
      EL11(1,3)=-V(4)*SDL
C
  113 CALL INERT(EMBAR,EL00,EL01,EYE00)
      CALL INERT(-EMBAR,EL11,EL01,EYE01)
      CALL INERT(-EMBAR,EL01,EL11,EYE10)
      CALL INERT(EMBAR,EL11,EL11,EYE11)
C
      DO 115 I=1,3
      DO 115 J=1,3
      EYE1(I,J)=EYE0(I,J)+EYE00(I,J)+EYE01(I,J)+EYE10(I,J)+EYE11(I,J)
      EYE2(I,J)=EYE01(I,J)+EYE11(I,J)
      EYE3(I,J)=EYE11(I,J)+EYE10(I,J)
  115 EYE4(I,J)=EYE0(I,J)+EYE00(I,J)+EYE11(I,J)
C
      G1(1,1)=CP2
      G1(1,2)=SP2
      G1(1,3)=0.0
C
      DO 120 I=1,3
      EMEG1(1,I)=OMEG(I)
  120 GT1(I,1)=G1(1,I)
C
C
C     CALCULATE G1  DOT 13  = A10 AT 122
C               1X3       3X3     1X3
C
      DO 122 I=1,3
      A10(I,1)=0.0
      DO 122 J=1,3
  122 A10(I,1)=A10(I,1)+G1(1,J)*EYE3(J,I)
C     CALCULATE 12 DOT GT1 =  A01  AT STATEMENT 121
C               3X3       3X1     3X1
C     CALCULATE 111 DOT GT1 =  A110 AT STATEMENT 123
      DO 123 I=1,3
      A01(I,1)=0.0
      A110(I,1)=0.0
      DO 123 J=1,3
  121 A01(I,1)=A01(I,1)+EYE2(I,J)*GT1(J,1)
  123 A110(I,1)=A110(I,1)+EYE1(I,J)*GT1(J,1)
C     CALCULATE  G1 DOT A110 = A11 AT 124
      A11(1,1)=0.0
      DO 124 J=1,3
  124 A11(1,1)=A11(1,1)+G1(1,J)*A110(J,1)
```

```
C
      DO 125 I=1,3
      DO 125 J=1,3
      AA(I,J)=EYE1(I,J)
      AA(I,4)=AO1(I,1)
      AA(4,I)=A10(1,I)
  125 AA(4,4)=A11(1,1)
C
      RHO(1)=S(1,3)
      RHO(2)=S(2,3)
      RHO(3)=S(3,3)
C
      DO 130 I=1,3
      RHO1(1,I)=RHO(I)
      RHOT(I,1)=-3.0*RHO(I)
  130 G2(I)=G1(1,I)
C
      CALL VECT1(RHO,EYE4,T1)
      CALL VECT1(OMEG,EYE4,T2)
      CALL VECT1(G2,EYE11,T3)
      CALL VECT2(EL01,OMEG,OMEG,EL11,T4)
      CALL VECT2(EL01,OMEG,G2,EL11,T5)
      CALL VECT2(EL01,G2,OMEG,EL11,T6)
      CALL VECT2(EL01,G2,G2,EL11,T7)
      CALL VECT2(EL11,OMEG,OMEG,EL01,T8)
C
C     CALCULATE   RHOT OUT RHO1 = RHOO  AT STATEMENT 132
C                 3X1      1X3    3X3
      DO 132  I=1,3
      DO 132  J=1,3
  132 RHOO(I,J)=RHOT(I,1)*RHO1(1,J)
C
      DO 135 J=1,3
  135 RHOO(J,J)=1.0+RHOO(J,J)
C
      CALL VECT3(EL01,RHOO,EL11,T9)
      CALL VECT3(EL11,RHOO,EL01,T10)
      CALL VECT3(OMEG1,EYE11,G1,T13)
      CALL VECT3(G1,EYE11,OMEG1,T14)
C
      CALL VECT1(RHO,EYE11,T15)
      CALL VECT1(OMEG,EYE11,T16)
C
      G1DOT(1,1)=-SP2*OMEG(3)
      G1DOT(2,1)=CP2*OMEG(3)
      G1DOT(3,1)=SP2*OMEG(1)-CP2*OMEG(2)
C
C     CALCULATE  T01  OUT G1DOT = T11   AND
C                T11  OUT G1DOT = T12   BELOW TO STATEMENT 136
      DO 136 I=1,3
      T11(I,1)=0.0
      T12(I,1)=0.0
      DO 136 J=1,3
      T11(I,1)=T11(I,1)+EYE01(I,J)*G1DOT(J,1)
      T12(I,1)=T12(I,1)+EYE11(I,J)*G1DOT(J,1)
  136 CONTINUE
C
      DO 140 I=1,3
      E0ST(I,1)=3.0*G*T1(I,1)-T2(I,1)-DELDOT*(T13(I,1)+T14(I,1))
     1-(DELDOT**2)*T3(I,1)+EMBAR*T4(I,1)+EMBAR*DELDOT*(T5(I,1)
```

```
     2+T6(1,1))+EMBAR*(DELDOT**2)*(7(1,1)+EMBAR*T8(1,1)+EMBAR*G
     3*(T9(1,1)+T10(1,1))-DELDOT*(T11(1,1)+T12(1,1))
  140 E1ST(1,1)=3.0*G*T5(1,1)-T16(1,1)-DELDOT*(T13(1,1)+T14(1,1))
     1-(DELDOT**2)*T5(1,1)+EMBAR*T6(1,1)+EMBAR*G*T10(1,1)
     2-DELDOT*T12(1,1)
C
C      CALCULATE   G1 DOT E1ST = E1ST AT STATEMENT 144
C                  1X3     3X1     1X1
      E1ST(1,1)=0.0
      DO 144 J=1,3
  144 E1ST(1,1)=E1ST(1,1)+G1(1,J)*E1ST(J,1)
      E1ST(1,1)=E1ST(1,1)+V(16)*DELDOT-V(15)*DEL
C
      DO 145 I=1,4
      DO 145 J=1,4
  145 AA1(I,J)=AA(I,J)
C
      DO 150 I=1,3
  150 ESTAR(I,1)=EG1ST(I,1)
      ESTAR(4,1)=E1ST(1,1)
C
      CALL INVERT(AA1,4)
C
C     CALCULATE  AA1 DOT ESTAR = TORQUE  AT STATEMENT 151
C                  4X4     4X1     4X1
      DO 151 I=1,4
      TORQUE(I,1)=0.0
      DO 151 J=1,4
  151 TORQUE(I,1)=TORQUE(I,1)+AA1(I,J)*ESTAR(J,1)
C
      W(1)=A(1,2)*OMEG(3)-A(1,3)*OMEG(2)
      W(2)=-A(1,1)*OMEG(3)+A(1,3)*OMEG(1)
      W(3)=A(1,1)*OMEG(2)-A(1,2)*OMEG(1)
      W(4)=A(2,2)*OMEG(3)-A(2,3)*OMEG(2)
      W(5)=-A(2,1)*OMEG(3)+A(2,3)*OMEG(1)
      W(6)=A(2,1)*OMEG(2)-A(2,2)*OMEG(1)
C
      DO 200 J=1,4
  200 DERY(J)=TORQUE(J,1)
      DERY(5)=Y(4)
C
      DO 210 J=1,6
  210 DERY(J+5)=W(J)
      DERY(12)=A7
C
      RETURN
      END
```

```
C*********************SUBROUTINE INPUT*********
      SUBROUTINE INPUT(DEPEND)
C
      COMMON/BLOCK1/AA,BA,AZ,OMEGA,EPS,NN,ISUN,ALPHA,ERROS
      COMMON/CONSTS/PI,TWOPI,RADIAN,FMU,DEGREE,SAR,CAR
      COMMON/XING/ALFAE,BETAE,GAMAE,PSI,OMEC(3)
      DIMENSION DEPEND(9),SXOMC(3),        PB(3,3)
      DIMENSION S(3,3),SA(3,3),                  EPC(3),EPEC(3)
C
      ALFAE=ALFAE*RADIAN
      BETAE=BETAE*RADIAN
      GAMAE=GAMAE*RADIAN
C
      SALFAE=SIN(ALFAE)
      CALFAE=COS(ALFAE)
      SBETAE=SIN(BETAE)
      CBETAE=COS(BETAE)
      SGAMAE=SIN(GAMAE)
      CGAMAE=COS(GAMAE)
C
      ANG1=CBETAE*CGAMAE
      ANG2=CBETAE*SGAMAE
      ANG3=SBETAE*SGAMAE
      ANG4=SBETAE*CGAMAE
C
      S(1,1)=ANG1+SALFAE*ANG3
      S(2,1)=-ANG2+SALFAE*ANG4
      S(3,1)=CALFAE*SBETAE
      S(1,2)=CALFAE*SGAMAE
      S(2,2)=CALFAE*CGAMAE
      S(3,2)=-SALFAE
      S(1,3)=-ANG4+SALFAE*ANG2
      S(2,3)=ANG3+SALFAE*ANG1
      S(3,3)=CALFAE*CBETAE
C
      PSI=PSI*RADIAN
      CPSI=COS(PSI)
      SPSI=SIN(PSI)
C
      BB(3,1)=CPSI
      BB(3,2)=SPSI
      BB(3,3)=0.0
      BB(1,1)=-BB(3,2)
      BB(1,2)=BB(3,1)
      BB(1,3)=0.0
      BB(2,1)=0.0
      BB(2,2)=0.0
      BB(2,3)=1.0
C
C     CALCULATE  BBT  DOT ST  = SA  AT STATEMENT 31
C                3X3      3X3    3X3
      DO 31 I=1,3
      DO 31 J=1,3
      SA(I,J)=0.0
      DO 31 K=1,3
   31 SA(I,J)=SA(I,J)+BB(K,I)*S(J,K)
C
      A1=(1.-EPS**2)
      A2=(1.+EPS*CPSI)
      A3=SQRT(A1)
      A4=CPSI+EPS
```

```
      RADIUS=A2*A1/A2
      RRX=RADIUS*CPSI
      RRY=RADIUS*SPSI
      VX=-A2*OMEGA*SPSI/A3
      VY=A2*OMEGA*A4/A3
      OMC(1)=0.0
      OMC(2)=(RRX*VY-RRY*VX)/RADIUS**2
      OMC(3)=0.0
C
      DO 50 I=1,3
      SXOMC(I)=0.0
      DO 50 J=1,3
   50 SXOMC(I)=SXOMC(I)+S(I,J)*OMC(J)
      DO 70 I=1,3
   70 OMEG(I)=OMBC(I)+SXOMC(I)*DEGREE
C
      L=0
      DO 80 I=1,2
      DO 80 J=1,3
      L=L+1
   80 DEPEND(L)=SA(I,J)
      DO 90 I=1,3
      OMEG(I)=OMEC(I)*RADIAN
C
   90 DEPEND(I+6)=OMEG(I)
      RETURN
      END
```

```
C*******************SUBROUTINE INERTO***************
C*****************INERTIA DYADIC IOTA ZERO***********
C
      SUBROUTINE INERTO(P,H,EYEO)
      COMMON/BODY/V(16)
      DIMENSION P(3,3),H(1,3),EYEO(3,3),R(1,3),S(1,3),
     1T(1,3),R1(3,3),S1(3,3),T1(3,3)
C
C
C     CALCULATE EM  DOT P   = H  AT STATEMENT 5
C                1X3      3X3  1X3
      DO 5 I=1,3
      H(1,I)=0.0
      DO 5 J=1,3
    5 H(1,I)=H(1,I)+V(J)*P(J,I)
      EMM=V(1)+V(2)+V(3)
      EMMI=1./EMM
      DO 10 I=1,3
      H(1,I)=H(1,I)*EMMI
   10 CONTINUE
C
      DO 20 J=1,3
      R(1,J)=P(1,J)-H(1,J)
      S(1,J)=P(2,J)-H(1,J)
      T(1,J)=P(3,J)-H(1,J)
C
   20 CONTINUE
C
C     CALCULATE (RT  DOT  R)*EM(1,1)   =R1      AND
C               (ST  DOT  S)*EM(1,2)   =S       AND
C               (TT  DOT  T)*EM(1,3)   =T1
C               3X1     1X3              3X3       BELOW TO STATEMENT 30
      DO 30 I=1,3
      DO 30 J=1,3
C
      R1(I,J)= R(1,I)*R(1,J)*V(1)
      S1(I,J)= S(1,I)*S(1,J)*V(2)
      T1(I,J)= T(1,I)*T(1,J)*V(3)
C
      EYEO(I,J)=R1(I,J)+S1(I,J)+T1(I,J)
      EYEO(I,J)=-EYEO(I,J)
   30 CONTINUE
C
      C=(R(1,1)**2+R(1,2)**2+R(1,3)**2)*V(1)+
     1(S(1,1)**2+S(1,2)**2+S(1,3)**2)*V(2) +
     2(T(1,1)**2+T(1,2)**2+T(1,3)**2)*V(3)
C
      DO 40 J=1,3
      EYEO(J,J)=EYEO(J,J)+V(J+6)+C
   40 CONTINUE
      RETURN
      END
```

```
C**********SUBROUTINE INERT*****
C**********COMPUTES ELEMENTS OF INERTIA DYADIC******
      SUBROUTINE INERT(EMBAR,ELA,ELB,EYE)
      DIMENSION ELA(1,3),ELB(1,3),EYE(3,3),U(1)
C
C
C     CALCULATE (ELA TRANSPOSE DOT ELB)*EMBAR = EYE AT 10
      DO 10 I=1,3
      DO 10 J=1,3
   10 EYE(I,J)=-EMBAR*(ELA(1,I)*ELB(1,J))
C
C     CALCULATE ELA DOT ELB TRANSPOSE = U AT 15
C
      U(1)=0.0
      DO 15 J=1,3
   15 U(1)=U(1)+ELA(1,J)*ELB(1,J)
      U(1)=U(1)*EMBAR
      DO 20 J=1,3
   20 EYE(J,J)=EYE(J,J)+U(1)
      RETURN
      END
```

```
C**********SUBROUTINE VECT1*****
C****** VECTOR PRODUCT AXB=A=Z  A AND Z ARE VECTORS,B IS A DYADIC
C******      X IS VECTOR PRODUCT, * IS DOT PRODUCT
      SUBROUTINE VECT1(A,B,Z)
      DIMENSION A(3),B(3,3),Z(3,1),        AAX(3,3),DUM(3,1)
      DO 10 I=1,3
   10 AAX(I,I)=0.0
      AAX(1,2)=-A(3)
      AAX(1,3)=A(2)
      AAX(2,1)=A(3)
      AAX(2,3)=-A(1)
      AAX(3,1)=-A(2)
      AAX(3,2)=A(1)
C
C
C     CALCULATE  B DOT A    = DUM    AND
C                 3X3    3X1     3X1
C               AAX DOT DUM = Z   BELOW  AT  STATEMENTS 14 AND 15
      DO 14 I=1,3
      DUM(I,1)=0.0
      DO 14 J=1,3
   14 DUM(I,1)=DUM(I,1)+   B(I,J)* A(J)
      DO 15 I=1,3
      Z(I,1)=0.0
      DO 15 J=1,3
   15 Z(I,1)=Z(I,1)+AAX(I,J)*DUM(J,1)
C
      RETURN
      END
```

```
C*******************SUBROUTINE VECT2 ******
C******* VECTOR PRODUCT AXBXCXD=Z  A,B,C,D AND Z ARE VECTORS
C******* X IS VECTOR PRODUCT
      SUBROUTINE VECT2(A,B,C,D,Z)
      DIMENSION A(3,3),B(3),C(3),D(3,3),AX(3,3),BX(3,3),CX(3,3),
     1          DUM1(3,1),DUM2(3,1),Z(3,1)
C
      DO 10 I=1,3
      AX(I,I)=0.0
      BX(I,I)=0.0
   10 CX(I,I)=0.0
      AX(1,2)=-A(1,3)
      AX(1,3)=A(1,2)
      AX(2,1)=A(1,3)
      AX(2,3)=-A(1,1)
      AX(3,1)=-A(1,2)
      AX(3,2)=A(1,1)
C
      BX(1,2)=-B(3)
      BX(1,3)=B(2)
      BX(2,1)=B(3)
      BX(2,3)=-B(1)
      BX(3,1)=-B(2)
      BX(3,2)=B(1)
C
      CX(1,2)=-C(3)
      CX(1,3)=C(2)
      CX(2,1)=C(3)
      CX(2,3)=-C(1)
      CX(3,1)=-C(2)
      CX(3,2)=C(1)
C
C
C     CALCULATE     CX  OUT  DT = DUM1       AND
C                   BX  OUT DUM1= DUM2       AND
C                   AX  OUT DUM2= Z          BELOW
C                  3X3       3X1   3X1
      DO 20 I=1,3
      DUM1(I,1)=0.0
      DO 20 J=1,3
   20 DUM1(I,1)=DUM1(I,1)+CX(I,J)*D(1,J)
      DO 30 I=1,3
      DUM2(I,1)=0.0
      DO 30 J=1,3
   30 DUM2(I,1)=DUM2(I,1)+BX(I,J)*DUM1(J,1)
      DO 40 I=1,3
      Z(I,1)=0.0
      DO 40 J=1,3
   40 Z(I,1)=Z(I,1)+AX(I,J)*DUM2(J,1)
      RETURN
      END
```

```
C********************SUBROUTINE VECT3 ********
C****** VECTOR PRODUCT AXB*C=Z  A,C AND Z ARE VECTORS,B IS A DYADIC
C****** X IS VECTOR PRODUCT, * IS DOT PRODUCT
      SUBROUTINE VECT3(A,B,C,Z)
      DIMENSION A(1,3),B(3,3),C(1,3),AX(3,3),        DUM(3,1),Z(3,1)
C
      DO 10 I=1,3
   10 AX(I,I)=0.0
      AX(1,2)=-A(1,3)
      AX(1,3)=A(1,2)
      AX(2,1)=A(1,3)
      AX(2,3)=-A(1,1)
      AX(3,1)=-A(1,2)
      AX(3,2)=A(1,1)
C
C
C     CALCULATE   B  DOT  CC  = DUM   AND (CC=C TRANSPOSE)
C                 AX DOT DUM  = Z    BELOW
C                3X3     3X1    3X1
      DO 20 I=1,3
      DUM(I,1)=0.0
      DO 20 J=1,3
   20 DUM(I,1)=DUM(I,1)+B(I,J)* C(1,J)
      DO 30 I=1,3
      Z(I,1)=0.0
      DO 30 J=1,3
   30 Z(I,1)=Z(I,1)+AX(I,J)*DUM(J,1)
      RETURN
      END
```

```
C**********SUBROUTINE INVERT****
C**********MATRIX INVERSION BY GAUSS-JORDAN ELIMINATION******
      SUBROUTINE INVERT(A,N)
      DIMENSION A(N,N),B(50),C(50),LZ(50)
      SUM=1.0
      DO 5 I=1,N
    5 SUM=SUM*A(I,I)
C
      AVG=10.0**(-ALOG10(SUM)/N)
C
      DO 6 I=1,N
      DO 6 J=1,N
    6 A(I,J)=A(I,J)*AVG
C
      DO 10 J=1,N
   10 LZ(J)=J
      DO 20 I=1,N
      K=I
      Y=A(I,I)
      L=I-1
      LP=I+1
      IF(N-LP) 14,11,11
   11 DO 13 J=LP,N
      W=A(I,J)
      IF(ABS(W)-ABS(Y)) 13,13,12
   12 K=J
      Y=W
   13 CONTINUE
   14 IF(Y.LT.1.E-8) GO TO 200
      YI=1.0/Y
      DO 15 J=1,N
      B(J)=A(J,K)
      A(J,K)=A(J,I)
      A(J,I)=-B(J)*YI
      A(I,J)=A(I,J)*YI
   15 C(J)=A(I,J)
      A(I,I)=YI
      J=LZ(I)
      LZ(I)=LZ(K)
      LZ(K)=J
      DO 19 K=1,N
      IF(I-K) 16,19,16
   16 DO 18 J=1,N
      IF(I-J) 17,18,17
   17 A(K,J)=A(K,J)-B(J)*C(K)
   18 CONTINUE
   19 CONTINUE
   20 CONTINUE
      DO 200 I=1,N
      IF(I-LZ(I)) 100,200,100
  100 K=I+1
      DO 500 J=K,N
      IF(I-LZ(J)) 500,400,500
  400 M=LZ(I)
      LZ(I)=LZ(J)
      LZ(J)=M
      DO 700 L=1,N
      B(L)=A(I,L)
      A(I,L)=A(J,L)
  700 A(J,L)=B(L)
  500 CONTINUE
```

```
  200 CONTINUE
C      MAKE IT A SYMMETRIC MATRIX
       DO 250 I=1,N
       DO 250 J=I,N
       AVG=(A(I,J)+A(J,I))*.5*RAVG
       A(I,J)=AVG
       A(J,I)=AVG
  250 CONTINUE
       RETURN
C
  260 N=-IABS(N)
       RETURN
       END
```

```
C********************SUBROUTINE EULER********
      SUBRLUTINE ELLER(Y,A,B,S)
C
      DIMENSION Y(1),A(3,3),B(3,3),S(3,3)
C
      B(3,1)=COS(Y(12))
      B(3,2)=SIN(Y(12))
       B(3,3)=0.0
      B(1,1)=-B(3,2)
      B(1,2)=B(3,1)
       B(1,3)=0.0
       B(2,1)=0.0
       B(2,2)=0.0
      B(2,3)=1.0
      A(1,1)=Y(6)
      A(1,2)=Y(7)
      A(1,3)=Y(8)
      A(2,1)=Y(9)
      A(2,2)=Y(10)
      A(2,3)=Y(11)
      A(3,1)=Y(7)*Y(11)-Y(8)*Y(10)
      A(3,2)=Y(8)*Y(9)-Y(6)*Y(11)
      A(3,3)=Y(6)*Y(10)-Y(7)*Y(9)
C
C
C     CALCULATE  AT DOT BT = S  AT 180
C                3X3    3X3   3X3
C
      DO 180 I=1,3
      DO 180 J=1,3
      S(I,J)=0.0
      DO 180 K=1,3
  180 S(I,J)=S(I,J)+ A(K,I)*B(K,K)
C
      RETURN
      END
```

```
C**************SUBROUTINE VECTRI*****************************************************
      SUBROUTINE VECTRI(A,B,D)
      DIMENSION A(1),B(1),D(1)
C
C     VECTRI CALCULATES THE VECTOR TRIPLE CROSS-PRODUCT (AXB)XB AND
C     PUTS THE RESULT IN D WHERE (AXB)XB = (-BDOTB)A + (BDOTA)B, THE
C     RESULT, D, IS NORMALIZED-- THUS D IS ORTHONORMAL
C
      B12=B(1)*B(1)
      B22=B(2)*B(2)
      B32=B(3)*B(3)
      A1B1=A(1)*B(1)
      A2B2=A(2)*B(2)
      A3B3=A(3)*B(3)
      D(1)=-A(1)*(B22+B32)+B(1)*(A2B2+A3B3)
      D(2)=-A(2)*(B12+B32)+B(2)*(A1B1+A3B3)
      D(3)=-A(3)*(B12+B22)+B(3)*(A1B1+A2B2)
      DMI=1.0/(SQRT(D(1)*D(1)+D(2)*D(2)+D(3)*D(3)))
      D(1)=D(1)*DMI
      D(2)=D(2)*DMI
      D(3)=D(3)*DMI
      RETURN
      END
```

Program Output

For each set of input data the run number and all of the initial primary satellite parameters are first printed out. The variable parameters are then computed and subsequently printed out at 2-minute time intervals throughout the 440 minutes of simulated satellite orbital motion. The computed printout includes:

TIME, min	Time in orbit after specification of initial values.
R, km	Magnitude of the radius vector from the earth's center to the satellite's center of mass.
RX, km	$R\cos\psi$
RY, km	$R\sin\psi$
ROLL, deg	Roll angle.
PITCH, deg	Pitch angle.
YAW, deg	Yaw angle.
ECLIPSED, dimensionless	Occultation parameter. ECLIPSED = 2; satellite is in sunlight. ECLIPSED = 1; satellite is in earth's shadow.

A typical printout follows. Only a small portion of the computed time history is shown since the remaining output has the same format.

RUN 149

M1,SIDE BOOM AND M4,DAMPER BOOM TIP MASS	=	0.11754	SLUGS
M2,MAIN BOOM TIP MASS	=	0.1592	SLUGS
M3,PAYLOAD MASS	=	8.7998	SLUGS
L1,SIDE BOOM AND L4,DAMPER BOOM LENGTH	=	35.00	FEET
L2,MAIN BOOM LENGTH	=	60.00	FEET
L3,DISTANCE FROM PAYLOAD C.G. TO HINGE	=	1.375	FEET
D1,SIDE BOOM AND D4,DAMPER BOOM DIAMETER	=	0.25	INCHES
D2,MAIN BOOM DIAMETER	=	0.50	INCHES
H1,SIDE,AND H4,DAMPER, BOOM THICKNESS	=	1.40E-03	INCHES
H4,MAIN BOOM THICKNESS	=	2.00E-03	INCHES
I(1,1),PAYLOAD ROLL INERTIA	=	4.00	SLUG-FT2
I(2,2),PAYLOAD PITCH INERTIA	=	4.00	SLUG-FT2
I(3,3),PAYLOAD YAW INERTIA	=	4.00	SLUG-FT2
PHI1,YAW ROTATION OF SIDE BOOM	=	-30.00	DEG
PHI2,YAW ROTATION OF HINGE AXIS	=	120.00	DEG
THETA1,ROLL ROTATION OF MAIN BOOM	=	0.0	DEG
THETA2,PITCH ROTATION OF MAIN BOOM	=	0.0	DEG
DELTA ZERO,NULL POSITION OF DAMPER BOOM	=	0.0	DEG
KD,DAMPER SPRING CONSTANT	=	85.00E-05	FT-LB/RAD
CD,DAMPER DAMPING CONSTANT	=	0.395	FT-LB-SEC/RAD

ECCENTRICITY	=	0.0	
SEMI-MAJOR AXIS	=7302.43E 00		KM
EARTH RADIUS	=6378.16E 00		KM
INITIAL TRUE ANOMALY	=	0.0	DEG
GRAVITATIONAL CONSTANT	=3986.13E 02		KM3/SEC2
OMEGA,MEAN ORBITAL RATE	=1011.75E-06		RAD/SEC
SUN ANGLE	=	30.00	DEG

ABSORPTIVITY	=	0.70	
LINEAR THERMAL COEFFICIENT OF EXPANSION	=1040.00E-08		IN/IN-F
THERMAL CONDUCTIVITY	=4167.00E-03		BTU/HR-IN-F
HEAT RADIATION OF THE SOURCE	=3065.00E-03		BTU/HR-IN2
THERMAL LAG TIME	=	0.0	MIN

INITIAL ROLL ANGLE	=	-10.000000	DEG
INITIAL PITCH ANGLE	=	-30.000000	DEG
INITIAL YAW ANGLE	=	30.000000	DEG

TIME	R	RX	RY	ROLL	PITCH	YAW	ECLIPSED
0.0	7302.43	7302.43	0.0	-10.00E 00	-30.00E 00	30.00E 00	2
2.00	7302.43	7248.67	884.41	-98.80E-01	-29.64E 00	29.82E 00	2
4.00	7302.43	7088.20	1755.80	-95.00E-01	-28.59E 00	29.30E 00	2
6.00	7302.43	6823.38	2601.35	-88.43E-01	-26.88E 00	28.51E 00	2
8.00	7302.43	6458.09	3408.59	-79.09E-01	-24.58E 00	27.49E 00	2
10.00	7302.43	5997.73	4165.55	-67.23E-01	-21.75E 00	26.35E 00	2
12.00	7302.43	5449.07	4861.39	-53.35E-01	-18.49E 00	25.17E 00	2
14.00	7302.43	4820.18	5485.55	-38.16E-01	-14.88E 00	24.03E 00	2
16.00	7302.43	4120.34	6028.95	-22.55E-01	-11.04E 00	22.99E 00	2
18.00	7302.43	3359.83	6483.59	-75.31E-02	-70.72E-01	22.09E 00	2
20.00	7302.43	2549.86	6842.78	59.51E-02	-31.00E-01	21.34E 00	2
22.00	7302.43	1702.35	7101.23	17.06E-01	76.11E-02	20.68E 00	2
24.00	7302.43	829.78	7255.13	25.18E-01	44.01E-01	20.06E 00	2
26.00	7302.43	-55.01	7302.22	29.96E-01	77.22E-01	19.39E 00	2
28.00	7302.43	-938.98	7241.80	31.27E-01	10.64E 00	18.58E 00	2
30.00	7302.43	-1809.14	7074.78	29.24E-01	13.09E 00	17.53E 00	2
32.00	7302.43	-2652.65	6803.59	24.11E-01	15.04E 00	16.19E 00	2
34.00	7302.43	-3457.11	6432.25	16.27E-01	16.47E 00	14.51E 00	2
36.00	7302.43	-4210.67	5966.21	61.32E-02	17.38E 00	12.46E 00	2
38.00	7302.43	-4902.24	5412.35	-58.47E-02	17.79E 00	10.05E 00	2
40.00	7302.43	-5521.64	4778.79	-19.21E-01	17.73E 00	73.11E-01	2
42.00	7302.43	-6059.75	4074.90	-33.49E-01	17.25E 00	42.66E-01	2
44.00	7302.43	-6508.66	3311.02	-48.23E-01	16.40E 00	96.13E-02	2
46.00	7302.43	-6861.74	2498.39	-62.95E-01	15.24E 00	-25.57E-01	2
48.00	7302.43	-7113.81	1648.98	-77.18E-01	13.84E 00	-62.48E-01	1
50.00	7302.43	-7261.16	775.29	-86.63E-01	12.25E 00	-99.15E-01	1
52.00	7302.43	-7301.60	-109.80	-94.80E-01	10.58E 00	-13.69E 00	1
54.00	7302.43	-7234.56	-993.28	-95.82E-01	87.30E-01	-17.29E 00	1
56.00	7302.43	-7061.01	-1862.14	-94.45E-01	69.06E-01	-20.95E 00	2
58.00	7302.43	-6783.51	-2703.59	-91.82E-01	51.16E-01	-24.54E 00	2
60.00	7302.43	-6406.15	-3505.23	-85.86E-01	33.42E-01	-28.06E 00	2
62.00	7302.43	-5934.48	-4255.28	-81.04E-01	18.28E-01	-31.57E 00	2
64.00	7302.43	-5375.45	-4942.68	-73.77E-01	37.26E-02	-34.89E 00	2
66.00	7302.43	-4737.27	-5557.32	-66.34E-01	-82.93E-02	-38.10E 00	2
68.00	7302.43	-4029.36	-6090.13	-57.98E-01	-18.70E-01	-41.10E 00	2
70.00	7302.43	-3262.13	-6533.29	-49.71E-01	-26.55E-01	-43.92E 00	2
72.00	7302.43	-2446.88	-6880.28	-41.47E-01	-32.32E-01	-46.51E 00	2
74.00	7302.43	-1595.61	-7125.97	-33.86E-01	-35.63E-01	-48.89E 00	2
76.00	7302.43	-720.84	-7266.76	-27.10E-01	-36.74E-01	-51.03E 00	2
78.00	7302.43	164.53	-7300.57	-21.59E-01	-35.60E-01	-52.96E 00	2
80.00	7302.43	1047.49	-7226.91	-17.59E-01	-32.43E-01	-54.66E 00	2
82.00	7302.43	1915.02	-7046.85	-15.35E-01	-27.39E-01	-56.17E 00	2
84.00	7302.43	2754.37	-6763.05	-14.99E-01	-20.76E-01	-57.48E 00	2
86.00	7302.43	3553.16	-6379.70	-16.61E-01	-12.84E-01	-58.63E 00	2
88.00	7302.43	4299.65	-5902.41	-20.14E-01	-39.64E-02	-59.62E 00	2

90.00	7302.43	4982.83	-5338.24	-25.45E-01	54.86E-02	-60.49E 00	2
92.00	7302.43	5592.67	-4695.47	-32.32E-01	15.11E-01	-61.23E 00	2
94.00	7302.43	6120.17	-3983.59	-40.43E-01	24.52E-01	-61.88E 00	2
96.00	7302.43	6557.57	-3213.07	-49.41E-01	33.31E-01	-62.45E 00	2
98.00	7302.43	6898.43	-2395.24	-58.84E-01	41.09E-01	-62.94E 00	2
100.00	7302.43	7137.73	-1542.14	-68.31E-01	47.51E-01	-63.36E 00	2
102.00	7302.43	7271.96	-666.34	-77.42E-01	52.23E-01	-63.71E 00	2
104.00	7302.43	7299.14	219.26	-85.80E-01	54.96E-01	-63.99E 00	2
106.00	7302.43	7218.86	1101.63	-93.16E-01	55.46E-01	-64.20E 00	2
108.00	7302.43	7032.30	1967.79	-99.27E-01	53.55E-01	-64.33E 00	2
110.00	7302.43	6742.22	2804.99	-10.40E 00	49.12E-01	-64.37E 00	2
112.00	7302.43	6352.88	3600.88	-10.72E 00	42.14E-01	-64.33E 00	2
114.00	7302.43	5870.01	4343.77	-10.89E 00	32.67E-01	-64.19E 00	2
116.00	7302.43	5300.74	5022.71	-10.92E 00	20.87E-01	-63.95E 00	2
118.00	7302.43	4653.42	5627.71	-10.82E 00	69.71E-02	-63.61E 00	2
120.00	7302.43	3937.60	6149.86	-10.61E 00	-86.89E-02	-63.17E 00	2
122.00	7302.43	3163.82	6581.47	-10.31E 00	-25.72E-01	-62.63E 00	2
124.00	7302.43	2343.46	6916.19	-99.37E-01	-43.67E-01	-61.99E 00	2
126.00	7302.43	1488.59	7149.09	-95.34E-01	-62.06E-01	-61.25E 00	2
128.00	7302.43	611.81	7276.75	-91.26E-01	-80.41E-01	-60.42E 00	2
130.00	7302.43	-273.97	7297.29	-87.46E-01	-98.24E-01	-59.48E 00	2
132.00	7302.43	-1155.72	7210.39	-84.25E-01	-11.51E 00	-58.44E 00	2
134.00	7302.43	-2020.46	7017.35	-81.94E-01	-13.06E 00	-57.30E 00	2
136.00	7302.43	-2855.45	6721.00	-80.78E-01	-14.45E 00	-56.05E 00	2
138.00	7302.43	-3648.40	6325.71	-81.01E-01	-15.65E 00	-54.70E 00	2
140.00	7302.43	-4387.66	5837.29	-82.77E-01	-16.64E 00	-53.24E 00	2
142.00	7302.43	-5062.30	5262.94	-86.17E-01	-17.41E 00	-51.68E 00	2
144.00	7302.43	-5662.44	4611.10	-91.20E-01	-17.95E 00	-50.03E 00	2
146.00	7302.43	-6179.20	3891.39	-97.79E-01	-18.27E 00	-48.28E 00	2
148.00	7302.43	-6605.00	3114.39	-10.57E 00	-18.36E 00	-46.45E 00	2
150.00	7302.43	-6933.56	2291.54	-11.48E 00	-18.25E 00	-44.53E 00	2
152.00	7302.43	-7160.05	1434.96	-12.46E 00	-17.93E 00	-42.54E 00	1
154.00	7302.43	-7281.14	557.24	-13.15E 00	-17.34E 00	-40.54E 00	1
156.00	7302.43	-7295.03	-326.67	-13.79E 00	-16.67E 00	-38.37E 00	1
158.00	7302.43	-7201.53	-1209.74	-13.90E 00	-15.72E 00	-36.21E 00	1
160.00	7302.43	-7002.01	-2073.01	-13.78E 00	-14.82E 00	-33.77E 00	2
162.00	7302.43	-6699.41	-2905.76	-13.61E 00	-13.79E 00	-31.13E 00	2
164.00	7302.43	-6296.18	-3695.72	-13.11E 00	-12.71E 00	-28.32E 00	2
166.00	7302.43	-5804.23	-4431.29	-12.74E 00	-11.52E 00	-25.21E 00	2
168.00	7302.43	-5224.84	-5101.62	-12.11E 00	-10.40E 00	-22.00E 00	2
170.00	7302.43	-4568.52	-5696.85	-11.44E 00	-91.48E-01	-18.60E 00	2
172.00	7302.43	-3844.96	-6208.20	-10.61E 00	-77.93E-01	-15.10E 00	2
174.00	7302.43	-3064.79	-6628.16	-97.43E-01	-63.59E-01	-11.52E 00	2
176.00	7302.43	-2239.50	-6950.55	-87.96E-01	-48.11E-01	-78.98E-01	2
178.00	7302.43	-1381.24	-7170.61	-78.42E-01	-31.46E-01	-42.91E-01	2
180.00	7302.43	-502.64	-7285.11	-69.05E-01	-13.48E-01	-73.56E-02	2
182.00	7302.43	383.34	-7292.36	-60.46E-01	58.44E-02	27.09E-01	2
184.00	7302.43	1263.69	-7192.26	-53.14E-01	26.46E-01	59.96E-01	2
186.00	7302.43	2125.44	-6986.27	-47.65E-01	48.18E-01	90.72E-01	2
188.00	7302.43	2955.90	-6677.43	-44.43E-01	70.69E-01	11.88E 00	2

APPENDIX E

EXAMINATION OF THE ANOMALOUS BEHAVIOR OF THREE GRAVITY GRADIENT SATELLITES

By

Robert L. Goldman

Research Institute for Advance Studies
Martin Marietta Corporation

(Because this study is required for the clear understanding of the basic publication, it is reproduced in its entirety from publication TR-71-07c, RIAS, Martin Marietta Corporation, March 1971.)

SUMMARY

The anomalous oscillatory behavior of three satellites orbited by the Naval Research Laboratory has been examined. The satellites, a part of the 160 series of experiments, were all hinged two-body gravity gradient configurations passively stabilized about their three principal axes by gravity gradient and damper torques. Two basic behavior patterns were observed. Either the satellites were stable with attitude perturbations less than $\pm 5^{\circ}$ or their behavior tended towards a low frequency rigid body oscillation dominated by large yaw motions and in some cases by yaw inversions. A causal relationship between sun angle and the character of satellite behavior was observed that appears to indicate that thermal distortion is a critical factor in a gravity gradient satellite's dynamic behavior. The behavior appeared to be further modified by the existence of response frequencies that were higher than anticipated values.

INTRODUCTION

Three-axis, passive, gravity gradient stabilization of spacecraft through the use of extendable booms has been demonstrated as a practical means for providing an earth-pointing equilibrium orientation (ref. 1). The success of these gravity gradient systems, however, has, for certain satellite configurations, been inexplicably associated with a low frequency anomalous oscillatory behavior. This unpredictable behavior has usually appeared as a sustained large-amplitude, rigid-body oscillation modified, in some cases, by one or more attitude inversions. A typical example of this type of behavior is illustrated in figure 1. Such a performance was clearly seen in the flight data collected during an initial series of gravity gradient experiments conducted by the Naval Research Laboratory (NRL) (ref. 2) and more recently in the data collected from the latest series of gravity gradient satellites orbited by NRL.

This new NRL flight test data is used in the present report as a basis for a further examination of a passive gravity gradient satellite's low frequency behavior. The investigation has been directed towards the collection, display, identification, interpretation and evaluation of data from three of these satellites, and is oriented to the objective of attempting to ascertain the essential ingredients of the behavior mechanism.

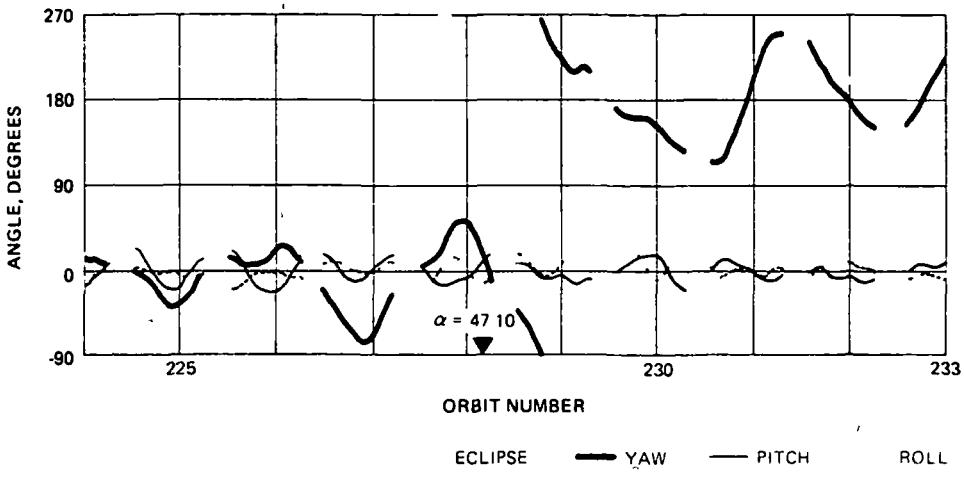

Figure 1 Typical Yaw Inversion, Satellite 163

The anomalous low-frequency behavior of a passive gravity gradient satellite can be viewed in its most general sense as an unstable interaction phenomenon involving coupling between internal dynamic properties of the satellite and external environmental energy sources. Depending upon the satellite's orbital distance and eccentricity, environmental energy sources (such as those due to aerodynamics, solar radiation and magnetic fields) may introduce destabilizing torques that are large when compared to the satellite's stabilizing gravity gradient torques (ref. 3). An adequate understanding of the dynamics of the anomalous behavior is required before any logical attempt can be made to eliminate the problem. The task that arises in the present study, therefore, is one that tries to find out which of the many internal and external system characteristics clearly dominates the unstable interaction phenomenon. Since the flexibility of a gravity gradient satellite's booms and the influence of solar pressure and thermal bending are generally suspected as being principal offenders in boom instabilities (refs. 4 to 9), they have been given principal consideration.

SPACECRAFT CHARACTERISTICS

The gravity gradient satellites in the NRL 160 series were launched together in the latter part of 1969 and successfully placed in a nearly circular 500 nautical mile orbit at an inclination of approximately 70° to the earth's equator. Their orbital parameters are summarized in Table 1. The satellites essentially moved along the same orbital path with a spacing of roughly 100 nautical miles between them. The orbital period and precession rate were such that the satellites came close (within 5°) to passing over the same point on the Earth's surface every 14 orbits.

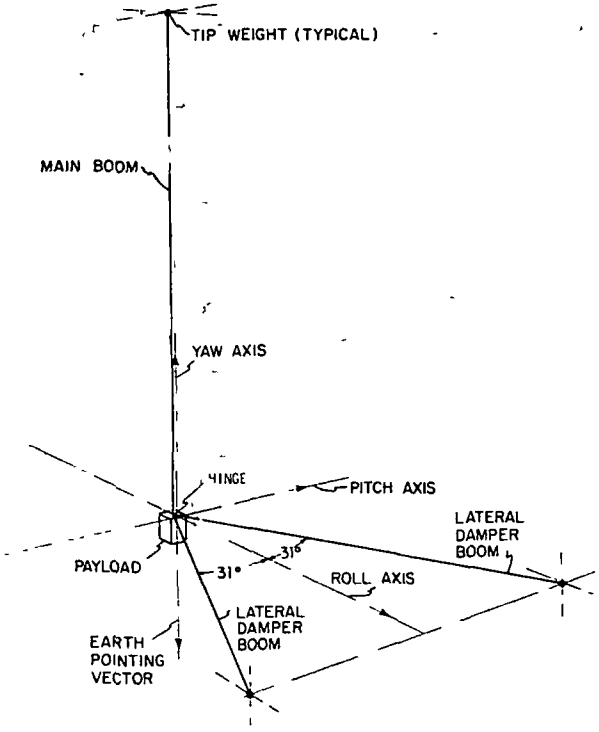

Figure 2 Satellite Geometry, Payloads 161 and 163

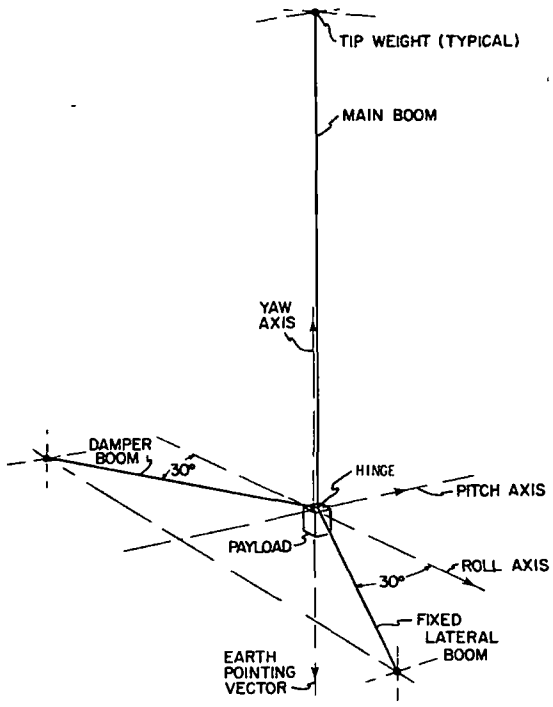

Figure 3 Satellite Geometry, Payload 164

Because of their susceptibility to rigid-body anomalous oscillations and their geometric similarity, three of these satellites, payloads 161, 163 and 164, shown in figures 2 and 3, have been singled out for examination. These particular satellites were hinged two-body configurations (ref. 10), passively stabilized about their three principal axes by gravity gradient and damper torques. The satellites were asymmetric with respect to both their geometrical shape and mass properties, but each had a plane of geometrical symmetry with respect to their principal axes. They each used three long extendable booms with a passive hinge damper attached to one or more of the booms. Tip weights were located at the deployed ends of the booms. The long booms and tip weights were needed in order to obtain a large enough moment of inertia for gravity torques to be effective, while the damper mechanism was designed to dissipate energy in order to inhibit tumbling and limit librational motions. Although active devices, such as momentum wheels and thrusters, were available on these payloads, their use was not required for stability. The important physical characteristics of the three satellite configurations are summarized in Table 2. The inertial properties listed in Table 2 are consistent with the definitions used in the formulation of the general equations of motion for a hinged two-body satellite given in reference 10.

Satellites 161 and 163

Gravity gradient satellites 161 and 163, illustrated in figure 2, have basically the same geometry. They differ mainly in their boom construction, a dissimilarity that makes examination of their motion attractive,

Table 1—Orbital Parameters

Parameter	Valve
Eccentricity	0.00203
Inclination	70.014°
Period	103.46 min/orbit
Perigee altitude	490 5 naut miles
Apogee altitude	506.5 naut miles
Orbital precession (eastward)	2.121 deg/day

Table 2—Satellite Physical Properties

Property	Units	Satellite		
		161	163	164
Payload weight	lb	235	247	283
Main boom tip weight	lb	5.28	5.28	5.12
Lateral tip weight (each)	lb	3 76	3 76	3.78
Main boom weight	gm/ft	6.866	4.584	6 866
Lateral boom weight (each)	gm/ft	2.709	4 584	2.709
Main boom length	ft	60	60	60
Lateral boom length	ft	37	37	35
Reduced inertias about hinge				
Main body pitch	slug-ft^2	641	631	623
Main body roll	slug-ft^2	641	631	623
Main body yaw	slug-ft^2	3	3	4
Secondary body pitch	slug-ft^2	240	243	220
Secondary body roll	slug-ft^2	87	85	73
Secondary body yaw	slug-ft^2	327	328	293
Total inertia about hinge				
Pitch	slug-ft^2	881	874	843
Roll	slug-ft^2	728	716	696
Yaw	slug-ft^2	330	331	297
Two-axis hinge				
Pitch spring	ft-lb/rad	0 182 x 10^{-2}	0.194 x 10^{-2}	
Roll spring	ft-lb/rad	0 382 x 10^{-3}	0.403 x 10^{-3}	
Pitch damper	ft-lb-sec/rad	0.162	0 155	
Roll damper	ft-lb-sec/rad	0.029	0.0268	
Single-axis hinge				
Spring	ft-lb/rad			0.714 x 10^{-3}
Damper	ft-lb-sec/rad			0.395
Damper stops		±27.5°	±27.5°	±29.5°

since observed variations in their librational behavior may possibly be due to differences in their boom properties. The three-axis, two-body gravity gradient stabilization system used on 161 and 163 (ref. 11) consisted of three extendable booms arranged in a symmetric pattern about the plane of the roll-yaw axes. The primary body was composed of the payload and the main boom; the secondary body consisted of the two lateral damper booms fixed in a V shape relative to each other. The lateral booms were nominally located in the horizontal pitch-roll plane. The secondary body was connected to the primary body through a two-axis (pitch and roll axes) hinge mechanism employing an eddy current damper and a torsion wire spring suspension system. Because of the inherent gyroscopic roll-yaw coupling in the libration of a gravity gradient satellite, restriction of the rotational hinge motion of the secondary body to two axes is theoretically sufficient to achieve three-axis damping of the entire satellite.

Self-extending SPAR BI-STEM booms manufactured by SPAR Aerospace Products, Ltd., of Canada were used on 161 (main boom 1/2" dia., lateral booms 1/4" diam.). Self-extending booms manufactured by the Westinghouse Electric Corp. of Baltimore, Md. were used on 163 (main and lateral booms 1/2" diam.). Both types of booms were interlocked, a feature which tended to give these booms a higher torsional stiffness than the open cross section booms used on earlier satellites. Perforations were provided on the Westinghouse booms in an attempt to better distribute the solar radiation energy picked up by the boom and thus reduce the magnitude of thermally induced boom distortions. The SPAR booms were not perforated.

Satellite 164

The basic geometry of satellite 164 is illustrated in figure 3. The three-axis, two-body gravity gradient stabilization system used on 164 (refs. 12 and 13) consisted of three extendable booms arranged in a symmetric pattern about the plane of the pitch-yaw axes. The booms were the interlocked, nonperforated SPAR BI-STEM type used on payload 161. The primary body was made up of the payload, main boom and front lateral boom (fixed to the payload); the secondary body consisted solely of the lateral damper boom. The lateral booms were nominally located in the horizontal pitch-roll plane. The secondary body (damper boom) was connected to the primary body through a single-axis hinge mechanism that constrained boom motion to a vertical plane. The hinge provided hysteresis damping torques and torsion wire spring restoring torques.

The design of this single axis damper configuration was based on the inertial coupling concept suggested by Tinling and Merrick (ref. 14). By skewing the horizontal principal axis of the secondary body (damper boom) out of the orbital plane, all motions become strongly coupled. Under these conditions, three-axis damping of the entire satellite is achieved by the single degree of freedom motion of the damper boom about its hinge.

FLIGHT DATA

The three satellites were equipped with attitude instrumentation for determining the Euler angle relationships in pitch, roll and yaw between the satellite's local vertical coordinate system and its body fixed axes. The angles in this case are defined in the usual sense so that in its preferred equilibrium orientation the satellite's body fixed axes are assumed to coincide exactly with its local vertical coordinate system (pitch axis with the orbital angular momentum vector, roll axis with the orbital velocity vector and yaw axis with the local vertical vector).

Attitude Reference System

The method of solving for these attitude angles, described in reference 2, depended upon an accurate determination in both local vertical and body fixed coordinates of the direction vectors to the sun and the Earth's magnetic field. A digital computer program, based on tracking data, was used to calculate these vectors in a local vertical coordinate system*; satellite sensor data was used to determine these same vectors in a body-fixed coordinate system. A digital computer orthogonal matrix transformation was then used to determine the desired Euler angle relationship between the two coordinate systems as defined by the two sets of identical vectors.

The sun data was obtained from a set of three Adcole solar sensors (Adcole Digital Solar Aspect System) manufactured by the Adcole Corp. of Waltham, Mass. These sensors had a pyramidal field of view of about 128° and were judiciously arranged on the top of the payload so that there was nearly complete coverage of the celestial sphere. However, certain fields of view (e.g., directly over the payload) were not covered, while others were covered by two sensors. The sensors measured the angles of the incident sunlight with respect to the body-fixed coordinate system of the spacecraft. These angles, in the form of digital outputs, were sampled and stored in the satellite's memory system.

The magnetic field data was obtained from a triaxial flux-gate magnetometer (Triaxial Magnetic Aspect Sensor) manufactured by the Schonstedt Instrument Co. of Reston, Va. The unit consisted of three sensors orthogonally aligned with the spacecraft's body-fixed axes. Each sensor produced an analog output voltage which was dependent upon the magnitude of the ambient magnetic field and the angle between the field vector and the sensor's axis. Sampled values of the three output signals, stored in the satellite's memory system, were later used to digitally compute the direction of the Earth's magnetic field vector in a body-fixed coordinate system. The digital program used in this computation included provisions for correcting the flight measurements for that portion of the ambient

* These calculations were based on an empirical formulation of the components of the Earth's magnetic field obtained by Jensen and Cain (see ref. 15) and the known Earth-Sun ecliptic relationship.

magnetic field emanating from the spacecraft. This correction was based on laboratory pre-flight measurements of the spacecraft's magnetic properties.

The accuracy of the attitude reference system depended not only upon the sensor resolution and alignment but also upon the accuracy of the tracking data, the computer formulation of the Earth's magnetic field and the magnetic field compensation. An independent check on the accuracy was obtained by comparing the scalar angle between the sun vector and the magnetic field vector in both the local vertical and body-fixed coordinate system. If the error difference between these two separate computations was less than 5° the results were considered to be acceptable.

Data Collection

The flight attitude data provided by NRL covered the first six months of satellite operation. It consisted of printed time histories of each satellite's pitch, roll and yaw attitudes as determined by the day-to-day interrogation of their memory storage systems. The memory systems stored about one day's worth of satellite sensor data sampled at a range of about one sample every 154 seconds*. These attitude plots were carefully compiled, edited and assembled in chronological order. After an initial review it became apparent that certain of these plots tended to capture the essential characteristics of each satellite's behavior. These individual plots were therefore singled out for further examination and have been reproduced in their entirety in Appendix A. They have been individually enhanced by tracing through the computed data points so as to bring out the distinctive features of each satellite's motions. For reference purposes the time for each south-north equatorial crossing, starting with Orbit 1 at launch, is also indicated.

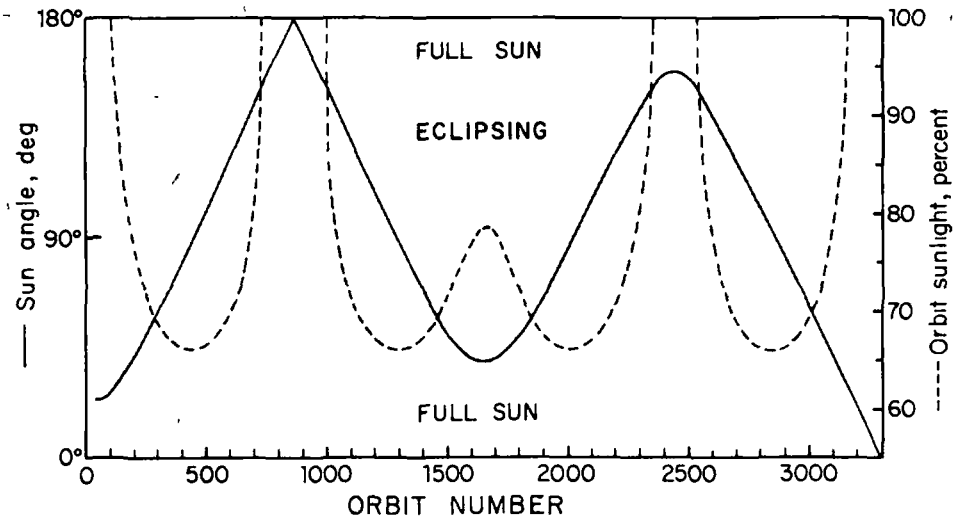

Figure 4 Solar Aspects Data for NRL 160 Series Satellites

* Real time interrogation was also available for the short period of time the satellites were in view of a ground station; during this time, data could be directly sampled at rates as high as one sample per second.

Solar aspect data for these satellites is shown in figure 4. The percent sun in figure 4 is indicative of the period in each orbit in which the satellite is not shaded by the Earth's shadow (eclipsed). The sun angle, α, in figure 4 is the angle between the sun vector and the normal to the satellite's orbital plane. When $\alpha=0°$, for example, the sun vector is perpendicular to one side of the orbit plane, when $\alpha=180°$ it is perpendicular to the other side, and when $\alpha=90°$ it is in the orbit plane. Because of symmetry, sun angles do not exceed 180°. Since sun angle, α, appeared to be such a significant parameter, it has been identified in the attitude plots in this report by marking the point in time at which a designated sun angle was reached.

SUMMARY OF OBSERVATIONS

An overall examination of the collected flight data for payloads 161, 163 and 164 leads to the general observation that there are two basic behavior patterns. The satellites are either stable with attitude perturbations less than $\pm5°$ or their behavior tends toward a low-frequency rigid-body oscillation dominated by large yaw motions. It is these two behavior patterns that are examined in the following discussion. The events leading into and through these patterns are described by referring to figures 5 to 7. The figures provide information on sun angle versus orbit number as well as the location of key events. They begin with the first orbit on day 273 of 1969 and end on day 144 of 1970. The broad lines (solid and dotted) superimposed on the sun angle line indicate the characteristic behavior patterns for those periods when actual flight data for each satellite was available. The figures are supplemented in the discussion by referring to copies of appropriate sections of the flight data in Appendix A and to the ground commands summarized in Table 3.

Satellite 161

This satellite displayed a simple form of anomalous behavior. It was either very stable or it oscillated in yaw. There were no yaw inversions. Pitch and roll motions were generally small and they did not appear to play a significant role in the behavior mechanism.

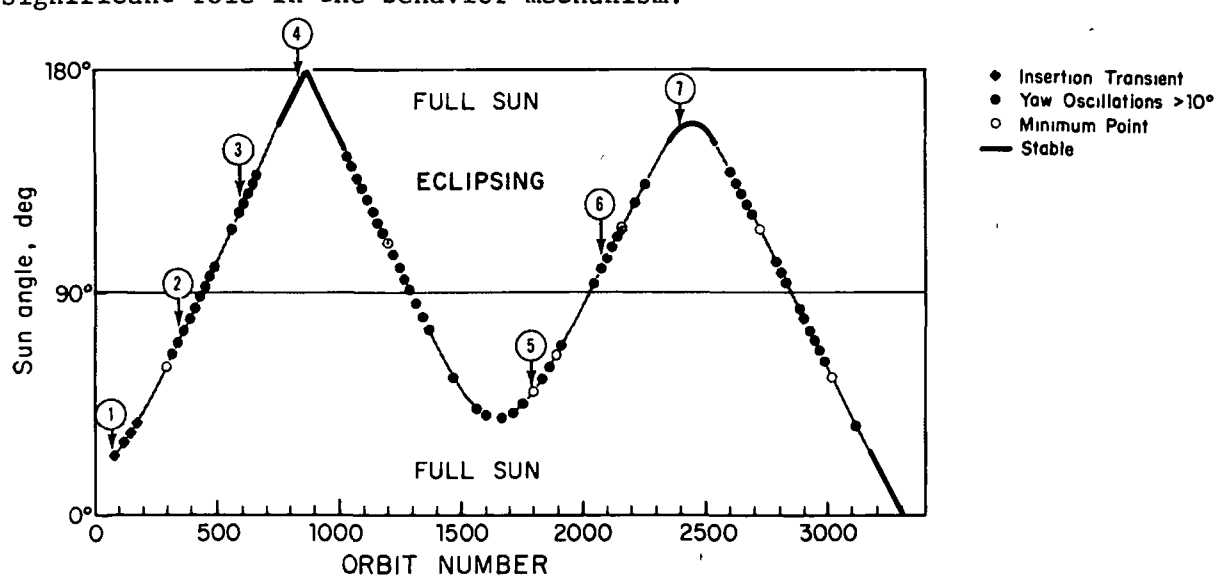

Figure 5 Sequence of Events, Payload 161

Table 3–Summary of Ground Commands

Payload	Orbit	Command
161,163	6	Primary modulation
163	7	Boom motor 1 on and off
164	7	Primary modulation
163	8	Lateral booms released
161	20	Lateral booms released
164	21	Lateral booms released
163	34	Thrusters 1 & 2 on and off, heaters 1 & 2 on
163	40	Heaters 1 & 2 off
163	48	Command main boom in and out
161,163	90	Command memory slow read
164		
161	145	Thrusters and heaters on and off
163	159	Thrusters and heaters on and off
164	159	Pitch momentum wheel on and off
161	325	Voltage control on
161	335	Thruster 1 on
161	394	Thruster 1 off
163	491	Pitch momentum wheel on
161	494	Thruster 2 on
163	494	Thruster 2 on
163	504	Thruster 2 off
161	506	Thruster 2 off
163	506	Pitch off
161	1096	Truster 2 on, pitch on
161	1099	Pitch off
164	1179	Pitch on
164	1180	Thruster 2 on
164	1185	Thruster 2 off, pitch off
163	1413	Thruster 2 on, pitch on
163	1415	Thruster 2 off
163	1418	Thruster 2 on
163	1420	Thruster 2 off, pitch off
161	1689	Pitch on
164	1689	PCM bad
161	1690	Pitch off
161	1703	Pitch on
161	1704	Thruster 1 on
161	1709	Thruster 1 off, pitch off
164	1689-2054	PCM inoperative
164	2054	Last orbit with successful command
163	2867	Pitch on
163	2868	Thruster 2 on
163	2877	Thruster 2 off, pitch off, thruster 1 on, yaw on due to failure of thruster 2
163	2884	Yaw off
163	2889	Yaw on
163	2896	Thruster 1 off
163	2898	Yaw off
163	2903	Yaw on
163	2908	Yaw off
161	3151	Heater 2 on to reduce charge current
161	3165	Heater 1 on for load
163	3165	Heater 1 on for load
163	3254	Heater 1 off
163	3262	Thruster 1 on, pitch on
163	3267	Thruster 1 off
163	3268	Thruster 1 on and off
163	3270	Pitch off
163	3276	Thruster 1 on and off
163	3277	Thruster 1 on
163	3282	Thruster 1 off
163	3290	Heater 1 on for load

At point 1, see figure 5 and Appendix A, shortly after insertion into orbit and in full sunlight, the satellite is oscillating as a rigid body in response to the insertion transient. The spacecraft has settled down into an inverted yaw position. Pitch motion is almost completely damped out, roll is decaying rapidly, and yaw is dieing out slowly.

Yaw motions continue to fall as the satellite enters into its first period of eclipsing orbits, reaching a minimum amplitude of less than $\pm 10^{\circ}$ at around point 2. After this point, however, the oscillations in yaw unexpectedly start to grow so that by the time point 3 is reached, the yaw oscillations are actually greater than they were at insertion. The yaw response frequency during this time was about .73 cycle-per-orbit, varying from .75 cycle-per-orbit at insertion to .69 cycle-per-orbit at point 3.

After the satellite enters its first period of full sunlight (orbit 720) the amplitude of this large yaw oscillation starts to decrease and is gradually replaced by a low amplitude, decaying one-cycle-per-orbit oscillation in yaw, pitch and roll. At point 4 the oscillation has just about disappeared and the satellite is extremely stable. After passing through the 180° sun angle position (a position in which the vector from the sun lined up with the satellite's pitch axis), the low amplitude one-cycle-per-orbit oscillation in yaw, pitch and roll very slowly reappears. This full sunlight region of stability ends as the satellite enters into its second period of eclipsing orbits, and the one cycle per orbit motion is gradually replaced by the .73 cycle-per-orbit, large amplitude yaw oscillation that was seen earlier.

The oscillation pattern that followed persisted for the next 1300 orbits (i.e., until the satellite was again in full sunlight). The behavior throughout this long period was repetitive. The yaw oscillation first gradually rose in amplitude, then, after reaching a maximum value, it slowly fell in amplitude; finally, after reaching a minimum value, it started rising all over again. The location of regions of minimum values are indicated on figure 5. A good view of this rise and fall pattern can be seen by examining the flight data in Appendix A near the minimum value at point 5 and the maximum value at point 6.

Coming out of this long period of eclipsing orbits, the satellite, at orbit 2240, enters its second period of full sunlight. As before, the yaw oscillations decrease and are gradually replaced by one-cycle-per-orbit perturbations in all three attitude traces, point 7. The sun angle on this pass, however, does not reach 180°, and the oscillations do not completely disappear as they did during the first full sun pass.

As the satellite leaves full sunlight and enters into a third period of eclipsing orbits, the oscillations again begin to grow. The low-amplitude one-cycle-per-orbit motions are replaced by the larger amplitude .73 cycle-per-orbit yaw oscillations, and the rise and fall pattern that was seen earlier is repeated. The whole behavior pattern, in fact, is repeated, starting all over again at orbit 3160 as the satellite enters into its third period of full sunlight.

Satellite 163

The behavior of this satellite was quite complex. It appeared to be susceptible to one per orbit pitch oscillations throughout its entire flight and large amplitude yaw oscillations and yaw inversions during periods of eclipsing orbits. The only prolonged periods of stability were during full sunlight.

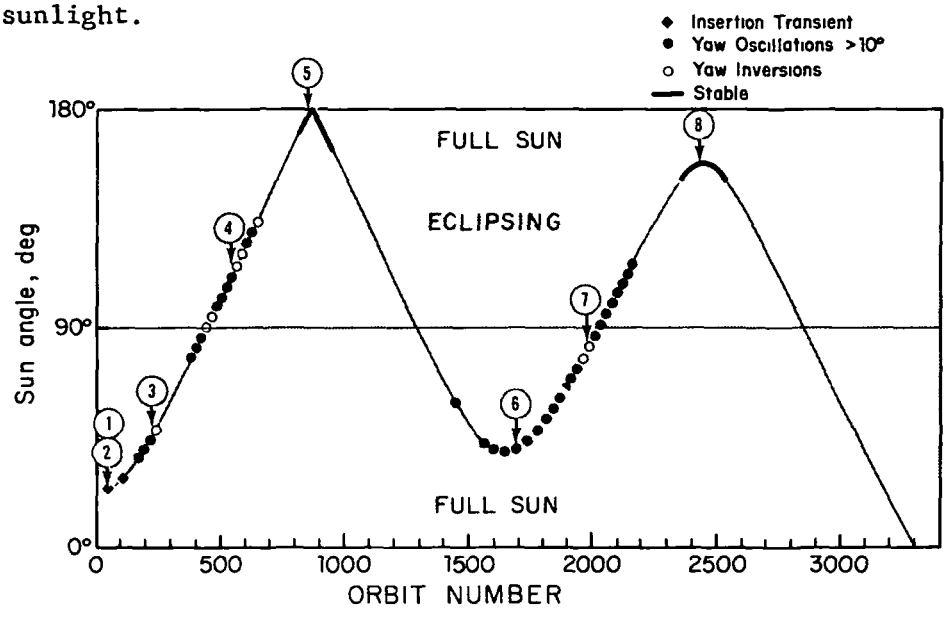

Figure 6 Sequence of Events, Payload 163

At point 1, see figure 6 and Appendix A, the satellite, captured in an inverted pitch position, is still responding to the insertion transient. Roll and yaw rigid body frequencies are damping out very slowly. Pitch, on the other hand, is responding at a one-cycle-per-orbit frequency and is exhibiting no tendency towards dieing out. At point 2 the 180° pitch error is successfully corrected by moving the main boom in and out. After this controlled inversion, the resulting transient in roll and yaw is still damped while pitch continues its sustained one-cycle-per-orbit response.

As the satellite makes it first entrance into eclipsing orbits, the yaw oscillations unexpectedly grow quite large. The satellite rapidly becomes unstable in yaw and by the time point 3 is reached, the behavior is so erratic that the satellite undergoes a yaw inversion. This undesirable yaw performance continues through point 4. In fact, during the entire first passage through eclipsing orbits the behavior is marked by numerous yaw inversions and several large amplitude oscillations in pitch and roll. The yaw frequency in this region seemed to generally be about 1/2 cycle-per-orbit.

The erratic behavior ends soon after the satellite enters its first period of full sunlight. By the time point 5 is reached the satellite is very stable with no pronounced attitude perturbations. This stability was probably maintained throughout the full sunlight period.

Although data for the time between orbit 940 and 1450 was lacking, it seems probable that the satellite again became unstable in yaw after entering its second period of eclipsing orbits. By the time points 6 and 7 are reached, the satellite's yaw behavior is again completely erratic, with several yaw inversions occurring near point 7. Large, one-cycle-per-orbit pitch oscillations are prevalent, while large yaw oscillations occur that appear to be a mixture of one-cycle-per-orbit motions and 1/2 cycle-per-orbit motions.

As the satellite continues into full sunlight the yaw instability once again disappears. At point 8 the satellite is again stable, its angular perturbations having been reduced to a relatively low level one-cycle-per-orbit oscillation in all three attitude traces. In all probability this stable characteristic continued until the next eclipsing period was entered.

Satellite 164

The behavior of this satellite was markedly different from that of 161 and 163. It was stable throughout its initial period of eclipsing orbits and unstable in yaw during its first excursion into full sunlight. This pattern did not persist, however, for during its second passage through eclipsing orbits its behavior rapidly deteriorated and the spacecraft ended up in a sustained, large amplitude yaw instability.

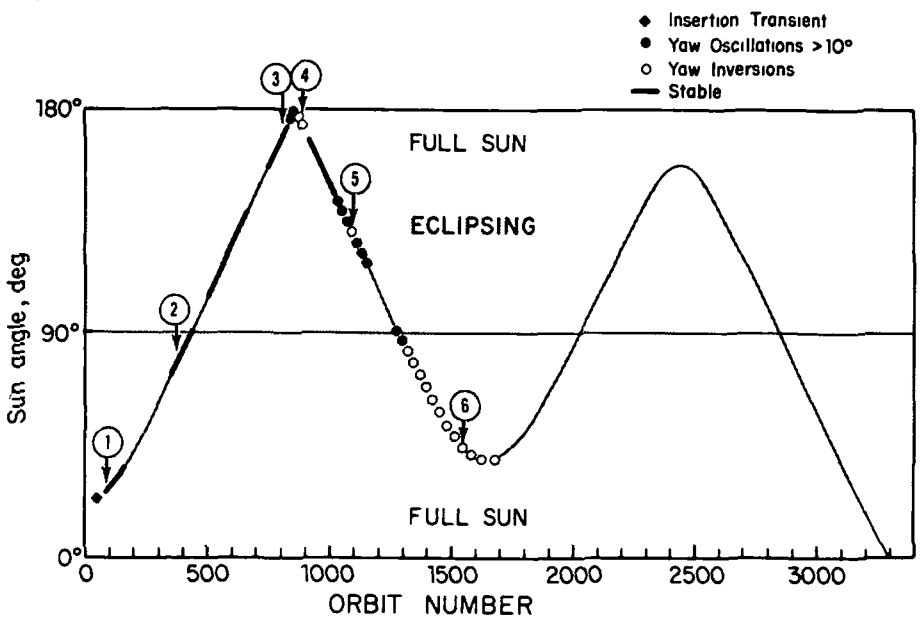

Figure 7 Sequence of Events, Payload 164

At point 1, see figure 7 and Appendix A, shortly after insertion and in full sunlight, the satellite has settled down into a well stabilized orbit. Its attitude in yaw is inverted* and the perturbations in pitch, roll and yaw are small. This satisfactory performance continues through points 2

* This inversion error was corrected in orbit 159 by energizing and de-energizing a pitch momentum wheel.

and 3. In fact, during the entire first passage through eclipsing orbits and first entrance into full sunlight all attitude errors are small. During the sequence of events from point 1 to point 3 there were only slight changes in attitude behavior; and in general the resulting small amplitude perturbations were confined to approximately one-cycle-per-orbit oscillations in pitch and 1/2 cycle-per-orbit oscillations in yaw.

As the satellite continues into the 180° sun angle position, the amplitude of the 1/2 cycle-per-orbit oscillation in yaw unexpectedly increases. The satellite rapidly becomes unstable and by the time point 4 is reached its behavior is completely erratic with numerous yaw inversions and several large amplitude oscillations in pitch and roll. Just as suddenly as the instability appeared, however, it ceases and by orbit 900 the erratic behavior has not only disappeared, but is followed for several days by a period of extremely stable operation.

Entering into the second period of eclipsing orbits the performance of the satellite begins to slowly degrade as the amplitude of the 1/2 cycle-per-orbit yaw oscillation gradually increases. Shortly before point 5 the satellite again breaks into an instability with several successive yaw inversions, ending up at point 5, in an inverted yaw position. What follows is a large amplitude, limit cycle oscillation in yaw at a frequency of about 1/2 cycle-per-orbit that persists through orbit 1130 and probably longer.

Data for the time between orbit 1130 and 1280 is lacking. Between orbits 1179 and 1185, however, the satellite was successfully inverted in yaw through the use of the pitch momentum wheel, so that when the satellite data is picked up again at orbit 1280 it is now in a limit cycle yaw oscillation about the 0° yaw position. Within the next few days the yaw amplitudes become excessive and the satellite's behavior is again completely erratic. Yaw inversions now occur nearly every day, and as typified by the traces near point 6, the instability persists to the very end*.

EVALUATION OF FLIGHT DATA

In seeking to provide an insight into those factors that most directly influenced the anomalous behavior of the three satellites, it became apparent that any attempt to single out one or two characteristics could not easily be substantiated solely on the available flight data. The complexity of actually defining (at least in a mathematical sense) the interaction phenomenon between a satellite's internal dynamic properties and its external environmental energy sources precludes the simple pin-pointing of these critical factors. For example, the effects of aerodynamic torques cannot be readily discerned without some additional measurements. Despite

* On orbit 1689 the PCM telemetry transmission from 164 was lost. Subsequent attempts to correct this malfunction or to send commands to the satellite were unsuccessful.

these restrictions, however, the observations summarized in the previous section indicate several relationships that warrant discussion.

Magnetic Torque

Although attitude responses due to variations in the Earth's magnetic field can be seen in the flight data, there is no evidence that the generating magnetic torques were large enough to contribute adversely to the anomalous behavior. For satellite 163 the effect, although small, seemed to be most pronounced in pitch as the satellite passed over the equator, see figure 8. Even the magnitudes of these small attitude perturbations are believed to be somewhat exaggerated due to computational inaccuracies resulting from slight errors in the magnetometer compensation factors and in the empirical description of the Earth's magnetic field.

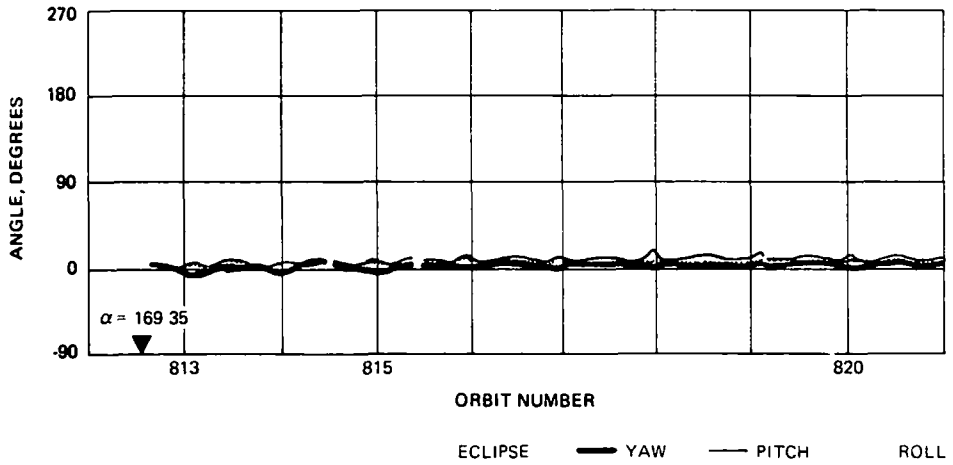

Figure 8 Magnetic Field Effect on Satellite 163

An interesting 14-orbit repetitive pattern can be seen in some of the flight data (e.g., orbits 606 to 620 on satellite 163). The pattern probably can be related to the Earth's magnetic field, since at the end of 14 orbits the satellite nearly retraces its path over the Earth's surface.

Solar Radiation

The relationship between sun angle and satellite behavior that can be seen in the flight data tends to indicate that the effect of either solar pressure or thermal bending due to solar radiation plays a significant role in a gravity gradient satellite's stability. Since a boom's thermal bending and twist is related to sun angle, it can be expected that a satellite's stability will be influenced by its thermal distortion properties.

The sudden instability of satellite 164 as it reaches the 180° sun angle position (see point 4 on figure 7) is a case in point. The instability appears to be related directly with the sun angle, disappearing as soon as the sun gets a few degrees away from 180°.

Similarly, in comparing data from 161 and 163, at least three regions of sun-related characteristic responses, illustrated in figure 9, can be discerned.

In Region 1 the satellites are in full sunlight with the sun nearly perpendicular to the orbit plane. Both satellites are quite stable with no pronounced attitude perturbations.

In Region 2 they are still in full sunlight but the sun is now inclined about 20° to the orbit plane. Although both satellites are still stable, a one-cycle-per-orbit perturbation appears in all three attitude traces.

In Region 3 the satellites have gone into an eclipsing orbit with the sun inclined about 50° to the orbit plane. Satellite 163 is now unstable in yaw with a period of about 2.0 orbits. Pitch perturbations on 163 continue at one-cycle-per-orbit. Satellite 161 has begun to undergo relatively large yaw oscillations with a period of about 1.5 orbits. Pitch and roll perturbations on 161 are now small.

Some perception into the mechanism of thermally induced instabilities of gravity gradient satellites can be deduced from Kanning's studies reported in reference 6. In this work the behavior of several gravity-oriented satellite configurations under the influence of solar radiation was examined. The effects of solar pressure torques as well as changing geometry and mass distributions due to thermal distortion on the performance of symmetrical and asymmetrical satellites were considered for a 1200 km orbit inclined 45° to the sun line. Kanning concluded that thermal distortion changes can be a critical consideration in the design of an asymmetrical satellite configuration. Although only one sun angle and only a few isolated configurations were examined, it appears that the simulated performance was significantly degraded (none of the cases examined were unstable) by the inclusion of thermal distortion.

An indication of the effect of sun angle on satellite stability can also be partially inferred from the recent study by Flanagan and Modi (ref. 16). They examined the behavior of a very simple representative satellite (no booms) under the influence of solar pressure (thermal distortion neglected) and found that in an elliptical orbit the sun angle significantly affected the satellite's response. Reviewing their work, it appears that the influence of sun angle would probably be much more pronounced for an asymmetrical satellite than for a symmetrical satellite.

Consideration of thermal bending and twist as a contributing factor to the anomalous behavior is complicated to a degree by the effect of "thermal twang" (ref. 4). The "thermal twang" excitation is associated with eclipsing orbits and is a repetitive disturbance that occurs every orbit. In full sunlight the booms are bent due to thermal distortion. Upon entering into the earth's shadow the booms return rapidly to an unbent position, introducing an impulse to which the satellite must respond. The reverse, of course, occurs as the booms enter into full sunlight. The shape of the resulting impulse can be broken down into a Fourier series so that sustained

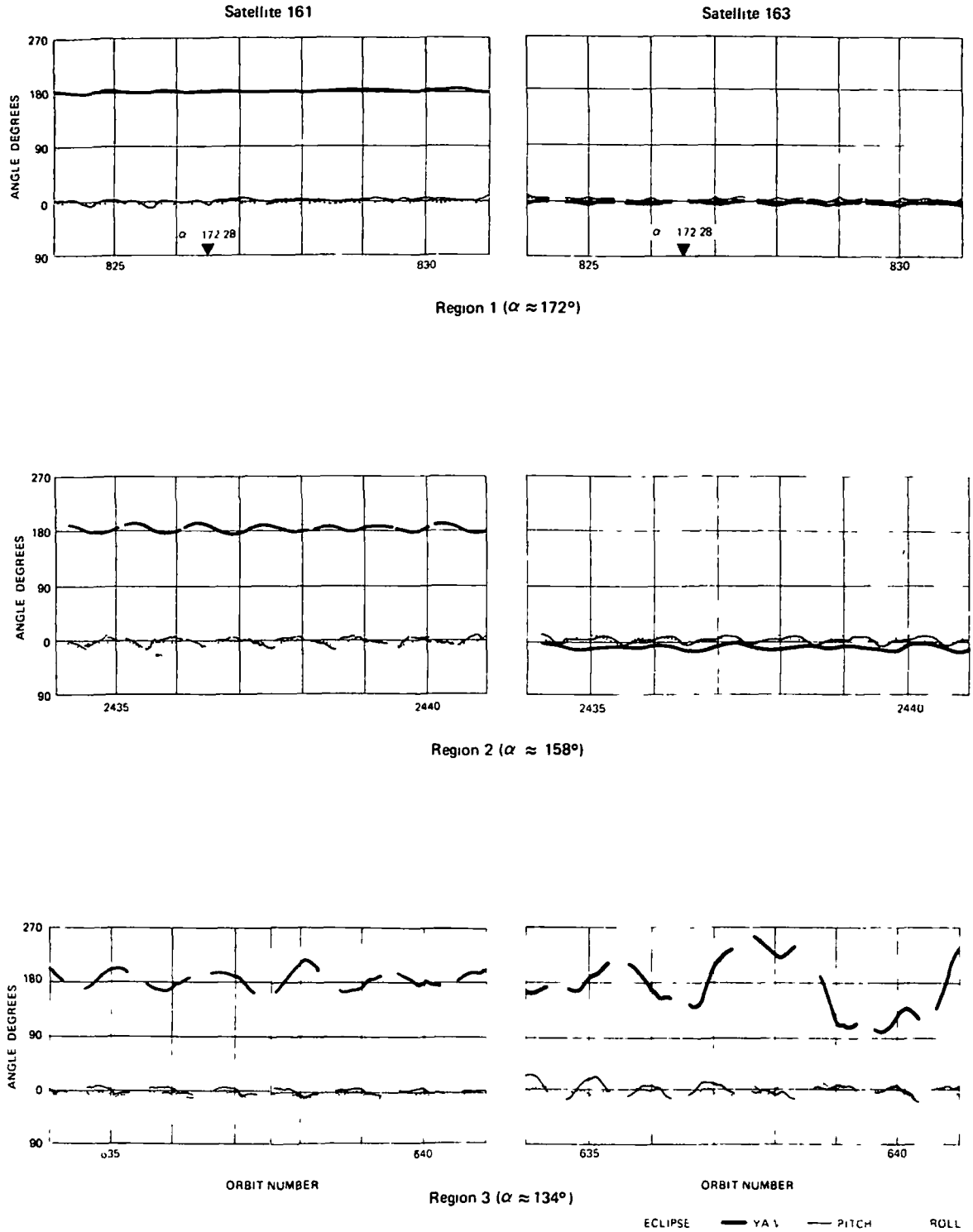

Figure 9. Effect of Sun Angle on Response, Satellites 161 and 163

satellite inputs can be anticipated at the orbital frequency and its harmonics. Since sustained responses during the anomalous performance of the three satellites were at frequencies that did not approach these "thermal twang" frequencies, it can be assumed that the behavior is not being driven solely by these impulses. The impulses on the other hand probably contribute to an instability mechanism and may be a feature in a feedback path that has not been accounted for.

Considerable evidence has previously been presented in references 7 to 9 that relates high frequency flexural oscillations of a sun-lighted boom with an instability that is sometimes referred to as thermal flutter. There were also some qualitative conjectures in references 2 and 3 that the low frequency anomalous behavior of a gravity gradient satellite is associated with thermal flutter. Although there is some evidence that the final degradation of satellite 164's behavior was coincident with a higher frequency boom oscillation, the preponderance of flight data tends to rule out thermal flutter as a controlling factor.

Dynamic Response Frequencies

The rigid body frequencies and stability of a hinged two-body satellite are controlled to a great extent by the size of the springs used in its damper unit. If the springs are too stiff, relative displacement between the two bodies is small and energy dissipation due to amplitude dependent damping is negligible. If the springs are not stiff enough, that is below some critical value, the satellite will oscillate about a cocked position. The ultimate selection usually involves an optimization procedure that ends up with springs that have stiffnesses that are slightly above the critical value.

The linearized equations for determining the small amplitude response of configurations such as 161 and 163, in which the hinge lies on the principal axes, leads to the characteristic equations given in Appendix B. Roll and yaw in such a case are decoupled from pitch. The characteristic equations for configuration 164, in which the hinge does not lie on a principal axis, are given in reference 12 and are somewhat more complex than the equations given in Appendix B. Roll and yaw in this case are not decoupled from pitch.

The theoretical response frequencies change as a function of spring stiffness and in the case of satellite 163 lead to the plots shown in figures 10 and 11. The plot for satellite 161 is similar. The pitch, roll and yaw frequencies for the selected pitch and roll springs are appropriately noted on these figures. In observing flight data one would expect that the frequencies during transient, and even during an anomalous performance, would bear some relationship to these characteristic frequencies. This, however, was not observed. Instead, as noted on figures 10 and 11, the flight frequencies for 161 and 163 (even at small amplitudes)* were close

* The pitch frequency observed in the flight data for 161 and 163 may be a response to a one-per-orbit excitation rather than a transient responses.

to the stiff spring frequencies, a condition which cannot occur without either assuming some change in the mechanical properties of the satellite (e.g., a locked damper spring) or by postulating an additional but unknown attitude-dependent torque.

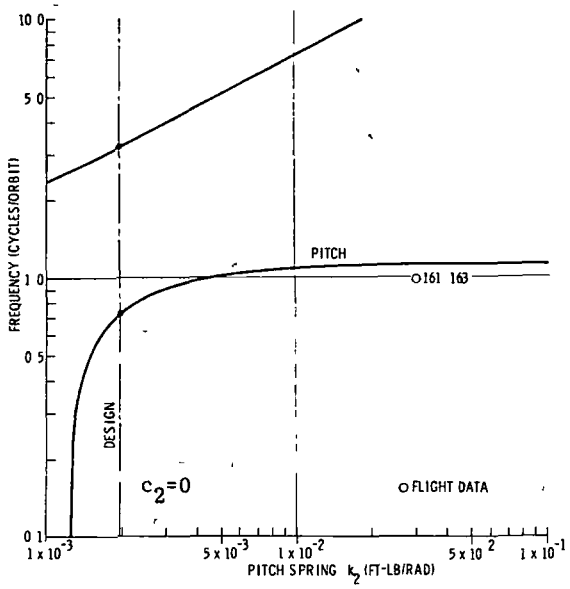

Figure 10. Pitch Frequency Variation with Spring Constant, Satellite 163

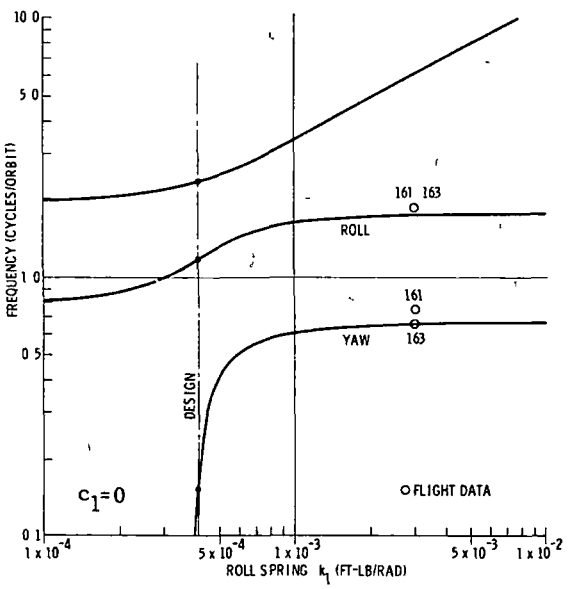

Figure 11. Roll-Yaw Frequency Variations with Spring Constant, Satellite 163

The observation that the roll frequency on 161 and 163 and the yaw frequency on 161 exceeded the theoretical rigid damper frequency is not easily explained without assuming some further change in the satellite's structural properties. Whether this change was due to an unanticipated variation in inertial properties or thermal bending is subject to speculation.

Because of the inertial coupling in a configuration such as 164, it is difficult to ascertain modal responses or to completely distinguish between pitch, roll and yaw disturbances. A configuration of this type, because of its inherent dependence on coupling for stability, is sensitive to both thermal distortion and variation in damper spring properties. Whatever the outcome of this coupling mechanism on 164, there is a change in its dynamic character, somewhere around orbit 1020, that leads to a rapid degradation in its behavior.

CONCLUDING REMARKS

The interaction phenomena observed in the flight data appear to establish a causal relationship between sun angle and the character of a satellite's response. Since thermal distortion and solar pressure are the two disturbance factors directly influenced by solar radiation, it can probably be assumed that they are influential in the anomalous behavior. Thermal distortion properties, bending and twist of each of the satellite's booms, may in fact be critical; even though a boom might be perforated to minimize thermal bending at normal sun angles, it still may deflect substantially at acute sun angles.

The observations related to discrepancies in the rigid body frequencies could be associated with a faulty hinge damper; however, the possibility of unanticipated boom deflections inhibiting the operation of the hinge cannot be ruled out. Further analytical clarification and classification of the mechanism of solar interaction is probably required. If a correct analytical model of this interaction can be obtained, then the chances of designing to avoid an instability are much enhanced.

A case in point is a configuration such as 164 that relies heavily on inertial coupling for three-axis stability. Such a configuration is particularly sensitive to thermal distortion, and it seems as if such a scheme should be avoided until a better understanding of thermal distortion effects is obtained.

A theoretical examination should be directed towards discerning the influence of thermal distortion and solar pressure on the long term or orbital stability of a satellite as opposed to boom stability. The study should consider a complete range of sun angles, boom thermal properties, damper unit properties, initial conditions, orbit eccentricity and eclipse times consistent with anticipated conditions.

REFERENCES

1. Fischell, R. E., and Mobley, F. F., "Gravity-Gradient Stabilization Studies with the DODGE Satellite", Tech. Memo. TG 1112, Applied Physics Lab., Johns Hopkins Univ., April 1970.

2. Raymond, F. W., Wilhelm, P. G., and Beal, R. T., "Gravity Gradient Flight Experience Acquired with the Naval Research Lab Satellites", Symposium on Gravity Gradient Attitude Control, Aerospace Corp., El Segundo, Calif., Dec. 1968.

3. Wiggins, K. E., "Relative Magnitudes of the Space-Environment Torques on a Satellite", AIAA Journal, vol. 2, no. 4, April 1964, pp. 770-771.

4. Foulke, H. F., "Effect of Thermal Flutter on Gravity Gradient Stabilized Spacecraft", Symposium on Gravity Gradient Attitude Control, Aerospace Corp., El Segundo, Calif., Dec. 1968.

5. Foulke, H. F., "Flight Analysis of Naval Research Laboratory Semi-Passive Stabilization Subsystem", Doc. No. 70SD5305, Space Division, General Electric Co., July 1970.

6. Kanning, G., "The Influence of Thermal Distortion on the Performance of Gravity-Stabilized Satellites", NASA TN D-5435, Nov. 1969.

7. Frisch, H. P., "Coupled Thermally-Induced Transverse plus Torsional Vibrations of a Thin-Walled Cylinder of Open Section", NASA TR R-333, Mar. 1970.

8. Merrick, V. K., "Instability of Slender Thin-Walled Booms Due to Thermally Induced Bending Moments", NASA TN D-5774, May 1970.

9. Beam, R. M., "On the Phenomenon of Thermoelastic Instability (Thermal Flutter) of Booms with Open Cross Section." NASA TN D-5222, June 1969.

10. Hartbaum, H., Hooker, W., Leliakov, I., and Margulies, G., "Configuration Selection for Passive Gravity-Gradient Satellites", Symposium on Passive Gravity-Gradient Stabilization, NASA SP-107, May 1965.

11. Leliakov, I., "Summary of Characteristics of a Small Three-Axis Controlled Gravity Gradient Satellite at Low Altitude", WDL-TN65-61, WDL Division, Philco Corp., Nov. 1965.

12. Barba, P. M., and Marx, S. H., "An Integrated 3-Axis Gravity Gradient Stabilization System", Symposium on Gravity Gradient Attitude Control, Aerospace Corp., El Segundo, Calif., Dec. 1968.

13. Anon., "Design and Performance of an Integrated, Hysteresis Damped, Gravity Stabilized Satellite", TR-DA 2091, Space and Re-Entry Systems Div., Philco-Ford Corp., July 1969.

14. Tinling, B. E., and Merrick, V. K., "Exploitation of Inertial Coupling in Passive Gravity-Gradient-Stabilized Satellites", J. Spacecraft and Rockets, vol. 1, no. 4, July-Aug. 1964, pp. 381-387.

15. Dudziak, W. F., Kleinecke, D. D., and Kostigen, T. J., "Graphic Displays of Geomagnetic Geometry", RM 63TMP-2 DASA 1372, General Electric Co., April 1963.

16. Flanagan, R. C., and Modi, V. J., "Attitude Dynamics of a Gravity Oriented Satellite under the Influence of Solar Radiation Pressure", Aero. J. of the Royal Aero. Soc., vol. 74, Oct. 1970, pp. 835-841.

APPENDIX A

SELECTED FLIGHT DATA

Page intentionally left blank

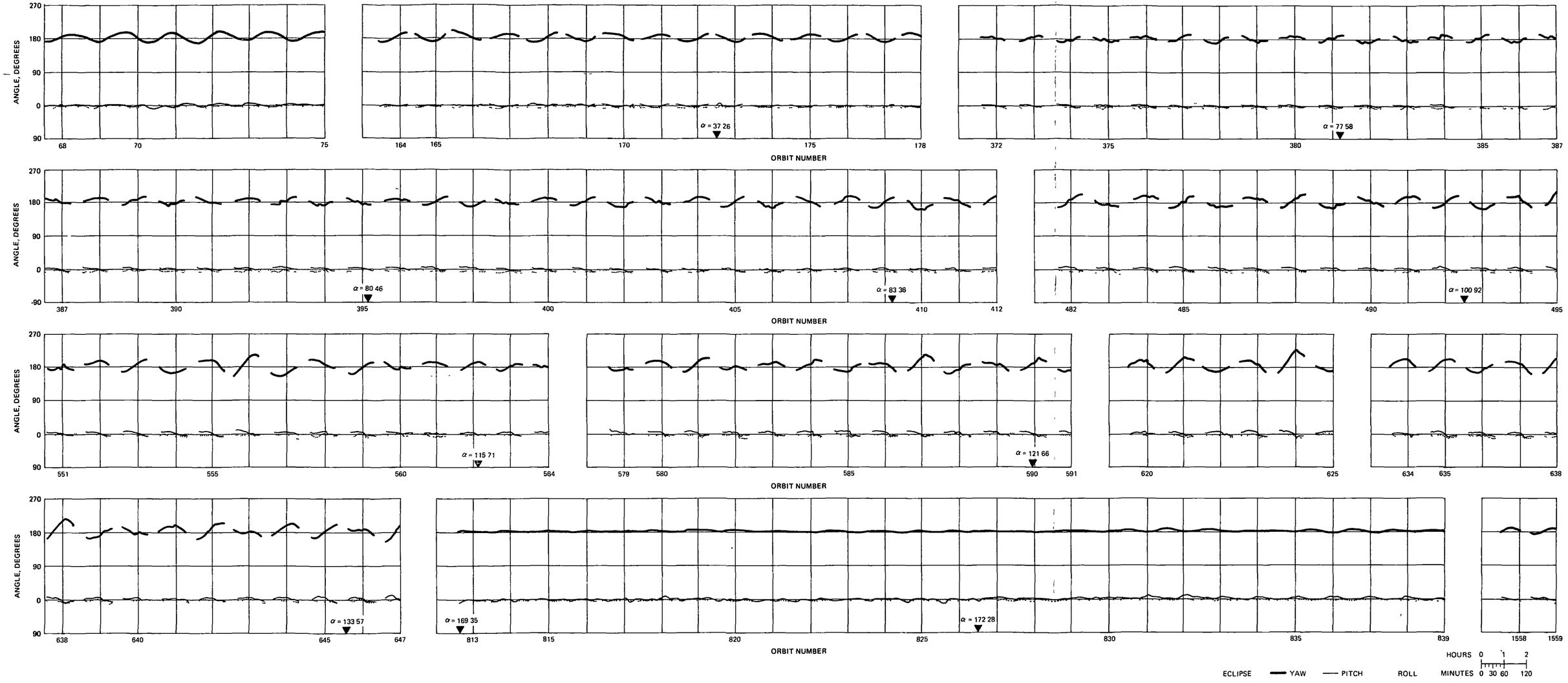

Figure A-1. Flight Data, Satellite 161

Page Intentionally Left Blank

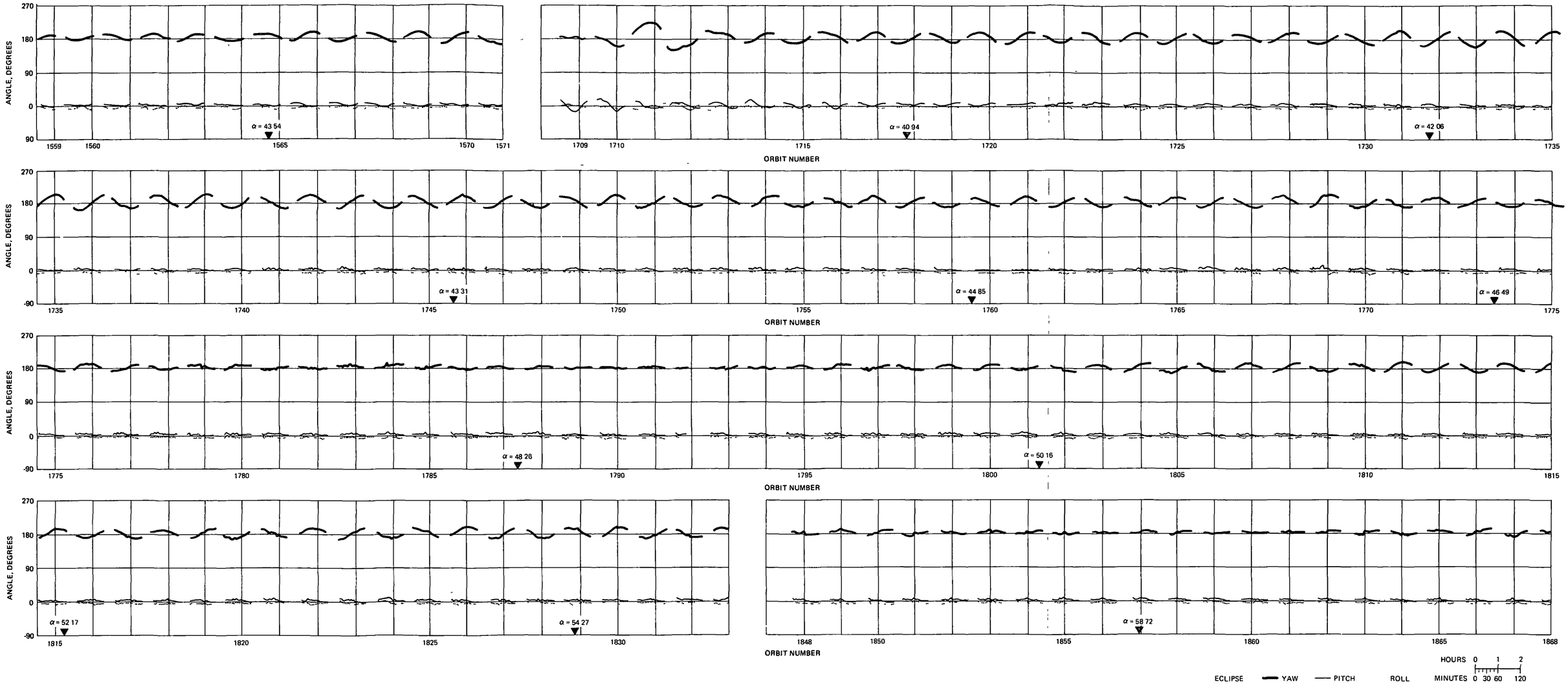

Figure A-1 (continued) Flight Data, Satellite 161

Page Intentionally Left Blank

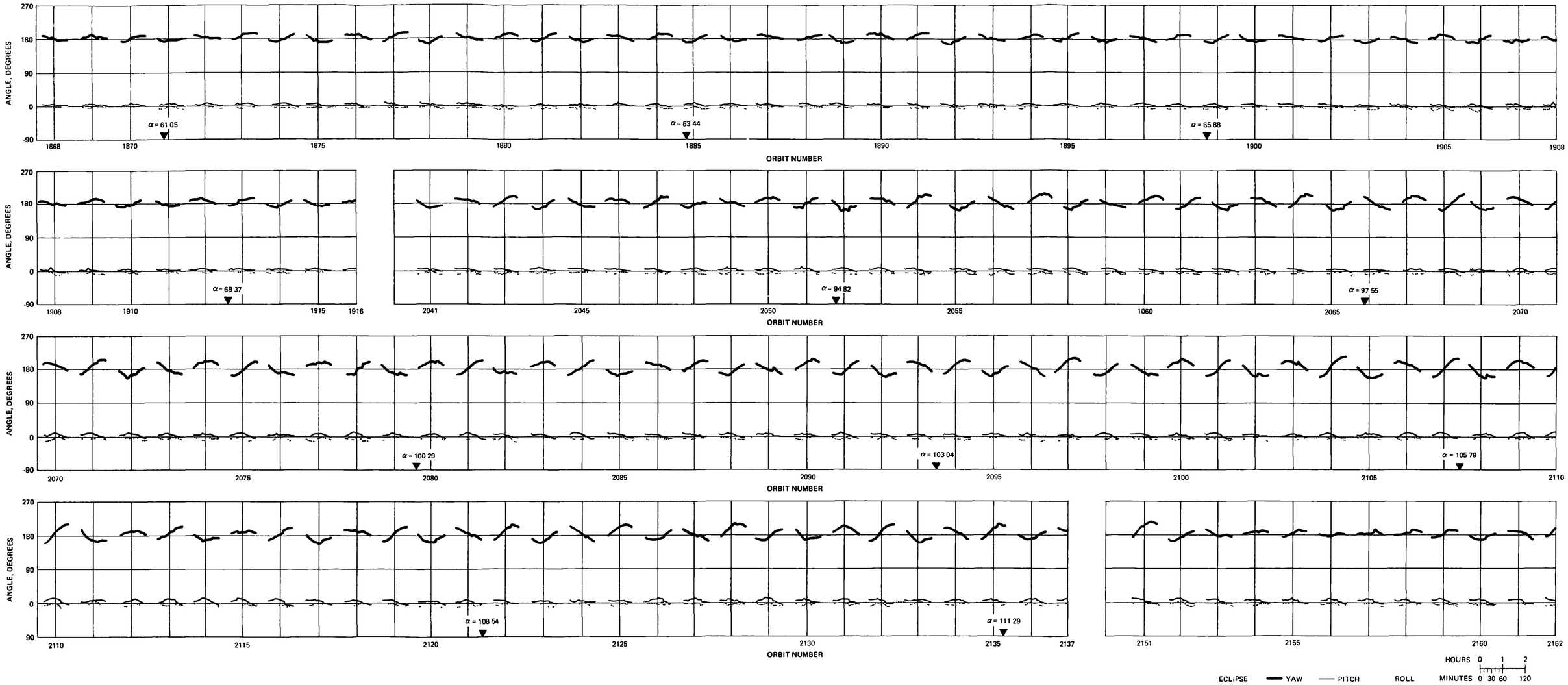

Figure A-1 (continued). Flight Data, Satellite 161

Page Intentionally Left Blank

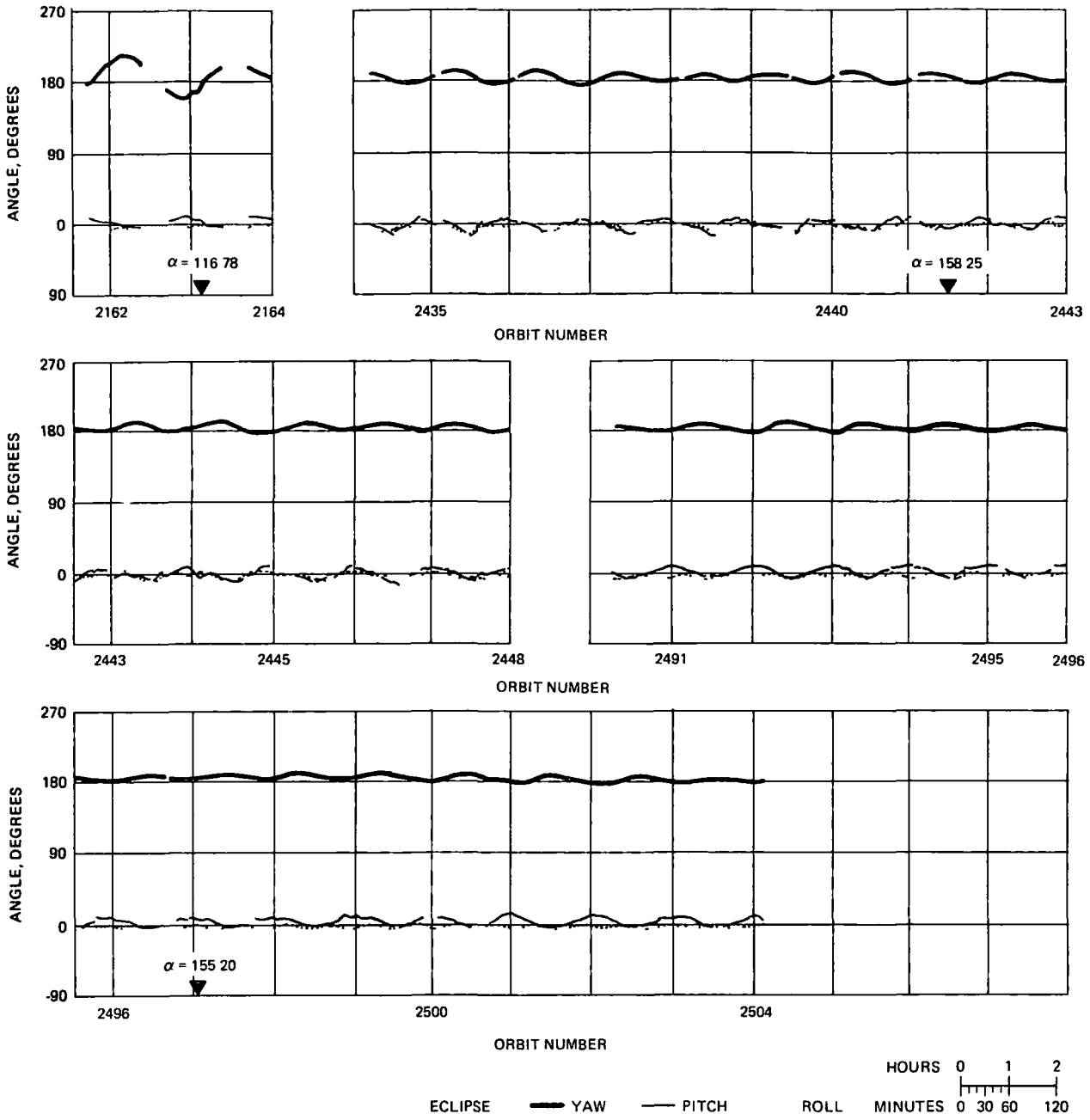

Figure A-1 (continued). Flight Data, Satellite 161

Page Intentionally Left Blank

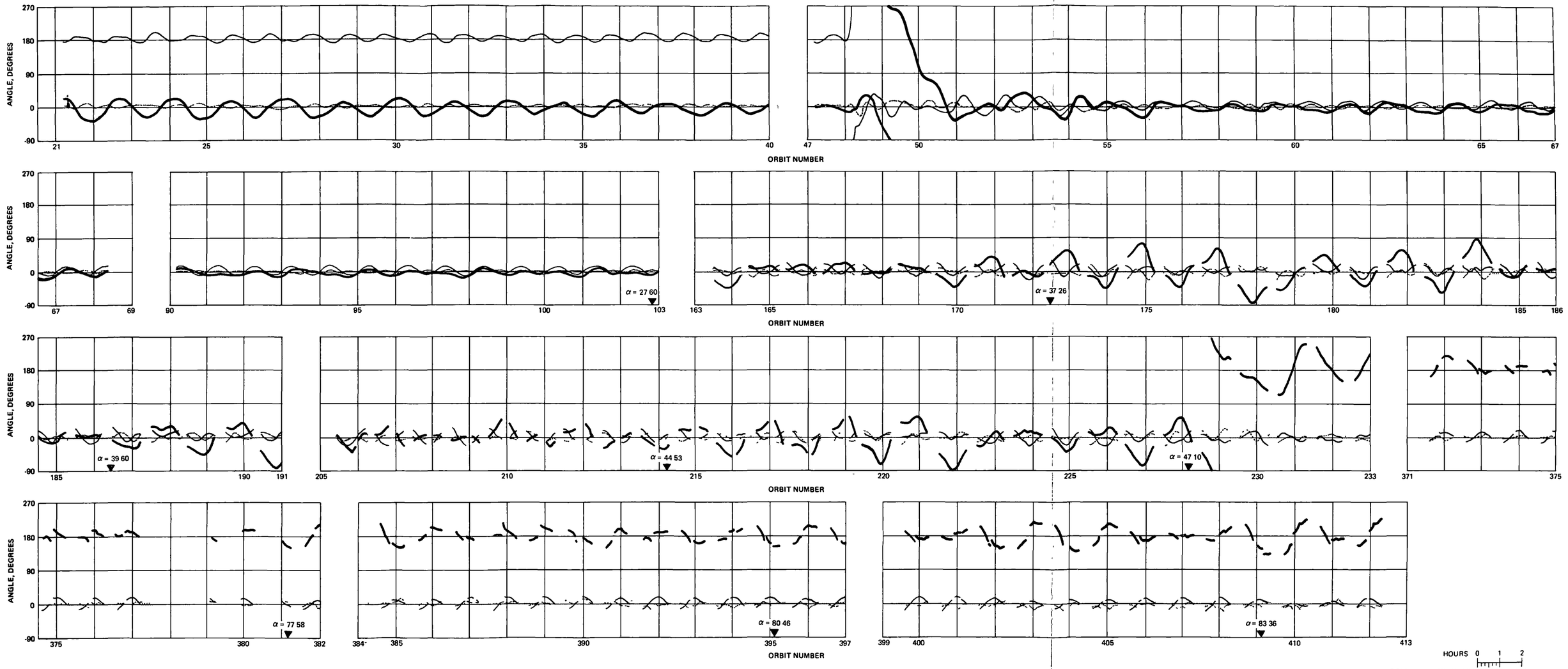

Figure A-2 Flight Data, Satellite 163

Page Intentionally Left Blank

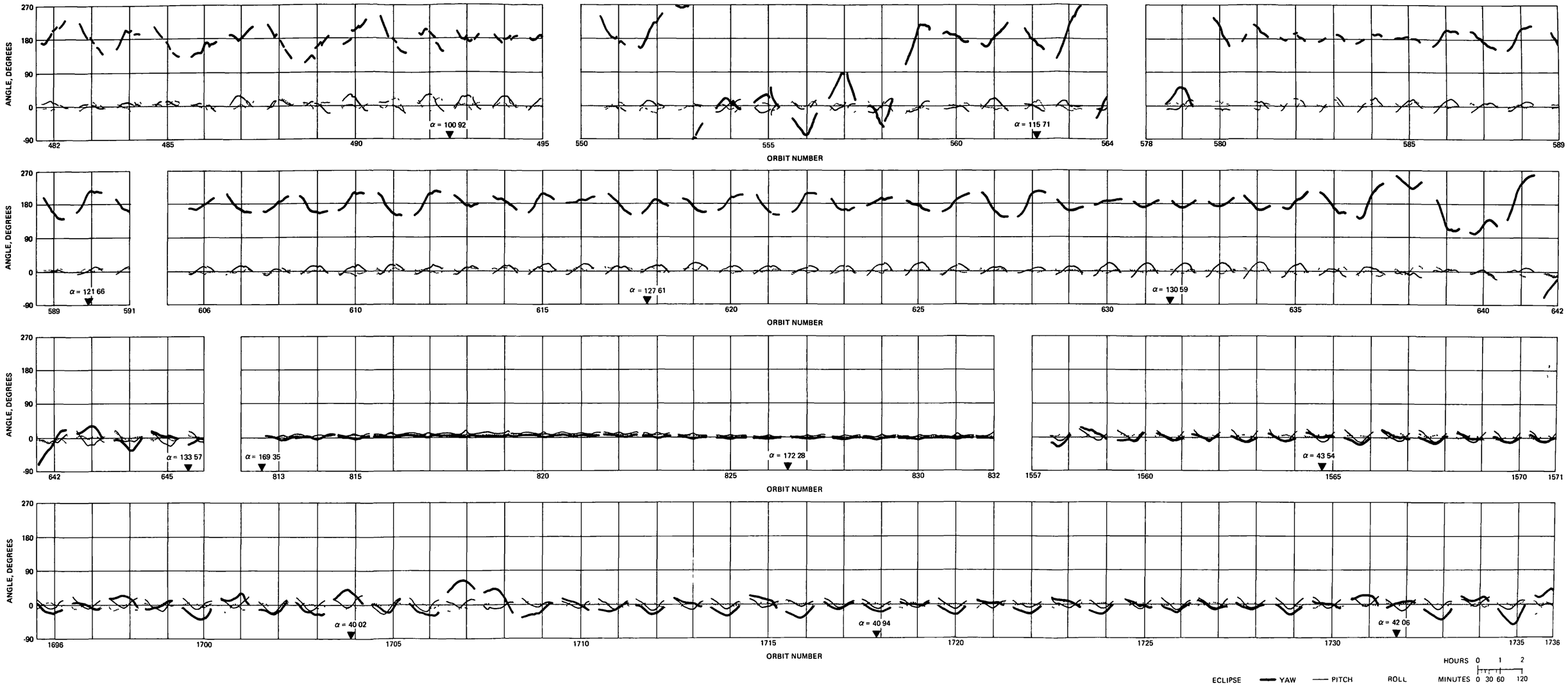

Figure A-2 (continued). Flight Data, Satellite 163

Page Intentionally Left Blank

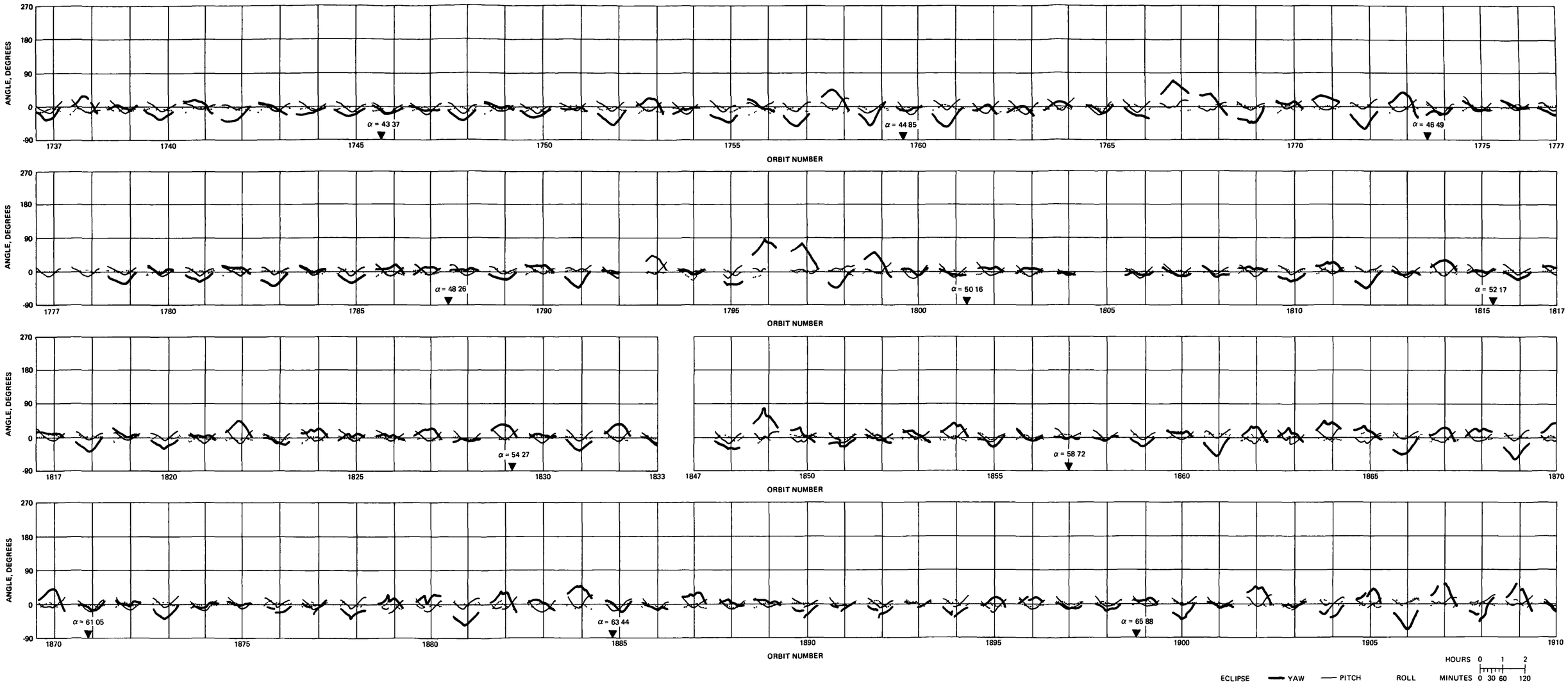

Figure A-2 (continued). Flight Data, Satellite 163

Page Intentionally Left Blank

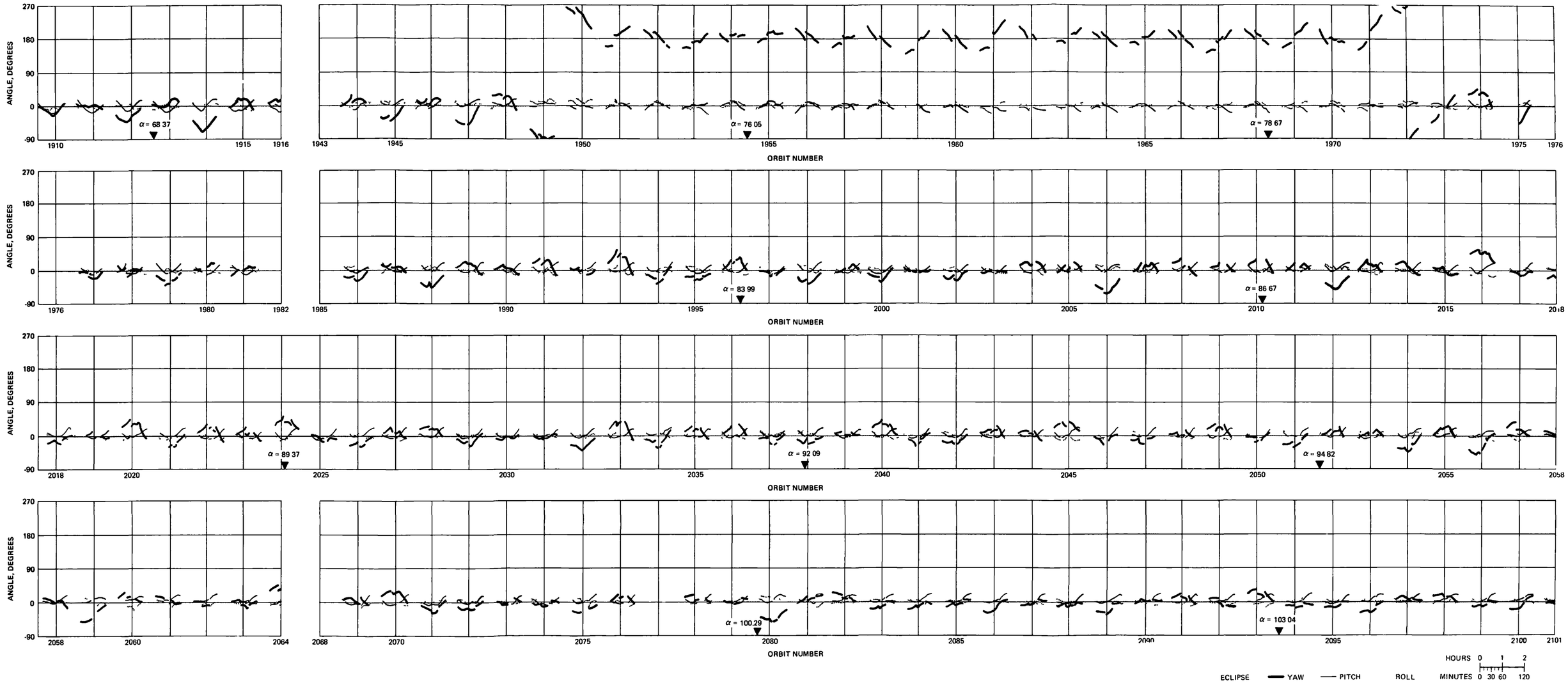

Figure A-2 (continued). Flight Data, Satellite 163

Page Intentionally Left Blank

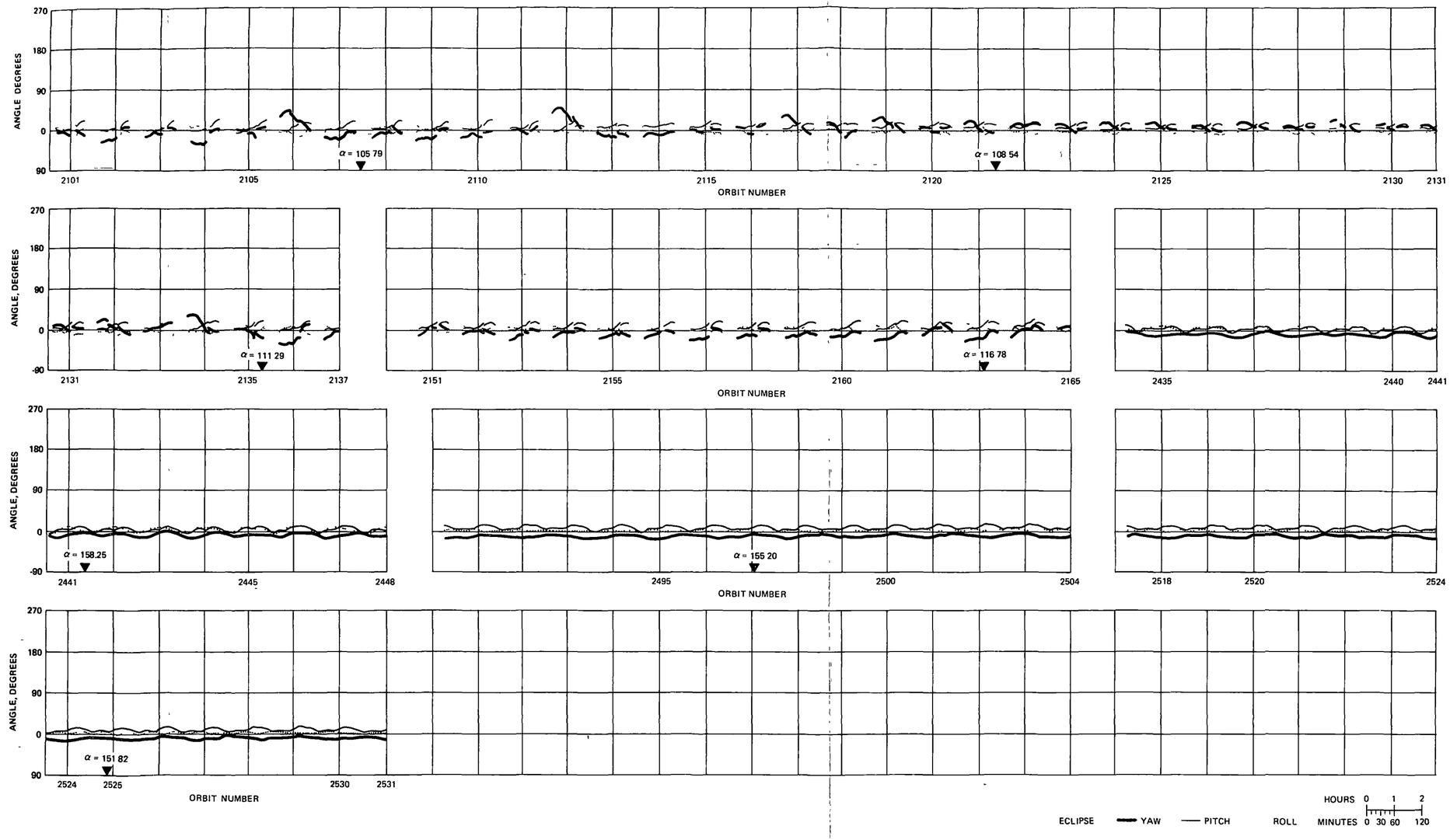

Figure A-2 (continued). Flight Data, Satellite 163

Page Intentionally Left Blank

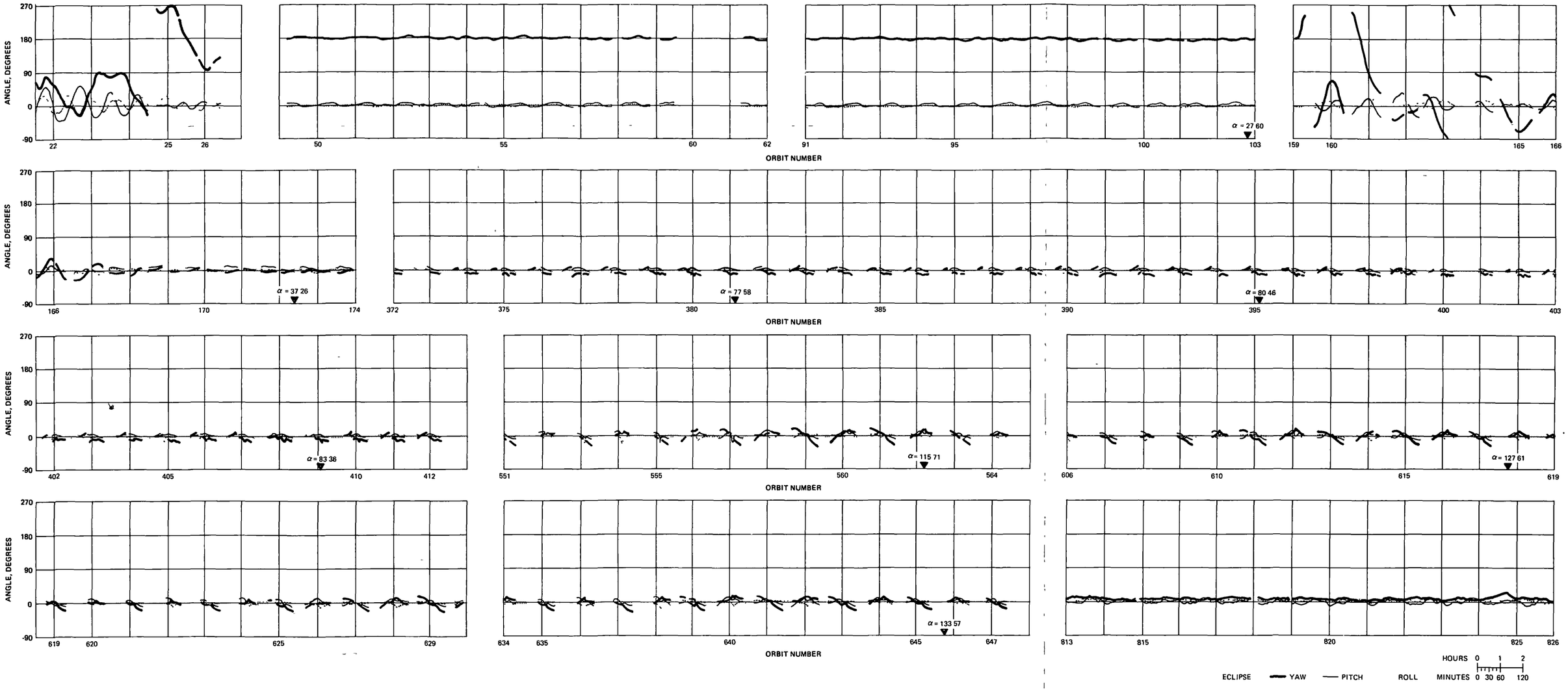

Figure A-3. Flight Data, Satellite 164

Page Intentionally Left Blank

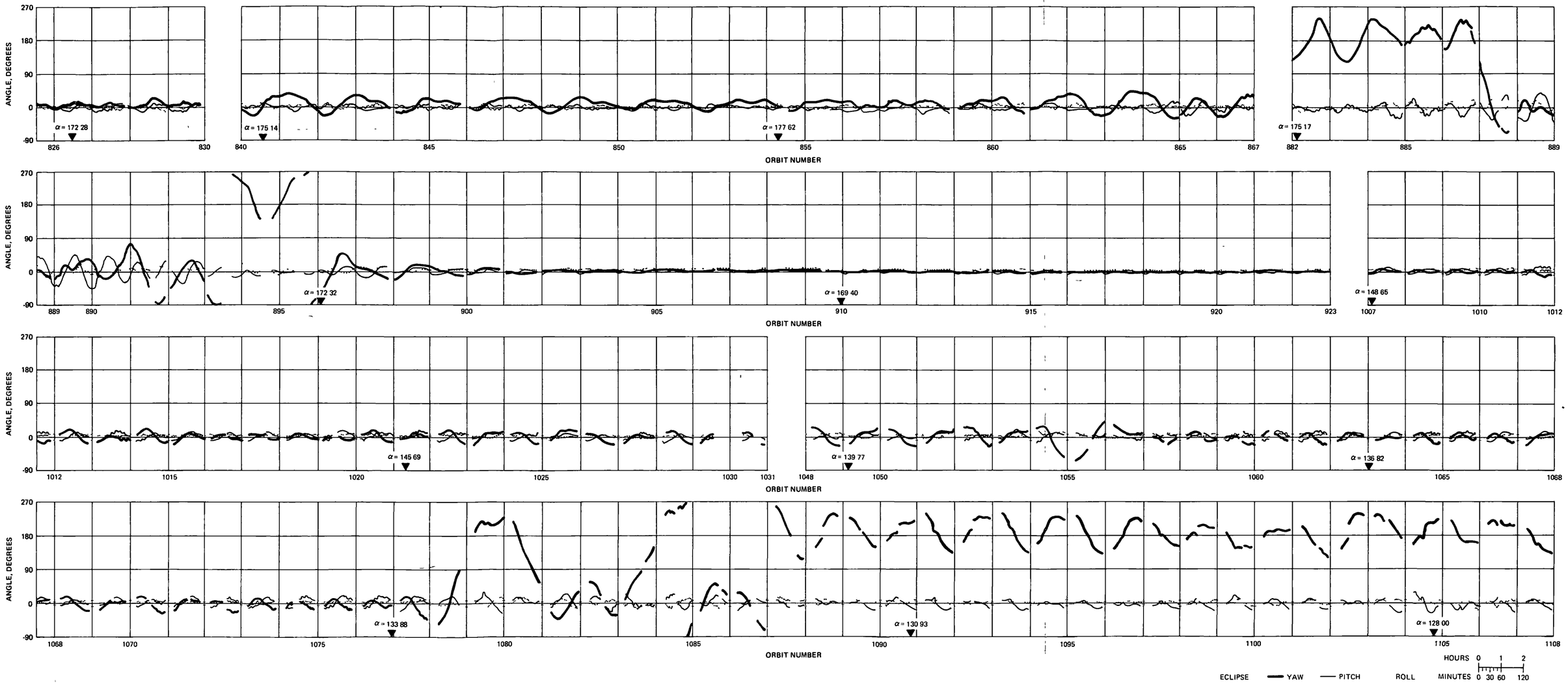

Figure A-3 (continued). Flight Data, Satellite 164

Page Intentionally Left Blank

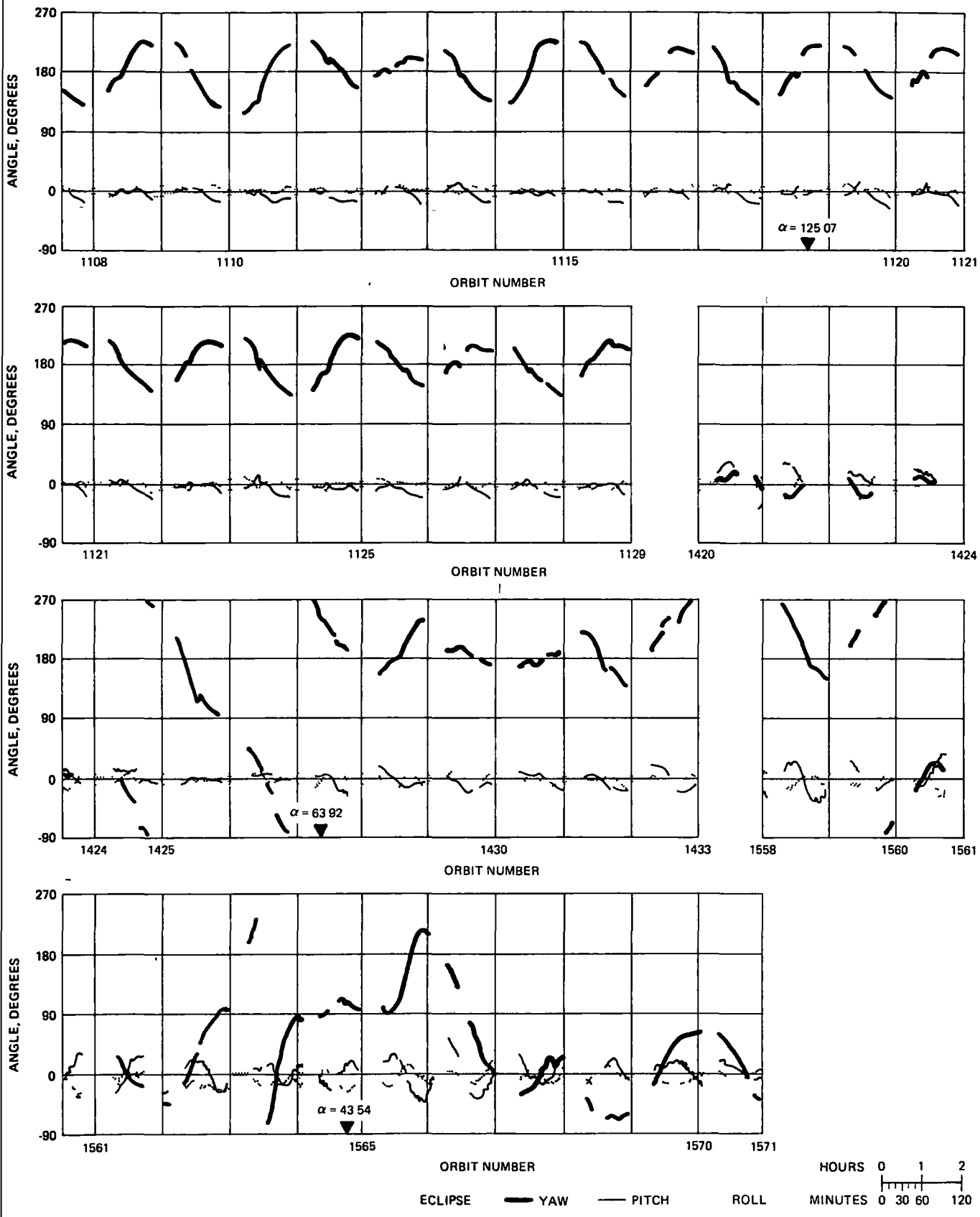

Figure A-3 (continued). Flight Data, Satellite 164

APPENDIX B

CHARACTERISTIC EQUATIONS

It can be shown that the small-angle attitude motion of a two-axis hinged, two-body satellite about its equilibrium position is described by the following set of linearized equations.

$$\ddot{\eta}_1 + C_1'(\dot{\eta}_1 - \dot{\eta}_2) + d_1\,\eta_1 - k_1'\eta_2 = 0 \qquad \text{(B-1)}$$

$$\ddot{\eta}_2 + C_2'(\dot{\eta}_2 - \dot{\eta}_1) + d_2\eta_2 - k_2'\eta_1 = 0 \qquad \text{(B-2)}$$

$$\ddot{\xi}_1 + C_1''(\dot{\xi}_1 - \dot{\xi}_2) + q_1\Omega\dot{\zeta} + u_1\xi_1 - \bar{k}_1\xi_2 = 0 \qquad \text{(B-3)}$$

$$\ddot{\xi}_2 + C_2''(\dot{\xi}_2 - \dot{\xi}_1) + q_2\Omega\dot{\zeta} + u_2\xi_2 - \bar{k}_2\xi_1 = 0 \qquad \text{(B-4)}$$

$$\ddot{\zeta} + (1 - f_1 - f_2)\Omega^2\zeta - \Omega f_1'\dot{\xi}_1 - \Omega f_2\dot{\xi}_2 = 0 \qquad \text{(B-5)}$$

where

$C_1' = C_2/I_2$, $\quad C_2' = C_2/I_5$

$k_1 = k_2/I_2$, $\quad k_2' = k_2/I_5$

$d_1 = 3\Omega^2(I_1 - I_3)/I_2 + k_1'$

$d_2 = 3\Omega^2(I_4 - I_6)/I_5 + k_2'$

$C_1'' = C_1/I_1$, $\quad C_2'' = C_1/I_4$

$q_1 = (I_1 + I_3 - I_2)/I_1$

$q_2 = (I_4 + I_6 - I_5)/I_4$

$u_1 = 4\Omega^2(1 - q_1) + k_1/I_1$

$u_2 = 4\Omega^2(1 - q_2) + k_1/I_4$

$\bar{k}_1 = k_1/I_1$ $\quad \bar{k}_2 = k_1/I_4$

$f_1 = (I_1 + I_3 - I_2)/(I_3 + I_6)$, $\quad f_2 = (I_4 + I_6 - I_5)/(I_3 + I_6)$

η_1 = pitch motion of primary body

η_2 = pitch motion of secondary body

ξ_1 = roll motion of primary body

ξ_2 = roll motion of secondary body

ζ = yaw motion

k_1 = roll spring constant

k_2 = pitch spring constant

C_1 = roll damping coefficient

C_2 = pitch damping coefficient

I_1, I_2, I_3 = roll, pitch and yaw inertia of primary body about hinge

I_4, I_5, I_6 = roll, pitch and yaw inertia of secondary body about hinge

Ω = 2π divided by orbital period

The pitch equations (B-1) and (B-2) are decoupled from the roll and yaw equations (B-3) to (B-5). The resulting characteristic equation in pitch is then

$$S^4 + (C_1' + C_2')S^3 + (d_1 + d_2)S^2 + (d_1C_2' + d_2C_1' - C_1'k_2' - C_2'k_1')S + (d_1d_2 - k_1'k_2') = 0 \qquad \text{(B-6)}$$

The roll and yaw equations (B-3) to (B-5) are all coupled, a result that makes the use of a damper only in roll practical. The characteristic equation in roll and yaw is

$$b_6S^6 + b_5S^5 + b_4S^4 + b_3S^3 + b_2S^2 + b_1S + b_0 = 0 \qquad \text{(B-7)}$$

where

$$b_0 = \Omega^2(1 - f_1 - f_2)(u_1u_2 - \bar{k}_1\bar{k}_2)$$

$$b_1 = \Omega^2(1 - f_1 - f_2)(C_2''u_1 + C_1''u_2 - \bar{k}_1C_2'' - \bar{k}_2C_1'')$$

$$b_2 = \Omega^2(1 - f_1 - f_2)(u_1 + u_2) + u_1u_2 - \bar{k}_1\bar{k}_2 + \Omega^2(f_1q_2\bar{k}_1 + f_2q_1\bar{k}_2 + f_1q_1u_2 + f_2q_2u_1)$$

$$b_3 = \Omega^2(1 - f_1 - f_2)(C_1'' + C_2'') + C_1''(u_2 + \Omega^2f_1q_2 + \Omega^2f_2q_2 - \bar{k}_2) + C_2''(u_1 + \Omega^2f_2q_1 + \Omega^2f_1q_1 - \bar{k}_1)$$

$$b_4 = \Omega^2(1 - f_1 - f_2) + u_1 + u_2 + \Omega^2(f_1q_1 + f_2q_2)$$

$$b_5 = C_1'' + C_2''$$

$$b_6 = 1$$

* U S GOVERNMENT PRINTING OFFICE 1975—635-049 / 71

"The aeronautical and space activities of the United States shall be conducted so as to contribute . to the expansion of human knowledge of phenomena in the atmosphere and space The Administration shall provide for the widest practicable and appropriate dissemination of information concerning its activities and the results thereof"

—NATIONAL AERONAUTICS AND SPACE ACT OF 1958

NASA SCIENTIFIC AND TECHNICAL PUBLICATIONS

TECHNICAL REPORTS Scientific and technical information considered important, complete, and a lasting contribution to existing knowledge

TECHNICAL NOTES Information less broad in scope but nevertheless of importance as a contribution to existing knowledge

TECHNICAL MEMORANDUMS Information receiving limited distribution because of preliminary data, security classification, or other reasons Also includes conference proceedings with either limited or unlimited distribution

CONTRACTOR REPORTS Scientific and technical information generated under a NASA contract or grant and considered an important contribution to existing knowledge

TECHNICAL TRANSLATIONS Information published in a foreign language considered to merit NASA distribution in English

SPECIAL PUBLICATIONS Information derived from or of value to NASA activities Publications include final reports of major projects, monographs, data compilations, handbooks, sourcebooks, and special bibliographies

TECHNOLOGY UTILIZATION PUBLICATIONS Information on technology used by NASA that may be of particular interest in commercial and other non-aerospace applications Publications include Tech Briefs, Technology Utilization Reports and Technology Surveys

Details on the availability of these publications may be obtained from

SCIENTIFIC AND TECHNICAL INFORMATION OFFICE

NATIONAL AERONAUTICS AND SPACE ADMINISTRATION

Washington, D.C. 20546